January 2014

# Organic Fluids and Passive Cooling in a Supercritical Rankine Cycle for Power Generation from Low Grade Heat Sources

Rachana Vidhi
*University of South Florida*, rachana@mail.usf.edu

Organic Fluids and Passive Cooling in a Supercritical Rankine Cycle for Power Generation from

Low Grade Heat Sources

by

Rachana Vidhi

A dissertation submitted in partial fulfillment
of the requirements for the degree of
Doctor of Philosophy
Department of Chemical and Biomedical Engineering
College of Engineering
University of South Florida

Major Professor: D. Yogi Goswami, Ph.D.
Elias K. Stefanakos, Ph.D.
Babu Joseph, Ph.D.
John Kuhn, Ph.D.
Mark Stewart, Ph.D.

Date of Approval:
July 8, 2014

Keywords: Efficiency, optimization, environmental heat sink, ground cooling, night-sky-radiative cooling

# DEDICATION

I dedicate this dissertation to my grandparents, who started the tradition of higher education in the family. Growing up in a well educated family provided me with the patience and perseverance required for doctoral work.

I dedicate this dissertation to my parents, who taught me to dream. My father encompassed the notion that I was capable to achieving anything I wanted if I put my heart and soul to it. My mother, who is the first one in the family to get a Ph.D., supported me with her motherly kindness and affection, as well as her experiences as a professional.

I dedicate this dissertation to my lovely sisters, my niece and my nephew, who have always been my biggest cheerleaders. They showed me to be happy even in the most adverse circumstances; to accept the challenge and not give in.

I dedicate this dissertation to friendship, a unique bond that joins strangers. I have been fortunate to find some great friends throughout my life, who shaped my personality. My friends at USF became my family away from home.

I dedicate this dissertation to my teachers, mentors and my students. All of them made such impacts on me, that are impossible to describe.

I dedicate this dissertation to all the renewable energy enthusiasts, who are constantly working in their own unique and subtle ways, in making the world a better place.

# ACKNOWLEDGMENTS

The number of people who have helped me in different ways makes me feel very fortunate and I would like to take this opportunity to show my gratitude towards all of them.

My advisor Dr. Yogi Goswami provided continuous support, encouragement, mentorship and the constructive criticism that helped me grow from a college student to a professional. Dr. Elias Stefanakos guided me with research and professional development during the last four years. The insight into technical analysis that I received from my committee members, Dr. Babu Joseph, Dr. John Kuhn and Dr. Mark Stewart, is invaluable.

Dr. Kyle Reed helped me not just with classes and programming, but mentored me throughout the Ph.D. program on several platforms. Dr. Vinay Gupta taught me how be a better educator when I assisted him for two courses. Dr. Sanjukta Bhanja and Dr. Sylvia Thomas provided moral support and comforted me whenever I needed any help. Dr. Sarada Kuravi guided me during the initial stage of my Ph.D. with data analysis and technical writing. Chemical Engineering department and the chair, Dr. Venkat Bhethanabotla provided financial support by hiring me as a teaching assistant.

This section would be incomplete without acknowledging my very helpful lab partners, classmates and students. And finally, I want to thank my parents and my sisters for their unstinting support, from across the world, that I always relied on. Even in the most difficult and stressful times, it was their encouragement that made me stronger.

**TABLE OF CONTENTS**

## LIST OF TABLES

# LIST OF FIGURES

vi

vii

## ABSTRACT

Low grade heat sources have a large amount of thermal energy content. Due to low temperature, the conventional power generation technologies result in lower efficiency and hence cannot be used. In order to efficiently generate power, alternate methods need to be used. In this study, a supercritical organic Rankine cycle was used for heat source temperatures varying from 125°C to 200°C. Organic refrigerants with zero ozone depletion potential and their mixtures were selected as working fluid for this study while the cooling water temperature was changed from 10-25°C. Operating pressure of the cycle has been optimized for each fluid at every heat source temperature to obtain the highest thermal efficiency. Energy and exergy efficiencies of the thermodynamic cycle have been obtained as a function of heat source temperature.

Efficiency of a thermodynamic cycle depends significantly on the sink temperature. At areas where water cooling is not available and ambient air temperature is high, efficient power generation from low grade heat sources may be a challenge. Use of passive cooling systems coupled with the condenser was studied, so that lower sink temperatures could be obtained. Underground tunnels, buried at a depth of few meters, were used as earth-air-heat-exchanger (EAHE) through which hot ambient air was passed. It was observed that the air temperature could be lowered by 5-10°C in the EAHE. Vertical pipes were used to lower the temperature of water by 5°C by passing it underground. Nocturnal cooling of stored water has been studied that can be used to cool the working fluid in the thermodynamic cycle. It was observed that the water temperature can be lowered by 10-20°C during the night when it is allowed to cool. The amount of water lost was calculated and was found to be approximately 0.1% over 10 days.

The different passive cooling systems were studied separately and their effects on the efficiency of the thermodynamic cycle were investigated. They were then combined into a novel condenser design that uses passive cooling technology to cool the working fluid that was selected in the first part of the study. It was observed that the efficiency of the cycle improved by 2-2.5% when passive cooling system was used.

**CHAPTER 1: INTRODUCTION**

Traditional methods of power generation generally require non-renewable sources of energy, such as coal, petroleum and natural gas; that are used to generate high temperatures in the power plants. The limited stock and environmental problems related to the fossil fuels have made it necessary to explore alternate sources of energy. There are several low to medium temperature heat sources, such as solar thermal, geothermal and waste heat, that are abundantly available and the amount of energy contained in those sources is high enough to fulfill all the energy requirements of the world [1]. However, the conventional power generation methods, such as a steam Rankine Cycle, result in very low efficiencies for these sources. As the efficiency of power conversion depends largely on source and sink temperatures; and the source temperature is low, other factors such as alternative configuration for the power cycle, appropriate working fluid, optimum operating pressure and lower sink temperature, need to be considered to obtain a viable method of power generation. A number of studies have analyzed the effects of aforementioned parameters separately. The objective of this study is to holistically combine different technologies to develop a novel design that can provide a comprehensive solution to the low temperature power generation.

Several configurations of thermodynamic cycles have been proposed to improve the efficiency of power generation when the heat source temperature is low, that include organic Rankine cycle (ORC), Kalina cycle, Goswami cycle, trilateral flash cycle and the supercritical Rankine cycle (SRC) [2-10]. These cycles have been studied with different working fluids that have the potential of giving high efficiency. Organic Rankine cycles (ORC) have performed

better compared to other thermodynamic cycles that convert low grade heat into power because of the simplicity in design and being more cost effective [7]. They use an organic fluid instead of steam to generate electricity from low temperature heat sources. They have been used as a bottoming cycle for a combined cycle power plant. It has been observed that the improvement in efficiency and the amount of power generated is generally sufficient to offset the cost of additional equipment needed.
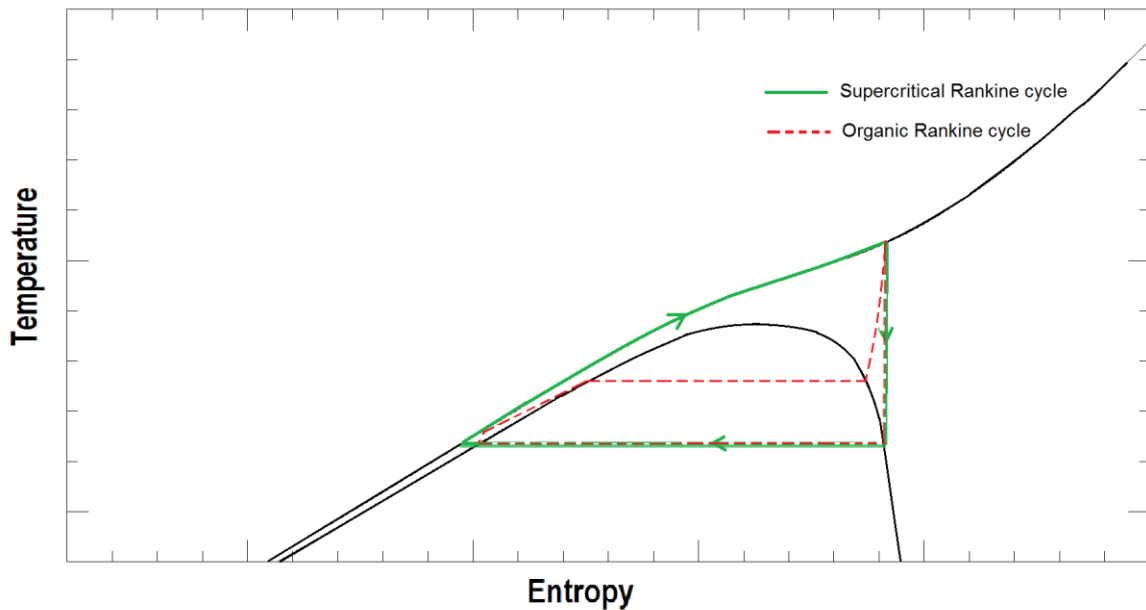


Figure 1. A supercritical Rankine cycle on a T-S diagram.

Conventional ORCs work under subcritical conditions and generally use pure working fluids. Since a pure fluid boils at a constant temperature (Figure 1), it results in a mismatch with the temperature profile of the heat source [8]. This mismatch results in higher losses in the heat exchange process, which can be reduced by the use of a supercritical Rankine cycle (SRC) [8]. In a SRC, shown in Figure 1, the working fluid is pressurized beyond its critical pressure and then it is heated isobarically directly to vapor phase. The superheated vapor then expands in the turbine where mechanical work is extracted. The turbine exhaust is then cooled to the liquid state in a

condenser and the condensed fluid is pumped back to the high pressure. A number of hydrocarbons and refrigerants have been studied as potential working fluids to be used in SRCs [8, 11-15]. It has been observed that these fluids give better efficiency in supercritical Rankine cycles than the conventional ORC [8, 12, 16-21].

The performance of a working fluid and the output of a power cycle are limited by different constraints that need to be considered while modelling the system for low temperature applications. The temperatures of geothermal, low concentration solar thermal and waste heat sources generally vary from less than 100 to over 200 °C [22]. There are also other limitations on the source side which restrict the heat exchanger/boiler performance and need to be accounted for while modeling the power block. For a geothermal source, the temperature of the geothermal fluid in a power plant, in general, cannot be lowered much below 80 °C to avoid precipitation of minerals and their deposition on the walls of the pipes. In the case of solar thermal plants, the temperature of some heat transfer fluids, such as a synthetic or mineral oil, cannot be lowered below 30-40 °C before it enters the collector field. The limitations on the sink side, which are posed by the ambient conditions, affect the cycle efficiency significantly. A lower value of sink temperature improves the overall efficiency, which may be difficult to achieve due to economic, environmental or social concerns. Water cooled condensers usually give lower sink temperatures but at many places, they cannot be used due to non-availability of water and environmental impacts. In those conditions, air cooled condensers remain the only acceptable choice. The air cooled condensers usually result in lower thermal efficiency associated with the added parasitic power losses and higher sink temperatures. Dry cooling using ambient air increases the sink temperature by 20-25°C and the reduction in thermal efficiency for a low temperature power generation system can be as high as 25%. Passive cooling methods such as a ground coupled

3

heat exchanger or night time radiative cooling lower the sink temperature and hence increase the overall efficiency of the power plant.

Use of earth as a heat sink can improve the performance by increasing the efficiency and lowering the fluctuations caused by the variation in the ambient air temperature. Although the ambient temperatures vary over the year by a large amount, the underground temperatures vary within a narrow range throughout the year. It has been observed that the temperature at a depth of few meters remains nearly constant at the average annual ambient temperature [23, 24]. Earth-to-air heat exchangers operate on the consistency of temperature below the surface of the earth to heat or cool the ambient air. Buried pipes are used through which air is circulated and the difference in temperatures is utilized for heating or cooling the air. This method has been used extensively for air-conditioning of buildings and greenhouses [24-36]. Another possible environmental heat sink is outer space to which heat can be rejected by radiation at night time. Since the sky temperature is much lower than the ambient air temperature, a surface exposed to the night sky can be cooled to a much lower temperature. However, the same surface needs to be protected from being heated during the day due to the incoming solar radiation. So, nocturnal cooling systems are generally equipped with an insulated cover that prevents daytime heating. This concept has also been used for air-conditioning of buildings in the form of roof-ponds [37-47]. All of these systems can be combined with the condenser of a power cycle that can use the air or water coming from a passive cooling system to cool the working fluid in the condenser. The cooling system of a power plant accounts for a major portion of the capital investment. Figure 2 shows the distribution of cost per kW power produced for Magnamax binary power plant located at Imperial Valley, California [48]. In order to have shorter payback period for such investment, it becomes necessary to employ more efficient condensers.
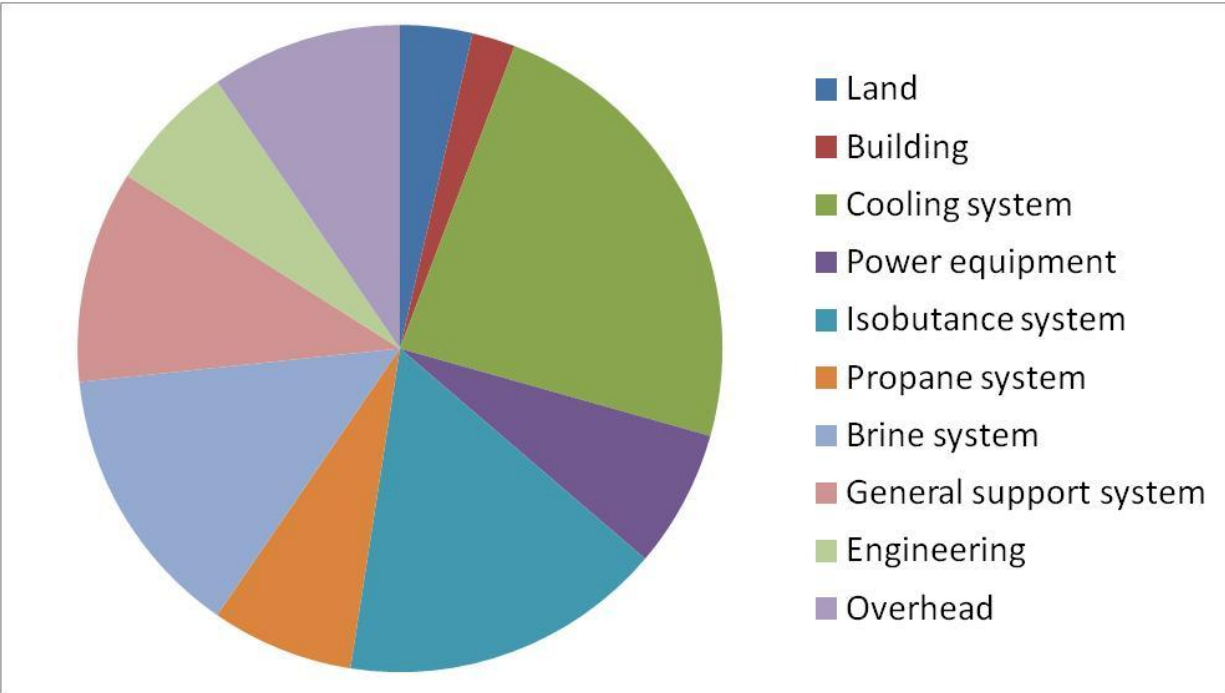
Figure 2. Cost distribution of a geothermal power plant.

In the current study, the effects of using organic refrigerants in a SRC and passive cooling in the condenser have been investigated for low temperature power generation. The power block and the ground coupled heat exchanger were first studied separately and then combined to get the complete system performance. In order to maximize the efficiency of a SRC operating in the low temperature range, a number of environmentally safe organic refrigerants were selected on the basis of their critical points to study the feasibility of their use as working fluids. The optimum pressure ratios for the selected fluids were obtained by investigating a wide range of pressure ratios for each source temperature. The system was then further analyzed for the working fluid giving the highest energy and exergy efficiencies. An earth-air-heat-exchanger (EAHE) was modeled and the results were used in the condenser of the SRC. Seasonal variation and its effect on the EAHE and eventually on the SRC efficiency were analyzed for the year round performance of the power generation system.

# CHAPTER 2: RESEARCH BACKGROUND

## 2.1 Supercritical Rankine Cycle

Supercritical Rankine cycle works on the same principle as an organic Rankine cycle but its operating pressure is higher than the critical pressure of the working fluid. Figure 3 shows a T-S diagram of a Supercritical Organic Rankine Cycle along with the temperature profile of a hot brine heat source. Since the fluid is in supercritical state during the heating process, it does not enter the two-phase region, while the sensible heat source transfers its heat to the working fluid. For a supercritical cycle, the energy loss is smaller than a conventional Rankine cycle because the thermal match between the heat source and the working fluid is better.
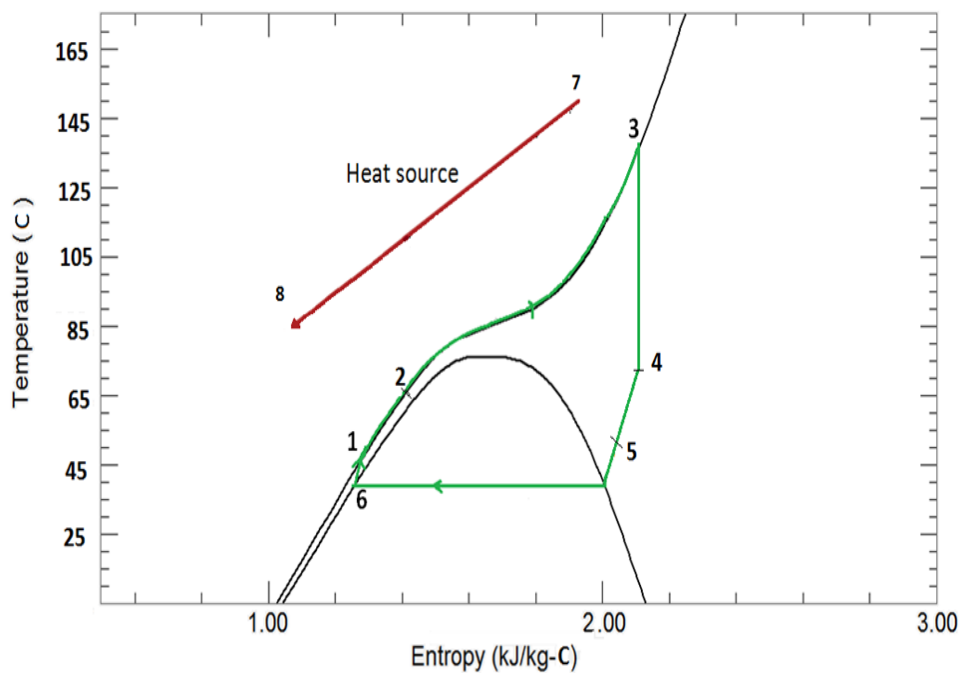


Figure 3. T-S diagram of a supercritical cycle with the temperature profile of the hot brine.

Figure 4 shows the T-S diagram for R-32 at various pressures. It can be seen that the temperature evolution during the heating process tends towards a straight line when the operating pressures are farther from the critical pressures. The same is true for other fluids as well. So, a higher operating pressure is preferable for a higher thermal efficiency of the heat exchange process. However, at high pressures, the required pump work will increase, and, more importantly, the material requirements would become more severe, thus increasing the cost. So an optimum operating pressure needs to be obtained for the highest overall efficiency and power output of the supercritical cycle.
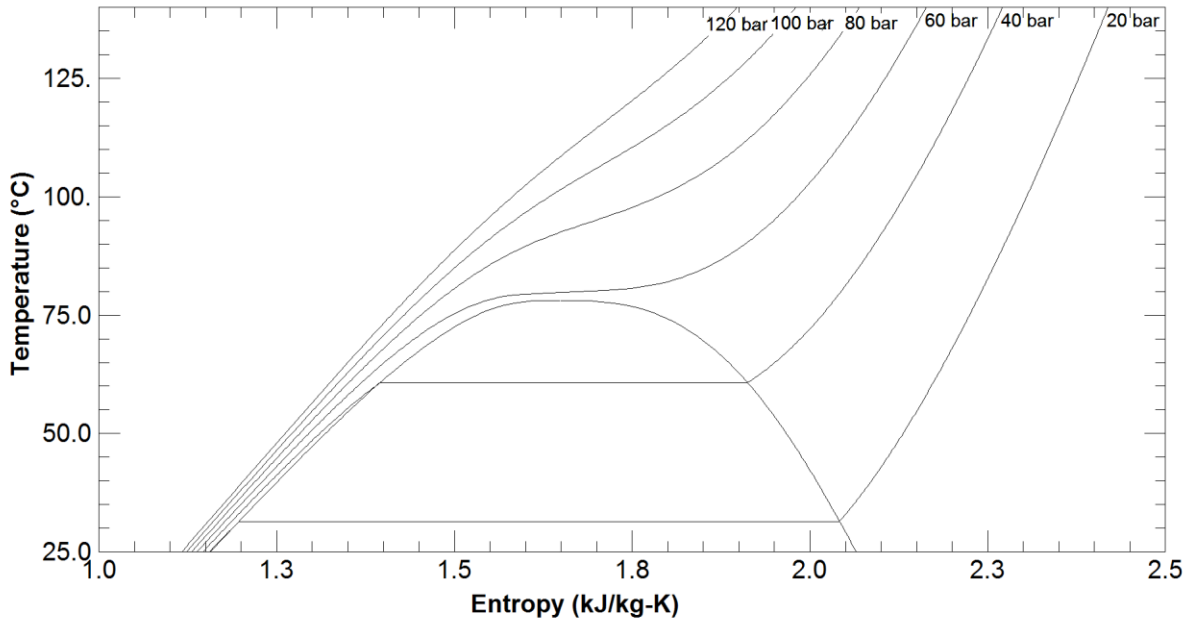


Figure 4. T-S diagram for R-32 at different pressures.

The choice of a working fluid depends on its physical and chemical properties as well as its environmental and economic aspects. Carbon dioxide is one such choice, being abundant, non-toxic, non-flammable and inexpensive. Zhang et al. [49-52] showed that the efficiency of a carbon dioxide based cycle is usually around 8-11% when the hot source temperature is close to 185°C and the cooling water temperature is between 7 and 10°C. Chen et al.[12] compared the

efficiency of a R-32 based ORC with a $CO_2$-based cycle under similar source and sink conditions and concluded that a R-32 based cycle gives higher efficiency than a $CO_2$ based cycle and operates at lower pressures. Also, the exergy efficiency and exergy density for a R-32 based cycle were found to be higher than a $CO_2$ based cycle. Bliem and Mines et al. [53-65] conducted a series of experiments to study the performance of a supercritical Rankine cycle for binary geothermal plants using propane-isopentane and isobutene-hexane family of hydrocarbons. They studied the performance of different equipment used in the experiments and the variation of heat transfer properties, when the heat source temperature was between 154 °C and 163 °C. Heberle et al. analyzed four working fluids for combined heat and power generation from geothermal sources and studied the effect of series and parallel circuits of ORC and heat production [66]. Guo et al. [67-69] studied combined power and heat generation systems for geothermal sources with temperatures less than 100°C. They considered a list of dry, wet and isentropic fluids and analysed them separately. Augustine et al. compared sub and supercritical binary Rankine cycles for 100 to 200°C geothermal source temperatures [21]. Air cooled condenser was considered in the modelling and most suitable working fluids along with the influence of parasitic losses in different conditions of cycle operation were reported. Lakew et al.[70] did parametric analysis for finding the working fluid that needs smallest equipment sizes but gives high power output. It was found that no fluid considered in the analysis required both smaller heat exchanger area and turbine size.

Mixtures of organic refrigerants have also been studied as potential working fluids [13, 16, 71-77]. Differences in boiling points and critical properties of the constituent fluids result in non-isothermal heating and condensation of the mixture in a thermodynamic cycle, which can reduce the exergy destruction in the heat exchanger. Chen et al.[16] have compared the

8

performance of zeotropic mixtures in a SRC with that of pure fluids in an ORC and found the performance of mixtures in the SRC better.

## 2.2 Passive Cooling

Passive cooling systems utilize natural means to produce cooling that may be used for various applications. Environmental heat sinks, i.e., ground, air or sky, are used to release heat from the system that needs to be cooled. Passive cooling methods have the potential to lower the sink temperature and hence increase the efficiency of power generation unit. Earth may be used as a heat sink to cool the ambient air or cooling water, which can then be used in the condenser to cool the working fluid. While using air as a coolant, the fluctuations caused by the variation in the ambient temperature can be reduced since the temperature at a depth of a few meters (~4 m) varies in a small range around the annual ambient temperature [23, 24, 78, 79]. Ground coupled heat exchangers, where coolant is circulated through buried pipes; operate on this consistency of temperature below the surface of the earth to cool the ambient air or water. This method has been used for air-conditioning of buildings and greenhouses [24-36, 80-88].

## 2.2.1 Earth-Air-Heat-Exchanger

Temperature of the soil under the surface of the Earth does not vary as much as the ambient air temperature and after certain depth, the temperature remains nearly constant throughout the year. The high thermal inertia of soil reduces the temperature variation and causes a lag between underground and ambient temperatures. This temperature difference can be utilized to cool the ambient air in summer and heat it in winter by passing it underground. Figure 5 shows a schematic diagram of an earth-air heat exchanger system. Ambient air is blown through the tunnels buried inside the ground using a fan (or a blower). As it flows through the tunnel, the air exchanges heat with the soil. In summer when the ground temperature is lower

9

than the ambient, heat is rejected into the ground. However, in the winter season, the ambient air temperature may be lower than the soil temperature. In this case, the air absorbs heat from the soil and the heated air is supplied to the air-conditioned space. This method can be used for lowering the temperature of the ambient air which is then used in the condenser of the power cycle. A closed loop system with water instead of air may be used at locations that are either far from a water body or use of water for condenser is prohibited for environmental or other social reasons.
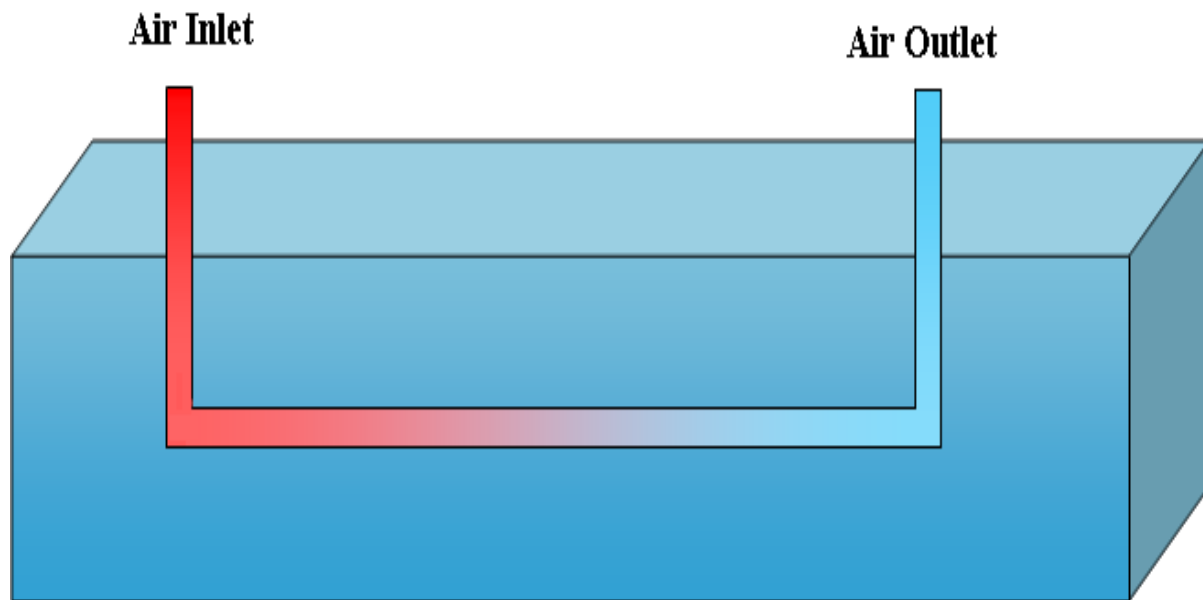


Figure 5. Schematic diagram of an earth-air heat exchanger.

Earth-air heat exchangers (EAHE) have been used for cooling of greenhouses and air-conditioning of buildings in many parts of the world [24, 27, 31, 35, 36, 89-96]. Goswami et al. compared the experimental observations [97] with the results obtained from a mathematical model for fixed mass flow rate and then used the mathematical model to determine the performance of different flow rates [98, 99]. Ileslamlou and Goswami analyzed an EAHE for a period of 90 days, in which the system was turned on for 16.5 hours in a day and then turned off for 7.5 hours [100, 101]. During the time it was on, the soil temperature increased with time,

although the increase was small, and then came down when the system was not operating. They noticed that the temperature after cool down was slightly higher than the initial temperature. Bansal and Sodha studied a system that was installed to meet the summer cooling requirements of a hospital situated near Delhi, India [27, 31]. It was observed that in summer, the dry bulb temperature could be lowered by as much as 15 °C in the EAHE. While in winter, 3-4 °C temperature rise was obtained. Mihalakakou studied the effect of various parameters, such as depth, length and diameter of pipes and effect of ground cover, on the performance of the EAHE [24, 32, 34, 102-108]. Trombe et al. [25, 109] conducted experiments on three identical systems coupled with each other. It was also observed that the decrease in air temperature was very rapid in the initial portion of the duct because the difference in the soil and air temperatures is the highest in the beginning and decreases later on. Eicker demonstrated the performance of the passive energy office building in Germany where different designs of ground cooling were examined and compared [110-112]. It was observed that the EAHE operated at a high coefficient of performance, of about 30, but it could only satisfy about 20% of the cooling load of the building. Ghosal et al. studied the effect of an EAHE on greenhouse temperature during the whole year for both summer cooling and winter heating [30, 113, 114]. It was observed that using an EAHE resulted in 7-8 °C higher temperature in winter and 5-6 °C lower temperature in summer compared to when EAHE was not in operation. Goswami [115] investigated the feasibility of using ground cooling in a Rankine cycle, when the soil temperature was 18 °C and the air temperature was 41 °C. It was observed that during the day, the performance of the plant with ground cooling was better than the air cooled solar thermal power plant.

Several parameters affect the performance of an earth-air heat exchanger, including but not limited to, the environmental factors, system design, location etc. Some of these parameters,

like location, seasonal and daily variation, solar radiation, soil temperature and properties, weather etc. cannot be controlled but affect the system performance significantly. For example, if the system is set up at a location that is close to a water body, its performance will be very different from the same setup located in a dry land area. A place with large temperature difference between summer and winter will have different results with EAHE than a place with near constant temperature all year round. Similarly different types of soil result in different thermo-physical properties and hence different performances of the EAHE. Since these factors have very large impact on the system performance but cannot be controlled, the design parameters are optimized according to the need. Pipe geometry, depth, mass flow rate, material use etc. are some parameters that are considered while designing a system to be used for a specific location. By appropriately designing a system, the climatic conditions can be used to their full advantage. This section describes these design parameters and their effects on the EAHE performance.

- Depth: As the lag between the ambient and underground temperature increases with depth, the performance of the EAHE system also improved by increasing the depth. However, it was generally observed that the performance improvement was negligible beyond a depth of 4 m [24, 31, 34, 35, 78, 90, 116].

- Length: Different pipe lengths have been used for various experimental projects as well as theoretical analyses [23, 24, 34, 35, 90, 117-120]. Longer pipes result in better thermal performance because the total heat transferred to or from the soil increases. However, the heat transfer rate becomes negligible as the air temperature inside the pipe gets closer to the soil temperature and further pipe length doesn't contribute towards lowering the air temperature.

- Pipe radius: Parametric analysis has been done by a number of researchers to study the effect of pipe radius. Pipe radius directly affects the convective heat transfer coefficient. Smaller pipe radius results in higher heat transfer coefficient and hence lower thermal resistance between air and soil [24, 34, 35, 118, 121, 122] . So, using a smaller pipe diameter should give lower outlet temperature in cooling mode and higher outlet temperature in heating mode. However, some researchers have observed an interesting trend where the outlet temperature first reduces with increasing radius and then increases. The point where the reversal starts is referred to as "critical radius" [116, 118, 120]. The reason for such trend is the combined effect of reducing heat transfer coefficient and increasing heat transfer area with increasing radius. Kumar et al. [118, 120] observed in their analysis that when the radius of the underground pipe was increased from 0.41 m to 0.52 m, the outlet temperature (in cooling mode) reduced. This suggested that the increase in surface area of the pipe dominated over the reduction of heat transfer coefficient. However, further increase in the pipe radius (0.58 and 0.70 m) resulted in higher outlet temperature, implying that the increase in surface area was not enough to overcome the effects of reducing heat transfer coefficient.

- Flow rate: Increase in flow velocity and hence the mass flow rate results in higher outlet temperature in cooling mode and lower outlet temperature in heating mode [24, 25, 34, 90, 98, 99, 109, 117, 118, 120]. Hence, lower flow rate is generally considered a favorable situation but the overall effects may not be the optimum. Bansal et al. studied the effect of flow velocity (2.0, 3.2, 4.0 and 5.0 m/s) for both heating and cooling mode and compared the results obtained in simulations with the experimental values [28, 29]. As the flow velocity was increased from 2.0 m/s to 5.0 m/s, the total time spent by the air

13

underground was reduced by 2.5 times, which dominated over the improvement in the heat transfer coefficient that increased by 2.3 times. They also noticed that even though the change in temperature was smaller at higher velocities, the heating or cooling effect per unit time was much more. So, an optimum flow rate may need to be obtained depending on the application.

- Ground cover and soil type: Different ground covers, like bare soil, grass-covered soil, sand-covered soil, high moisture soil etc., result in different underground temperatures and thermal properties [90, 106, 107, 123, 124]. Soil with higher moisture content results in better performance because its thermal conductivity is increased, leading to improved heat transfer between the soil and the underground pipes. Goswami et al. showed the variation of thermal conductivity with time and moisture content and proved its effect on the performance of the EAHE [99-101]. It was observed that as the soil around the pipe got heated by the passing air, the moisture dissipated from the pipe vicinity and the thermal conductivity of the soil was lowered from the initial value of 1.1 W/m-K to less than 0.8 W/m-K. However, when the system was turned off for 3 hours, the moisture content was restored and the thermal conductivity increased to 0.9 W/m-K.

- Pipe material and thickness: Thermal conductivity of the pipe material adds to the thermal resistance in the heat transfer. However, since the thickness of the pipe is generally only a few millimeters, different materials do not induce much difference in thermal performance [28, 29, 90, 122].

- Time: For analyzing the performance of EAHE, earth is usually considered as an infinite source/sink. So, the underground temperature is assumed constant and it is a valid assumption for short duration use. Even if the underground temperature is affected by the

EAHE system, the change is generally negligible However, continued use for a long period of time results in discharge/extraction of a large amount of heat to/from the earth. This results in the change of temperature in the region surrounding the underground tube. Ileslamlou and Goswami analyzed an EAHE for a period of 90 days, in which the system was turned on for 16.5 hours in a day and then turned off for 7.5 hours [100, 101]. During the time it was on, the soil temperature increased with time, although the increase was small, and then came down when the system was not operating. They noticed that the temperature after cool down was slightly higher than the initial temperature. The same behavior continued for the entire period of time, resulting in an overall increase of the outlet temperature by 2 °C [100, 101].

### 2.2.1.1 Configurations

Different designs have been proposed and practiced all over the world depending upon the application requirements, ease of establishment, economic considerations, heat exchanger studies and experiments. The most common design is a single pipe heat exchanger buried at a fixed depth [27, 30, 31, 34, 100, 101, 104, 125, 126]. However, a number of researchers have studied multiple pipe systems as well [35, 126]. Figure 6 (a) and (b) show the schematic of such a system where multiple pipes buried underground are connected in series and parallel, respectively. The series configuration is generally used when the fluid needs to be cooled to a lower temperature while the parallel configuration is preferred when the heat load is higher. While modeling a multiple pipe system, an additional term for the thermal resistance caused by the mutual interactions of the pipes must be considered. This term is halved for the pipes that are on the sides.
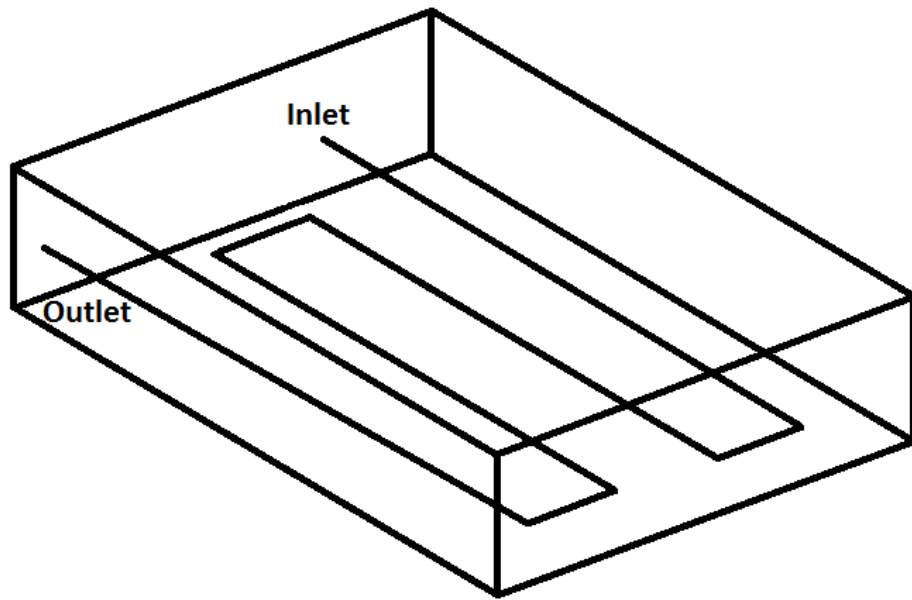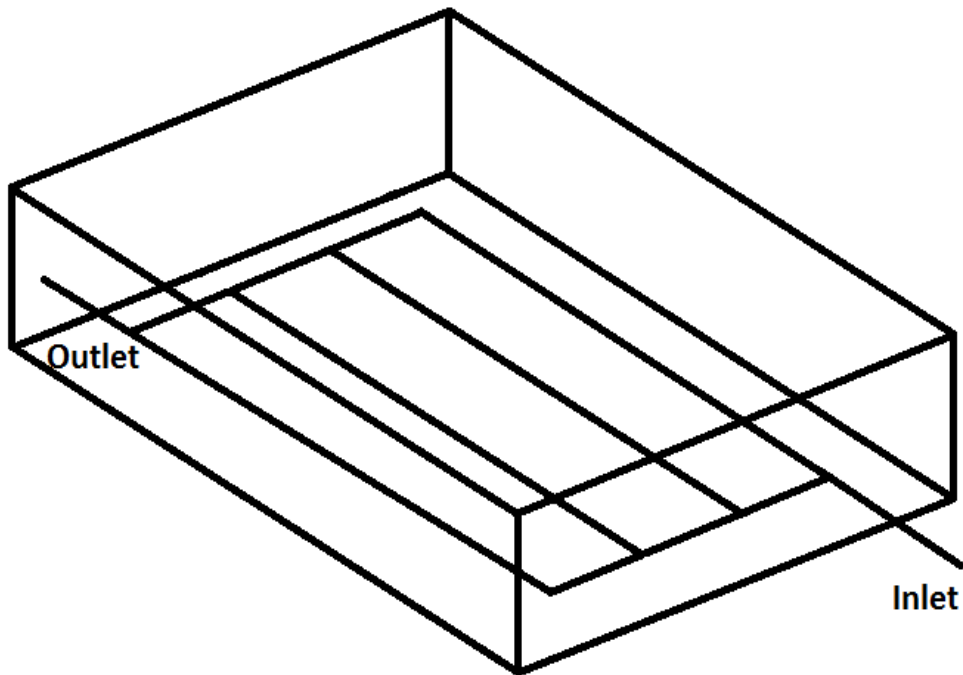
Figure 6. Configurations of multiple pipes EAHE. (a) Series (b) Parallel.

Hamada et al. performed experiments on a modified design for underground heat exchanger that could be installed without digging and was more economic [127]. Figure 7 shows the installation process for the new design using no-dig method. They observed that using this system, energy consumption during installation was decreased by 78% while the annual primary energy consumption was reduced by 29% over the vertical underground system. The payback period also reduced to less than one year compared for both energy and carbon emission, which were 4.6 and 6.9 years respectively for the conventional system.
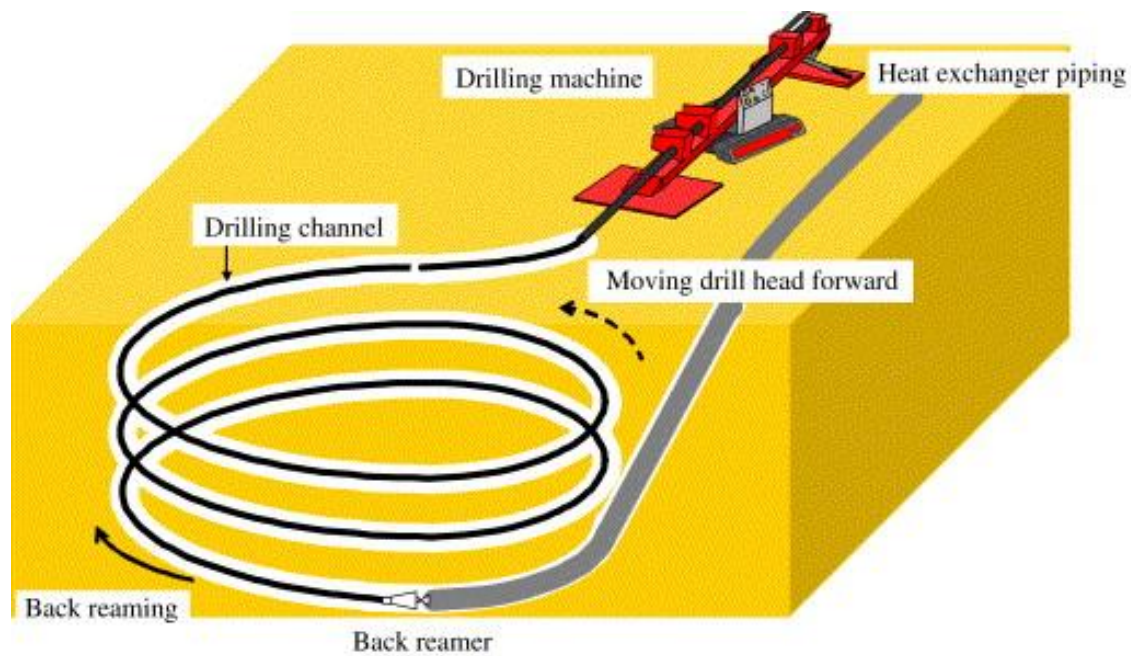


Figure 7. Installation process using no-dig method. [127] (Copyright permission in Appendix B).

### 2.2.1.2 Models

A number of analytical and numerical models have been successfully applied to analyse the earth-air-heat-exchanger systems. The analytical models are generally based on solving the differential equations for heat transfer and energy balance with some simplifying assumptions, while the numerical solutions use the discretization of the heat transfer elements for one, two or three dimensional analysis. Neural network and genetic algorithm techniques have also been

used for predicting the outlet air temperature by extensive training of the model using the experimentally obtained data [119, 128, 129]. The relevant features and involved equations (for analytical models) of these models are summarized in Table 1, along with the location of experimental study.

Table 1. Models used for EAHE analysis.

| Reference | Model details | Location |
|---|---|---|
| Cucumo [130] | 1-D heat transfer in soil when air temperature is sinusoidal in time.<br><br>$$T_{air}(t) = T_{air,av} + \Delta T_a \cos\left(2\pi\left(\frac{t - t_a^*}{t_0}\right)\right)$$<br><br>$$T(x,t) = T_{air,av} + \frac{\Delta T_a e^{-x\sqrt{\pi/t_0\alpha}}}{\sqrt{1+2\beta+2\beta^2}} \cos\left(2\pi\left(\frac{t-t_a^*}{t_0}\right) - x\pi t0\alpha\right)$$<br><br>$$\beta = \frac{k}{h}\left(\frac{\pi}{\alpha t_0}\right)^{\frac{1}{2}}$$ | Ahmedabad, India [131], Greensboro, NC [99], Athens, Greece [132] |
| Goswami et al. [98-101] | 2-D Pseudo-analytical iterative solution. Pipe was divided into several elements and output from first was considered as input to second and so on.<br><br>$$T_n = \begin{cases} \frac{[(1-U/2)T_{n-1}+UT_s]}{1+U/2} & \text{unsaturated} \\ \frac{\left[(1-U/2)T_{n-1}+\frac{(W_{n-1}-W_n)}{C_p}H_{fg}+UT_s\right]}{1+U/2} & \text{saturated} \end{cases}$$ | Greensboro, NC, Gainesville, FL |
| Mihalakakou [105] | Parametric model to determine overall heat transfer coefficient, U using on pipe length, radius, velocity and depth.<br><br>$$U = a_0 + a_1(L) + a_2(L)^2 + a_3(L)^3$$<br><br>The coefficients of this polynomial were determined using empirical relations. | Athens, Greece |

Table 1. (continued)

| | | |
|---|---|---|
| Trombe [25] | 1-D heat transfer analysis on several pipe elements.<br><br>$$T(x) = T_{soil} + (T_0 - T_{soil}) \exp\left(-\frac{x}{mC_p R_{th}}\right)$$<br><br>$$R_{th} = \frac{1}{hA} + \frac{\Delta x}{kA}$$ | Toulouse, France |
| Gauthier [133] | 3-D numerical model. The region was divided into small control volumes and finite difference scheme was used to solve heat transfer equation over each. | Quebec, Canada |
| Kumar [119] | 2-D model using Neural Networks. | Mathura, India |
| Kumar [129] | 2-D model using Genetic Algorithms. | Mathura, India |
| Vaz [95, 96] | Numerical solution based on finite volume method using ANSYS FLUENT. | Viamao-RS, Brazil |
| Liu [134] | 3-D numerical model in cylindrical coordinates. Pipe was divided into elemental discs (Figure 8).<br><br>$$T_{air,j+1}^t = T_{air,j}^t - \frac{\Delta z\, hA}{\dot{m}C_{p,air}}\left(T_{air,j}^t - T_n^t\right)$$ | Chongqing, China |
| Hollmuller [135, 136] | 2-D numerical model. Pipe was divided into several elements and energy balance was performed on each element iteratively.<br><br>$$T_i = T_{i-1} + \frac{Q_{friction} - Ah(T_{i-1} - T_{tube})}{(C_{p,air} + C_{p,vap}W_{air})\rho_{air}\dot{V}_{air}}$$<br><br>$$W_i = W_{i-1} - \frac{Ah(W_{i-1} - W_{tube})}{C_{p,air}\rho_{air}\dot{V}_{air}\Delta t}$$ | Switzerland |
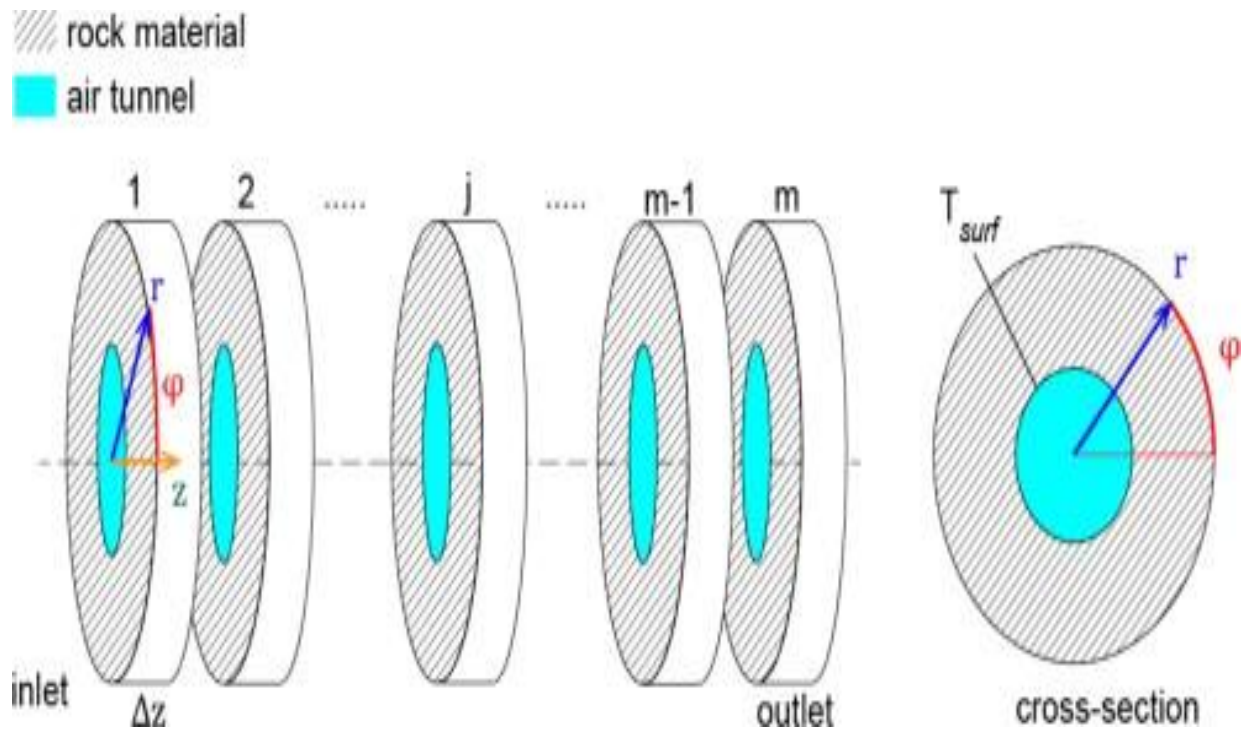
Figure 8. Radial cross-sections of pipe and surrounding soil. [134] (Copyright permission in Appendix B).

## 2.2.2 Ground Coupled Water Cooling

Another mode of utilizing earth as a heat sink is to pass water through underground pipes which rejects heat to the surrounding soil and colder water is obtained at the outlet. The ground coupled water cooling system works on the same principle as an EAHE; and uses the difference in temperature of the underground soil and warmer water coming out of an air-conditioning system [82, 88, 137-149]. Figure 9 shows the schematic of a ground coupled heat exchanger where water enters from one end of a U-tube and comes out of the other after exchanging heat with the soil. This system has generally been used for air-conditioning applications and pre-heating of domestic hot water. These systems have been proven to save annual energy and operating cost of air-conditioning, but are still not very widely used due to high initial investment [81, 82, 141, 142].

20
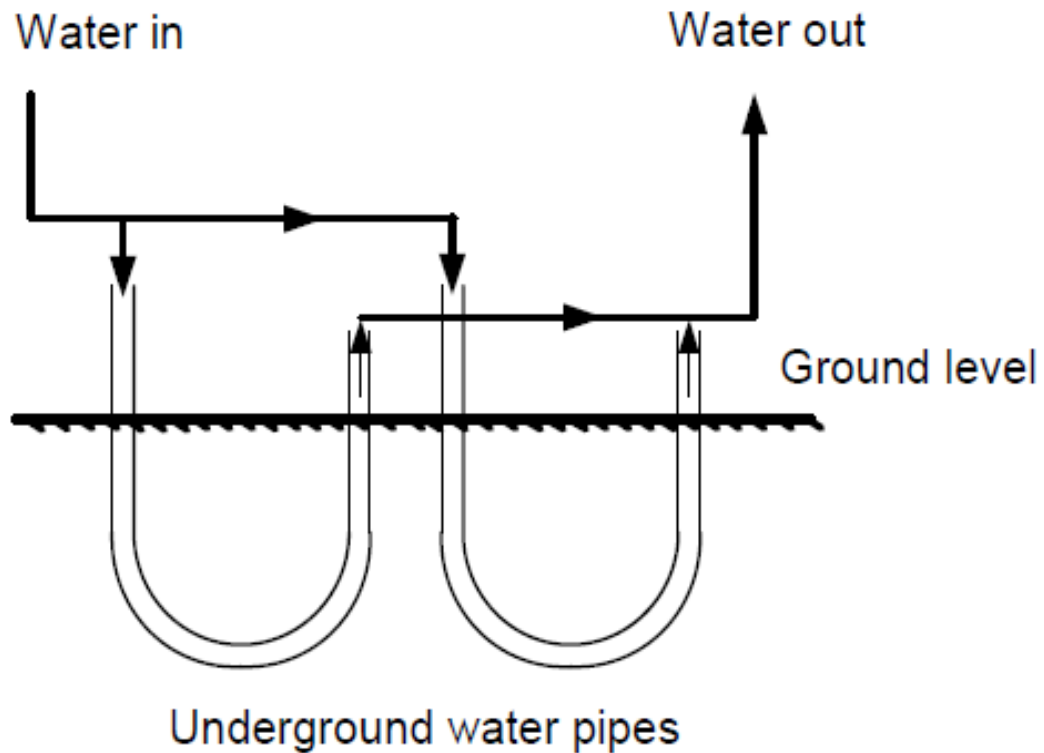
Figure 9. Schematic of a ground coupled water cooling system.

### 2.2.2.1 Configurations

Different configurations have been proposed for the GCHPs. The underground pipes can be placed in horizontal trenches or vertical boreholes [81, 82, 86, 141]. Figure 9 shows the vertical boreholes while Figure 10 shows examples of horizontal configurations that have been studied in the recent years. The horizontal trenches are installed generally when sufficient land area is available for digging [82, 85, 88]. If the area is limited or landscape disruption needs to be avoided, vertical boreholes are preferred. In the recent years, "slinky" shapes ground heat exchangers have also been studied (Figure 11) that allow more pipes in a smaller area, but prevent the natural recharge of the soil temperature to the accumulation of larger quantity of heat in a smaller area [88, 150-152].
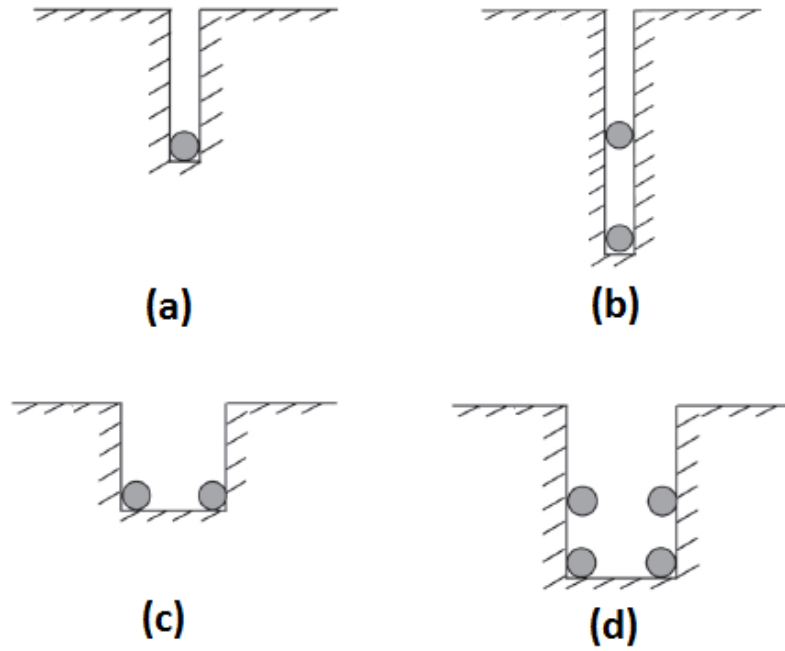
Figure 10. Horizontal ground heat exchanger. (a) Single pipe per trench (b) Two pipes (over/under) (c) Two pipes (side by side) (d) Four pipes per trench. [82] (Copyright information in Appendix B).
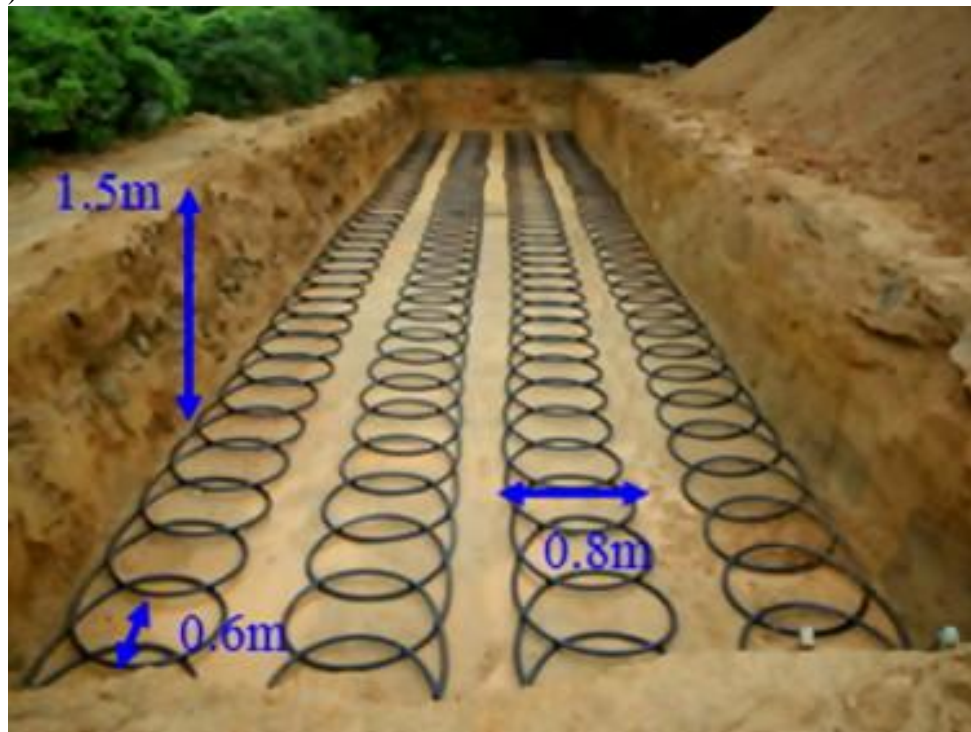


Figure 11. Slinky coil ground heat exchanger. [150] (Copyright information in Appendix B).

*2.2.2.2 Models*

The models proposed for analyzing the ground source heat exchangers generally require the calculation of overall heat transfer coefficient and thermal resistance [143, 153-156]. Since the depths of the boreholes are very large, the soil temperature is assumed constant at the average annual temperature [81, 141, 143, 153, 154, 157, 158]. Table 2 shows the details of the different models that have been used and verified for the study of GCHP.

Table 2. Ground source water cooling models.

| Reference | Model description | Location |
|---|---|---|
| Zeng [157] | Thermal resistances between fluid and soil ($R_{11}$), and that between two pipes ($R_{12}$ and $R_{13}$) were calculated separately (Figure 12). $$R_{11} = \frac{1}{2\pi k_b}\left[\ln\left(\frac{r_b}{r_p}\right) - \frac{k_b - k}{k_b + k}\ln\left(\frac{r_b^2 - D^2}{r_b^2}\right)\right] + R_p$$ $$R_{12} = \frac{1}{2\pi k_b}\left[\ln\left(\frac{r_b}{\sqrt{2}D}\right) - \frac{k_b - k}{2(k_b + k)}\ln\left(\frac{r_b^4 + D^4}{r_b^4}\right)\right]$$ $$R_{13} = \frac{1}{2\pi k_b}\left[\ln\left(\frac{r_b}{2D}\right) - \frac{k_b - k}{k_b + k}\ln\left(\frac{r_b^2 + D^2}{r_b^2}\right)\right]$$ | N/A |
| Bose [159] | 1-D model for thermal resistance. $$R_b = \frac{1}{2\pi k_b}\ln\left(\frac{r_b}{\sqrt{N}r_p}\right) + R_p$$ | N/A |
| Hart [160] | Ground is treated as an infinite medium and borehole as an infinite line source with $q_1$ heating rate per unit length. $$T_g(r,t) = T_0 + \frac{q_1}{4\pi k}\int_{\frac{r^2}{4\alpha t}}^{\infty}\frac{e^{-u}}{u}du$$ | N/A |
| Sanaye [81, 141] | Total thermal resistance between the pipe and the soil is calculated. $$R_{total} = \frac{1}{h_w\pi D_i 2L} + \frac{\ln\left(\frac{D_o}{D_i}\right)}{2\pi k_p 2L} + \frac{F}{U_s\pi D_o 2L}$$ | Tuscaloosa, Alabama |
| Lee [161] | 3-D solution using finite difference method in rectangular coordinates. | N/A |

Table 2. (continued)

| Muraya [162] | Heat transfer analysis was performed using transient finite-element method. | N/A |
|---|---|---|
| Li [163] | 3-D finite volume model was developed using triangular mesh. | Harbin, China [164] |
| Bernier [156] | Mean fluid temperature was calculated using thermal resistances and g-function [165]. $$T_f(t) = T_g + qR_b + \frac{q}{2\pi k} g\left(\frac{t}{t_s}, \frac{r_b}{H}\right)$$ | Le Bourget-du-Lac, France [166] |
| Cui [167] | Numerical solutions using finite element method. | Hong Kong |
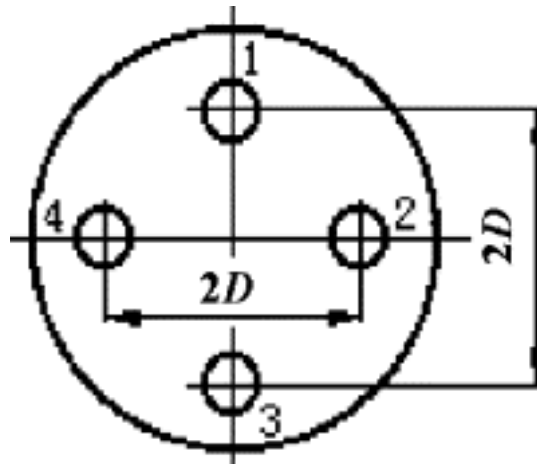


Figure 12. Cross-sectional view of 2 U-tube boreholes. (Copyright permission in Appendix B).

### 2.2.3 Night Sky Radiative Cooling

The temperature of the outer space is about 4 K [168], which is the coldest available heat sink for passive cooling. A sky-facing surface can be cooled during the night by exchanging infrared radiation with the space. According to Parker [169], a sky-facing surface at 27°C on a clear desert night can lose heat at a rate of 75 W/m². However, the rate of cooling is strongly dependent on the ambient humidity and cloudiness, and goes down to 60 W/m² for a humid

climate, 40 W/m$^2$ with 50% cloud cover, and 7 W/m$^2$ under completely overcast sky [169]. The temperature of water can be lowered as much as 8℃ below the ambient temperature on a clear night in a desert using this method. The use of spectrally selective surfaces can increase the temperature drop to as much as 20°C below the ambient [170]. Such surfaces have high emittance between wavelengths 8 to 13 μm and low absorption outside this region. Al-Nimr et al. [171] observed that using night sky radiative cooling, the mean temperature of a 120 $l$ water storage tank with a 0.6 m$^2$ radiative cooling panel and 0.2 m depth could be reduced by 15°C in one night implying a heat rejection of 13 MJ/m$^2$ to the sky. In another study by Ali [38], the water temperature of a 0.5 m deep tank with 1 m$^2$ surface area was lowered from an initial value of 23.8-27.1°C to a final value of 17.2-18.9°C.

Nocturnal cooling was traditionally used in ancient civilizations for space cooling and ice production [172]. More recently it has also been considered for cooling of buildings [173, 174]. Yellott and Hay used a roof pond with a movable cover where the water stored in a shallow reservoir at was cooled at night and covered during the day to prevent it from heating [46, 47, 175]. Radiative cooling has also been considered for lowering the temperature of cooling water in the condenser of thermal power plants. For a CSP plant operating at a high temperature of 80-100°C, the efficiency can be improved by 50-100% by using night sky cooling in the condenser [176]. Olwi et al. [177] proposed the idea of using a pond covered by a radiator plate to cool the hot water coming from the condenser of a power plant. Figure 13 depicts a schematic of the system [177]. The hot water from the power plant enters close to the surface of the pond. It is cooled inside the pond and the cold water is withdrawn from the bottom. A separating screen is used to prevent mixing of the top hot water layer with the bottom storage layer. A prototype experimental pond was also studied at a University Farm in Hada Al-Sham, Saudi Arabia [170].

The pond was covered with a white painted aluminum sheet. They observed a heat rejection rate of 50 W/m$^2$ from the pond at night time.
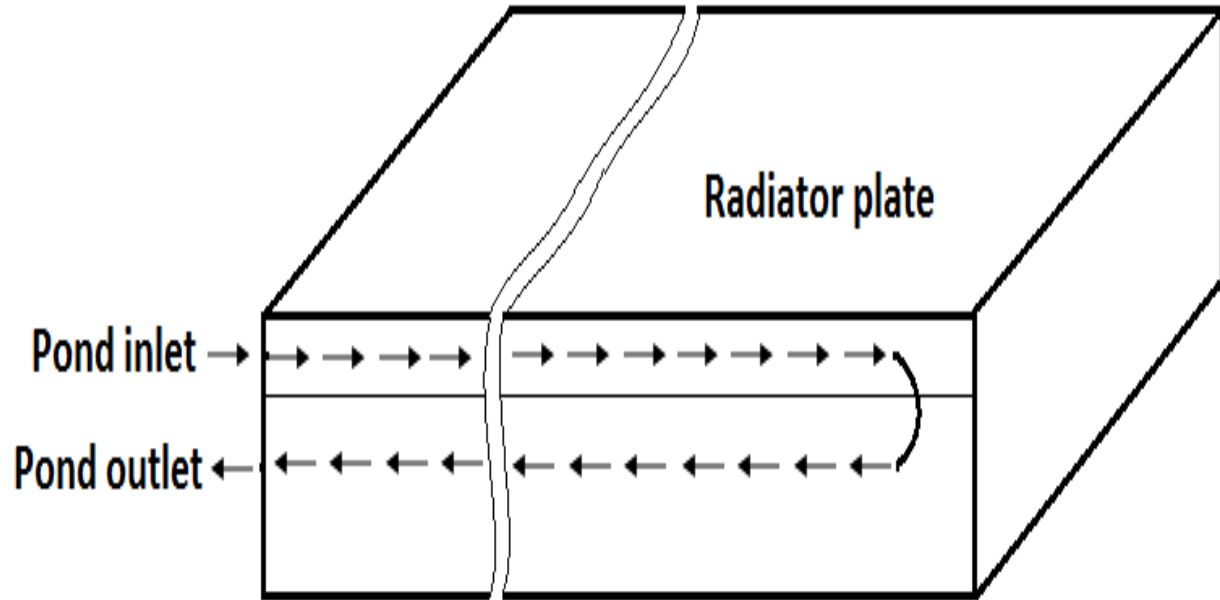


Figure 13. Night sky radiative cooling system used to cool the hot water from the power plant (redrawn from [17]).

Although the night sky cooling has been shown to be an effective cooling technique especially in arid areas, an important limitation is its inability to cool during daytime and limited effectiveness at locations with high humidity. Because of the night time limitation, the net cooling period using night sky cooling is less than 11 h/day [178]. Therefore, additional alternative methods, such as ground coupling, are needed for cooling during the day.

*2.2.3.1 Models*

Several different models have been proposed to calculate the radiative heat loss from a water reservoir. Table 3 lists different models that have been proposed in the last few decades and experimentally verified.

Table 3. Different models that have been proposed for nocturnal cooling.

| Ref. | System description | Model details/ underlying assumptions | Experiment location |
|---|---|---|---|
| Meir [179] | Inclined radiator panel connected with a water reservoir. | Lumped model using [180] and [181] $$\frac{q}{A} = \varepsilon_w \sigma \left( T_w^4 - T_{sky}^4 \right) + h_c (T_w - T_a)$$ $$h_c = 3.1 + 4.1v$$ $$T_{sky} = T_a \left( 0.711 + 0.0056 T_{dp} + 0.000073 T_{dp}^2 \right)^{0.25}$$ | Oslo, Norway |
| Erell & Etzion [173, 182, 183] | Flat place radiator to cool a building. | Lumped model using a linearized form of Stefan-Boltzmann law given by [184] $$R_{net} = 4 \varepsilon_w \sigma T_{air}^2 \left( T_w - T_{sky} \right)$$ $$h_c = 1.8 + 3.8v \ (W/m^{2 \circ}C)$$ | Sede-Boqer, Israel |
| Ali [168] | Open loop system with a warm water tank feeding to two parallel plate radiators. | Lumped model applied on number of elements along the radiator. Sky radiation calculations were based on [185] | Assiut, Egypt |
| Tang & Etzion [45, 186] | Roof pond with gunny bags floating on water surface. | Roof pond is thermally stratified along the depth. Sky radiations were calculated using [187] $$h_c (T_a - T_g) - (0.7581 + 0.4257v)(P_w - \emptyset P_a)^{0.7} - \varepsilon_w \sigma \left[ T_g^4 - T_{sky}^4 \right] - U_{gw} (T_{w1} - T_g)$$ $$= H_1 \rho_w C_{pw} \frac{dT_g}{dt}$$ Stratification: $$\frac{k_w}{h_1} \left( T_{w,i-1} + T_{w,i+1} - 2T_{w,i} \right) = h_1 \rho_w C_p \frac{dT_{w,i}}{dt}$$ | Seder Boker, Israel (Results are shown in [43]) |

Table 3. (continued)

| | | | |
|---|---|---|---|
| Tang & Etzion [186] | Roof pond with movable insulation. | Roof pond is assumed to have perfect thermal stratification during the day and full mixing at night.<br><br>$$h_c(T_a - T_w) -$$ $$(0.2253 + 0.2464v)(P_w - \emptyset P_a)^{0.82} -$$ $$\varepsilon_w \sigma[(T_w + 273)^4 - T_{sky}^4] = H_1 \rho_w C p_w \frac{dT_w}{dt}$$<br>$$T_{sky} = \varepsilon_{sky}^{0.25} T_a$$<br>$$\varepsilon_{sky} = 0.754 + 0.0044 T_{dp}$$ | Seder Boker, Israel (Results are shown in [43]) |
| Sodha et al. [44, 188] | Open roof pond. | Lumped model with constant convective and radiative heat transfer coefficients.<br><br>$$m_w \frac{dT_w}{dt} = \frac{\varepsilon_w \sigma(\bar{T}_w^4 - (\bar{T}_a - 12)^4)(T_a - T_w)}{\bar{T}_w - \bar{T}_a}$$<br>$$+0.884 \left[(\bar{T}_w - \bar{T}_a) + \frac{p_w - \varphi p_a}{268.9 \times 10^3 p_w} T_w\right]^{\frac{1}{3}} (T_a - T_w)$$<br>$$+14.385 \times 10^{-3} \left[(\bar{T}_w - \bar{T}_a) + \frac{p_w - \varphi p_a}{268.9 \times 10^3 p_w} T_w\right]^{\frac{1}{3}}$$<br>$$(R_1(T_w - \varphi T_a) + R_2(1 - \varphi))$$ | New Delhi, India |
| Clus et al. [189] | Funnel shaped radiative due condenser. | CFD analysis. | Corsica Island, France |
| Jain [190] | Roof pond with movable insulation. | Lumped model with Fourier expansion of energy balance equation. Heat transfer coefficients were determined using [191-193].<br><br>$$m_w C_p \frac{dT_w}{dt} = (2.8 + 3.0v)(T_a - T_w)$$ $$+ \varepsilon_w \sigma(T_a^4 - T_{sky}^4)$$<br>$$T_{sky} = T_a - 6$$ | Rajasthan, India |

Table 3. (continued)

| Rincon et al. [194] | Roof pond with movable insulation. | Numerical solution using finite volume approach. Measured hourly data for outdoor temperature and solar irradiance is used. | Maracaibo, Venezuela |
|---|---|---|---|
| Ali [38] | Thermally uninsulated open tank. | Heat transfer analysis on each wall of the tank was performed using lumped model. Sky radiation was calculated using [193]. $$m_w C_p \frac{dT_w}{dt} = Q_{conv,a-w} + Q_{conv,tkw-w}$$ $$+ Q_{conv,tkb-w} - Q_{evap,w-a}$$ $$- Q_{rad,w-sky}$$ $$Q_{rad,w-sky} = A\varepsilon_w\sigma\left[(T_w + 273)^4 - T_{sky}^4\right]$$ $$Q_{evap,a-w} = A(0.2253$$ $$+ 0.2464v)(P_w - \emptyset P_a)^{0.82}$$ $$Q_{conv,a-w} = Ah_c(T_a - T_w)$$ | Assiut, Egypt |
| Ito & Miura [195, 196] | Radiator panels connected with a storage tank. | Lumped model using radiative heat transfer calculation based on [193]. $$q = 4\varepsilon_w\sigma T_a^2(T_w - T_{sky}) + h_c(T_w - T_a)$$ | Atsugi, Japan |
| Spanaki et al. [197] | Roof pond covered with a floating cloth. | Analysis of the thermally stratified tank is done using the model given by Tang et al. [45, 186]. $$h_c(T_a - T_g) -$$ $$(0.7581 + 0.4257v)(P_w - \emptyset P_a)^{0.7} -$$ $$\varepsilon_w\sigma\left[T_g^4 - T_{sky}^4\right] - U_{gw}(T_{w1} - T_g)$$ $$= H_1\rho_w C_{pw}\frac{dT_g}{dt}$$ | Heraklion city, Greece |

Table 3. (continued)

| Dobson [198] | Radiator panel connected to a water storage tank. | Steady state lumped model for both radiator and storage tank. Sky emissivity is calculated using [199].<br><br>$$\dot{m}C_p(T_2 - T_1) = \varepsilon_w A\sigma[T_w^4 - T_{sky}^4]$$<br>$$+ (a + bv)A(T_w - T_a)$$<br>$$a = 0.8, b = 0 \; if \; v < 0.076 m/s$$<br>$$a = 3.5, b = 0 \; if \; v < 0.45 m/s$$<br>$$a = 1.8, b = 3.8 \; if \; 1.35 < v < 4.5 m/s$$ | Seder Boker, Israel [200] |
|---|---|---|---|

The following generic model can be concluded after the review of these models:

$$m_w C_p \frac{dT_w}{dt} = Q_c + Q_e + Q_r$$

where $Q_c$, $Q_e$ and $Q_r$ are the convective, evaporative and radiative heat transfer terms and can be given by the following generic equations 1-6.

$$Q_c = h_c A(T_w - T_a) \tag{1}$$

$$h_c = a_1 + b_1 v \; \left(\frac{W}{m^{2\circ}C}\right) \tag{2}$$

Here, v is the wind velocity in m/s and $a_1$ and $b_1$ are empirical constants.

$$Q_e = (a_3 + b_3 v)(P_w - \emptyset P_a)^{c_4} \tag{3}$$

$$P_a = a_4 \exp(b_4 + c_4(T)^{d_4}) \tag{4}$$

$$Q_r = A\varepsilon_w \sigma(T_w^4 - T_{sky}^4) \tag{5}$$

Here, $a_3$, $b_3$, $c_3$, $a_4$, $b_4$, $c_4$ and $d_4$ are empirical constants and $T_{sky}$ is the effective sky temperature given by:

$$T_{sky} = \varepsilon_{sky}^{0.25} T_a \; (K) \tag{6}$$

where $\varepsilon_{sky}$ is a function of the dew point temperature and is obtained experimentally for different locations.

Several models have been proposed to calculate the effective sky temperature that in turn depends on the sky emissivity. The following section gives the details of different equations.

### 2.2.3.2 Effective Sky Temperature

Even though the temperature of outer space is much lower, the effective temperature for radiative heat transfer is influenced by the earth's atmosphere, cloud cover, humidity and wind velocity. Different empirical correlations have been proposed to predict the effective sky temperature and have been compared with the experimental data. These are described in Table 4.

Table 4. Different expressions for sky emissivities.

| Ref. | Model | Location |
|---|---|---|
| Tang [187] | $\varepsilon_{sky} = 0.754 + 0.0044 T_{dp}$ | Negev Highlands, Israel |
| Berdahl and Fromberg [201] | $\varepsilon_{sky} = 0.741 + 0.0062 T_{dp}$ during night<br><br>$\varepsilon_{sky} = 0.727 + 0.0061 T_{dp}$ during day | Arizona, Maryland,<br><br>Missouri |
| Berdahl and Martin [202, 203] | $\varepsilon_{sky} = 0.711 + 0.56 \left( \dfrac{T_{dp}}{100} \right) + 0.73 \left( \dfrac{T_{dp}}{100} \right)^2$ | Arizona, Texas, Maryland,<br><br>Missouri, Florida, Nevada |
| Centeno [204] | $\varepsilon_{sky} = 0.56 + 0.08 P_v^{0.5}$ | Venezuela |
| Berger [205] | $\varepsilon_{sky} = 0.77 + 0.0038 T_{dp}$ | Carpentras, France |
| Chen [206, 207] | $\varepsilon_{sky} = 0.736 + 0.00577 T_{dp}$ during night<br><br>$\varepsilon_{sky} = 0.732 + 0.00635 T_{dp}$ during day | Nebraska and Texas |

All of these models were obtained by empirical correlations and are applicable for their respective locations and the environmental conditions they have been tested for. They can be compared with the experimentally obtained values of sky emissivity. The sky emissivity value is experimentally calculated by measuring the incoming long wave radiations, IR and ambient temperature as shown in equation 7.

$$IR = \sigma \varepsilon_{sky} T_a^4 \tag{7}$$

where σ is the Stefan Boltzmann constant equal to 5.67 x $10^{-8}$ W/m$^2$/K$^4$. So, if the measured values for incoming radiation and ambient temperature are available, emissivity can be calculated. The error in calculation due to the measurement error in the radiation and temperature can be obtained by the error analysis of the above equation.

$$\varepsilon = \frac{IR}{\sigma T_a^4}$$

$$d\varepsilon = \frac{d(IR)}{\sigma T_a^4} - IR \frac{d(T_a)}{\sigma T_a^5}$$

$$So, \Delta\varepsilon_{max} = \frac{\Delta(IR)_{max}}{\sigma T_a^4} + IR \frac{\Delta(T_a)_{max}}{\sigma T_a^5} \tag{8}$$

The experimental values for incoming long wave radiation and ambient temperature are available for the NREL Solar Radiation Research Laboratory in Boulder, Colorado. Figure 14 shows the comparison of the sky emissivity models with the experimental data obtained from the values obtained from the NREL website for June 1$^{st}$, 2012 [208]. Most of these models show similar behavior, except for the Centeno model [204]. Table 5 shows the root mean square errors (RMSE) for all these models. It can be observed that the RMSE is smallest for the model proposed by Berdahl & Martin [202]. This is also the most widely used model and has been verified for different locations in the United States.
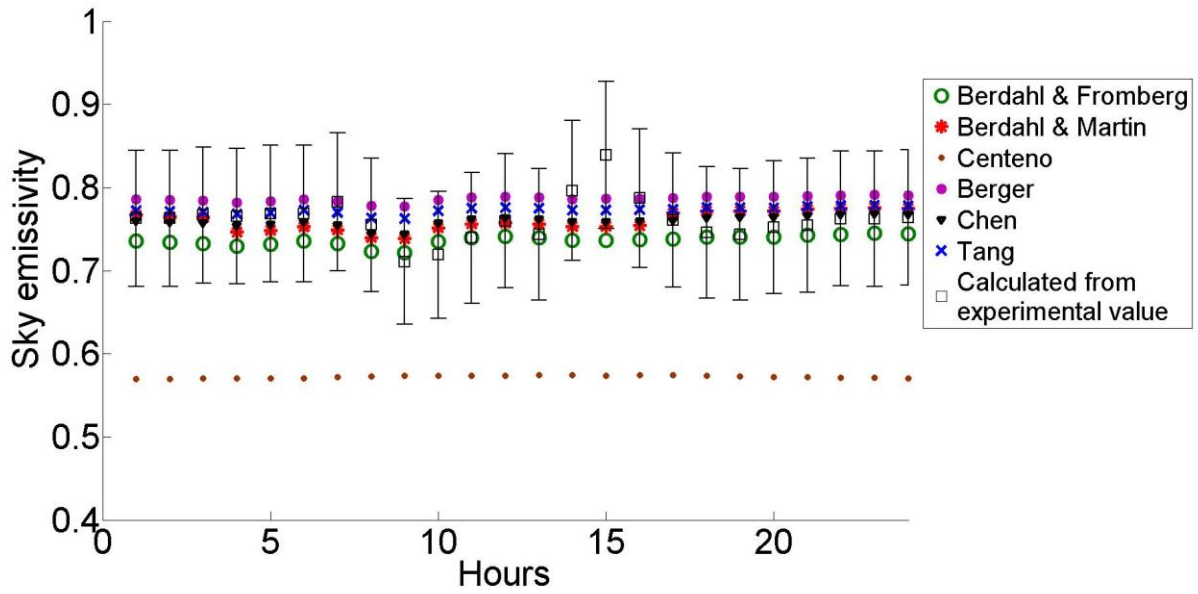
Figure 14. Comparison of different sky emissivity models with the experimental data.

Table 5. Mean error for different sky emissivity models.

| S. No. | Model | Root mean square error in emissivity value |
|--------|-------|--------------------------------------------|
| 1. | Berdahl & Fromberg | 0.0350 |
| 2. | Berdahl & Martin | 0.0272 |
| 3. | Centeno | 0.1907 |
| 4. | Berger | 0.0348 |
| 5. | Chen | 0.0246 |
| 6. | Tang | 0.0270 |

# CHAPTER 3: OPTIMIZATION OF SUPERCRITICAL RANKINE CYCLE

## 3.1 Thermodynamic Model

Figure 15 shows a schematic of the thermodynamic cycle that was simulated using CHEMCAD and MATLAB. The pump (unit 1) pressurizes the working fluid to its high pressure (stage 2), and then the pressurized fluid passes through the pre-heater (recuperator) before entering the vapor generator (stage 3). In the boiler heat exchanger, the working fluid is heated to its superheated vapor phase by the hot brine from a geothermal, solar thermal or waste heat source. The vaporized fluid in the supercritical state (stage 4) then enters the turbine and undergoes adiabatic expansion, generating power. The fluid from the turbine exit passes through the recuperator and cools down before entering the condenser at stage 6. When the turbine exit temperature is not higher than the pump outlet temperature, the recuperator (unit 2) is bypassed. A water cooled condenser (unit 5) is used for condensing the working fluid, which then enters the pump and the power cycle is completed.

The hot water used in the boiler heat exchanger is a sensible heat source which rejects the heat to the working fluid and leaves the heat exchanger at a lower temperature (stage 8). The water used in the condenser heat exchanger runs in an open loop and the warmer water leaves the heat exchanger (stage 10). The pinch temperatures in both the boiler and condenser are assumed to be 5°C.[1]

---

[1] This chapter was published in the ASME Journal of Energy Resources Technology. Copyright permission is included in Appendix B.
Rachana Vidhi, Sarada Kuravi, D. Yogi Goswami, E. K. Stefanakos, Adrian Sabau, "Organic fluids in a supercritical Rankine cycle for low temperature power generation". Journal of Energy Resources Technology, 135, 042002, 2013.
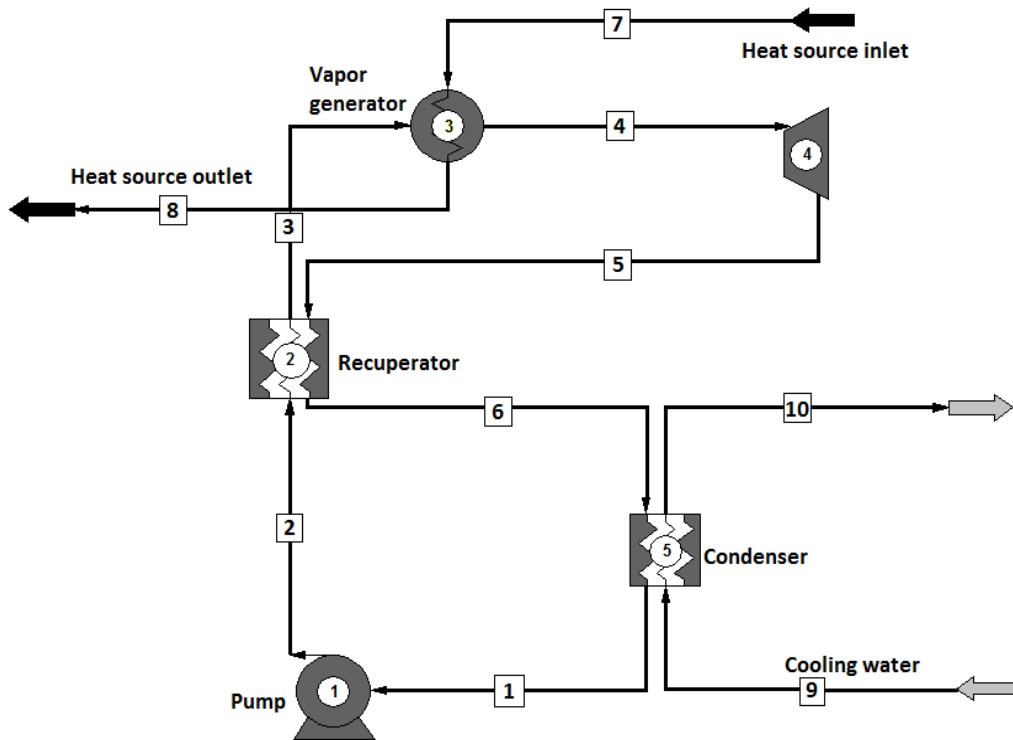
Figure 15. Layout of the cycle simulated in CHEMCAD. The numbers in the square blocks indicate the fluid condition; the numbers in the circles refer to equipment unit.

## 3.2 Operating Conditions

The thermodynamic cycle operates in the supercritical region for all the fluids considered. In this study, the pump and turbine were both assumed to work at 85% efficiency. The coolant temperature in the wet cooled condenser was varied from 10 to 25 °C. The lower value of the coolant temperature allows the working fluid to come out of the turbine at a lower pressure, leading to higher cycle efficiency. Simulations were performed for the heat source temperatures varying from 100 to 200 °C in steps of 5°C and coming down to 80 °C after passing through the boiler. In each simulation, the vapor quality at the turbine exit was kept higher than 95% in order to ensure proper performance of the turbine. If the amount of liquid increases in the turbine, droplets of liquid start forming that could damage the turbine blades[3, 209]. In addition, the pinch point in the recuperator was kept between 7 °C to 9 °C.

35

### 3.3 Comparison of Thermal Efficiency for $CO_2$ and R32 Based Cycle

According to the first law of thermodynamics, thermal efficiency of a power cycle is given as:

$$\eta_{th} = \frac{W_{out}}{Q_{in}} = \frac{W_{out,turbine} - W_{in,pump}}{Q_{in}} \tag{9}$$

The cycle efficiencies, without considering the efficiencies of the heat exchangers, are shown in Figure 16 (a) and (b). It is clear that the R32 based cycle gives better efficiencies than the $CO_2$ based cycle at a fixed heat source temperature while operating at a much lower pressure. For example, at 200 °C, an efficiency of 18.3% is obtained for R32 based cycle whereas the $CO_2$ based cycle obtains 16.5% efficiency. Also, as the source temperature is reduced, the efficiency of the $CO_2$ based cycle reduces at a faster rate. The difference in efficiencies for R32 and $CO_2$ based cycles was larger when the turbine efficiency was lower (see Figure 16 (b)).
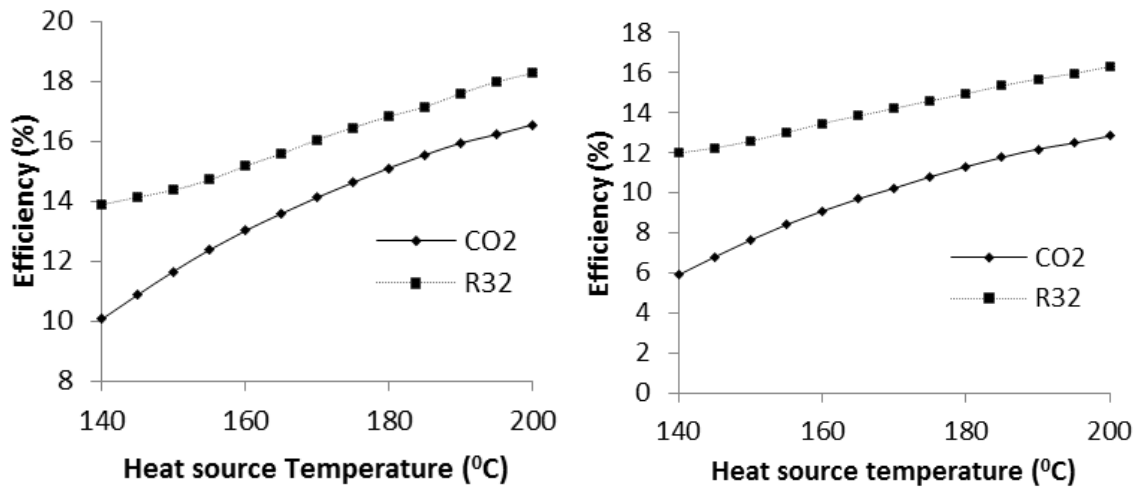


(a) Turbine efficiency 85%   (b) Turbine efficiency 75%

Figure 16. Thermal efficiencies of CO2- and R32-based supercritical Rankine cycles at 85% and 75% turbine efficiencies.

**3.4 Fluid Selection Criteria**

Performance of an organic working fluid in a supercritical cycle depends largely on its critical properties. Chen et al. [8] classified a number of fluids on the basis of their thermo-physical properties and environmental impacts. Different fluids were sorted for their potential as working fluids. The following parameters were found to be important in the selection:

- Critical temperature: Critical temperature is a key parameter in the selection of working fluids. If the critical temperature is too high, the cycle will work in or close to the sub-critical region and the efficiency will be low. If the critical temperature is too low, condensation at the given cooling condition will not be possible.

- Critical pressure: Both the energy and exergy efficiencies depend on the thermal match between the heat source and the working fluid. If the fluid is pressurized far above its critical point in the supercritical region, the fluid temperature profile during heating will be straighter and will match better with that of the heat source. So, if the critical pressure of the fluid is lower, pressurizing it to a higher pressure to increase its performance will be easier.

- Environmental Concerns: Refrigerants that are derived from Chlorofluoro carbons (CFC) and hydrochlorofluoro carbons (HCFC) are known to be the ozone depleting substances[13]. We considered fluids with zero ozone depletion potential and are non-flammable, non-toxic and stable in the temperature and pressure range selected for this study [13, 14, 49-52].

Table 6 shows the different fluids considered for this study, their chemical names and their critical properties.

Table 6. List of fluids studied and their critical properties.

| Fluids | Chemical name | Critical temperature (°C) | Critical pressure (MPa) |
|---|---|---|---|
| R23 | Trifluoromethane | 16.14 | 4.83 |
| R32 | Difluoromethane | 78.11 | 5.78 |
| R143a | 1,1,1-Trifluoroethane | 72.71 | 3.76 |
| R134a | 1,1,1,2-Tetrafluoroethane | 101.05 | 4.06 |
| R170 | Ethane | 32.18 | 4.87 |
| R125 | Pentafluoroethane | 66.02 | 3.62 |
| R218 | Octafluoropropane | 71.87 | 2.64 |

The thermo-physical properties of the working fluids are predicted using the Peng – Robinson equation of state, given by the following equations:

$$P = \frac{RT}{V-b} - \frac{a(T)}{V(V+b) + b(V-b)} \tag{10}$$

where

$$a(T) = 0.45724 \frac{R^2 T_c^2}{P_c} m(T)$$

$$b = 0.07780 \frac{RT_c}{P_c}$$

$$m(T) = \left\{1 + k\left(1 - \sqrt{T/T_c}\right)\right\}^2$$

$$k = 0.37464 + 1.54226\omega - 0.26992\omega^2$$

Here, V is the molar volume, $T_c$ and $P_c$ are the critical temperature and pressure, respectively, $\omega$ is the acentric factor of the species, and R is the universal gas constant. Calculation of properties using the Peng – Robinson equation of state is simple and is valid for a large number of fluids in a much wider range of temperature and pressure. Although this

equation of state has certain limitations, the error in determining the properties is within acceptable limits [210].

In the analysis, two different cases were considered. In the first case, the pressure ratio in the cycle is fixed for all the fluids. In the second case, the minimum cycle pressure is kept constant at the lowest pressure at which that fluid can be condensed completely at the given sink temperature, while the maximum pressure is varied to obtain the optimum operating pressure. Table 7 shows the minimum pressure obtained for each fluid. The analysis for the second case would provide the best thermal efficiency that can be achieved for each fluid at every heat source temperature.

Table 7. Condensation pressures of the working fluids.

| Fluid | Condensation pressure (Bar) at 20 °C |
|:---:|:---:|
| R23 | 40 |
| R32 | 15 |
| R143a | 11 |
| R134a | 5.8 |
| R170 | 37 |
| R125 | 12 |
| R218 | 7.5 |

**3.5 Thermal Efficiency at Fixed Pressure Ratio**

In this section, the pressure ratio is fixed at 5 and the variation of thermal efficiency is found as a function of the heat source temperature for each fluid. Figure 17 shows the results obtained for each fluid. It can be observed from the figure that the efficiency of the cycle increases with increase in the heat source temperature. This is consistent with the fact that higher

operating temperatures lead to higher cycle efficiencies. The slope of the efficiency curve increases at the minimum temperature where the recuperator is used. As can be observed from the figure, not all the fluids can be used in the power cycle for the entire temperature range. For example, R32 could not be used for temperatures lower than 135 °C. This is because, at lower temperatures, the vapor quality in the turbine drops to less than 90%. It was observed that the R125 and R143a based cycles gave the highest efficiencies at high temperatures, while at low temperatures, the R218 based cycle was the most efficient. In addition, R218 could be used even at temperatures as low as 90°C unlike other fluids.
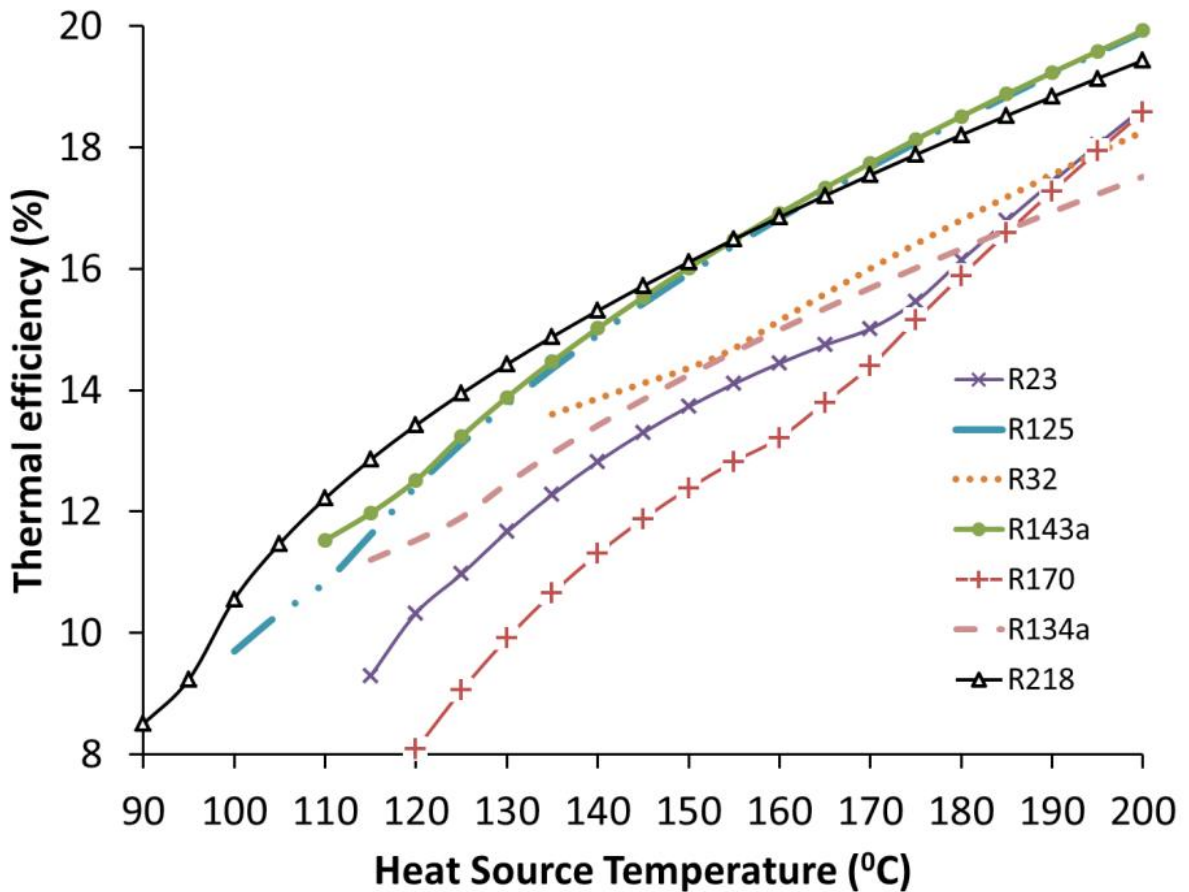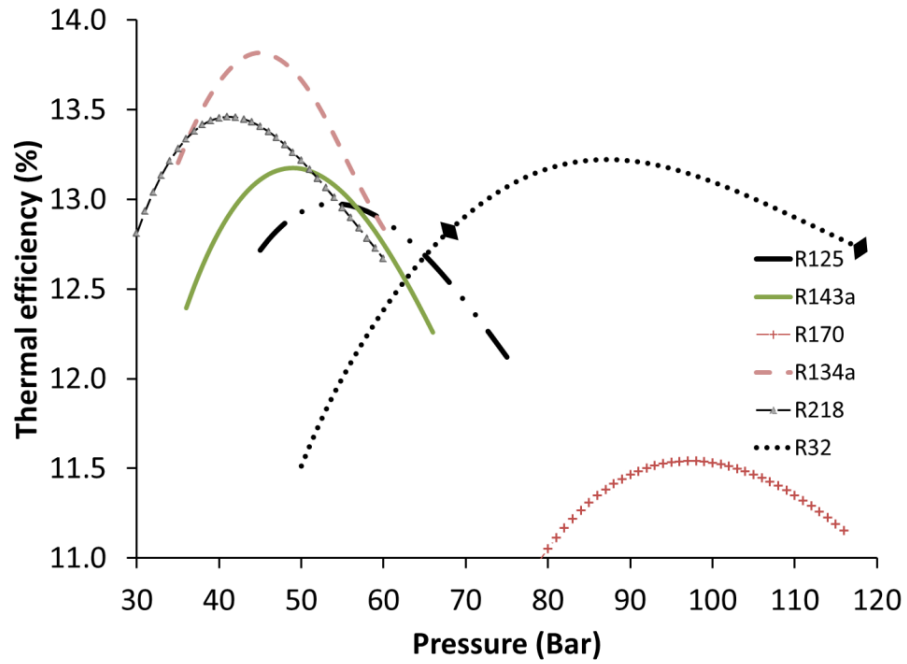


Figure 17. Thermal efficiency vs. heat source temperature at a constant pressure ratio of 5.

**3.6 Effect of Pressure on Thermal Efficiency**

For all the working fluids considered in this analysis, the pressure ratios were varied to study their effect on the thermal efficiency of the power cycle. For this analysis, the condensation pressure was kept the same for each fluid (as given in Table 7) to ensure complete condensation at the condenser outlet, and the turbine inlet pressure is varied in steps of 1 bar to obtain the optimum point. This process was repeated for different heat source temperatures. Figure 18 - Figure 21 show the variation of thermal efficiency as a function of operating pressure and pressure ratio for each fluid at different heat source temperatures. Since the cycle can be operated with all the working fluids at temperatures between 125 °C to 200 °C, the same heat source temperatures were used for each fluid for further analysis. It was observed that first the thermal efficiency increases with increasing pressure ratio and then decreases for each working fluid. For R32 however, the maximum efficiency was achieved at a pressure where the vapor fraction in the turbine becomes lower than 95%. As shown in the Figure 18 (a) and (b), the portion of graph bounded by the arrows signifies the range where the vapor quality in the turbine was poor and those pressures cannot be used. Similar behavior was obtained at every source temperature for R32 but we only considered the pressures where turbine vapor quality was more than 95%. It was also observed that the optimum pressure of R170 was the highest while the optimum pressure ratio was the lowest at all source temperatures. Since R170 has low critical temperature and hence high condensation pressure, even very high operating pressures give low optimum pressure ratios. Such low pressure ratios resulted in lower value of the turbine work output while the necessity to increase the pressure in the pump to a very high value increased the pump work input compared to other refrigerants and eventually lower thermal efficiency was

obtained. Furthermore, for R134a, that has high critical temperature and so low condensation pressure, a high value of pressure ratio could be obtained at lower operating pressures.



(a)
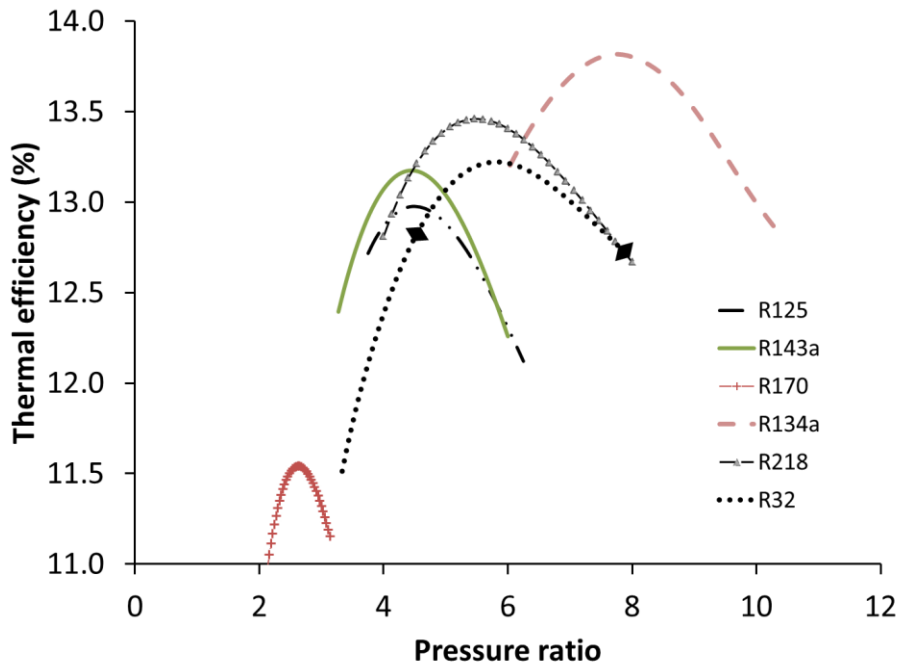


(b)

Figure 18. Thermal efficiency of the SRC at 125 °C heat source temperature and 10 °C sink temperature.

(a)



(b)

Figure 19. Thermal efficiency of SRC at 150 °C heat source temperature and 10 °C sink temperature.
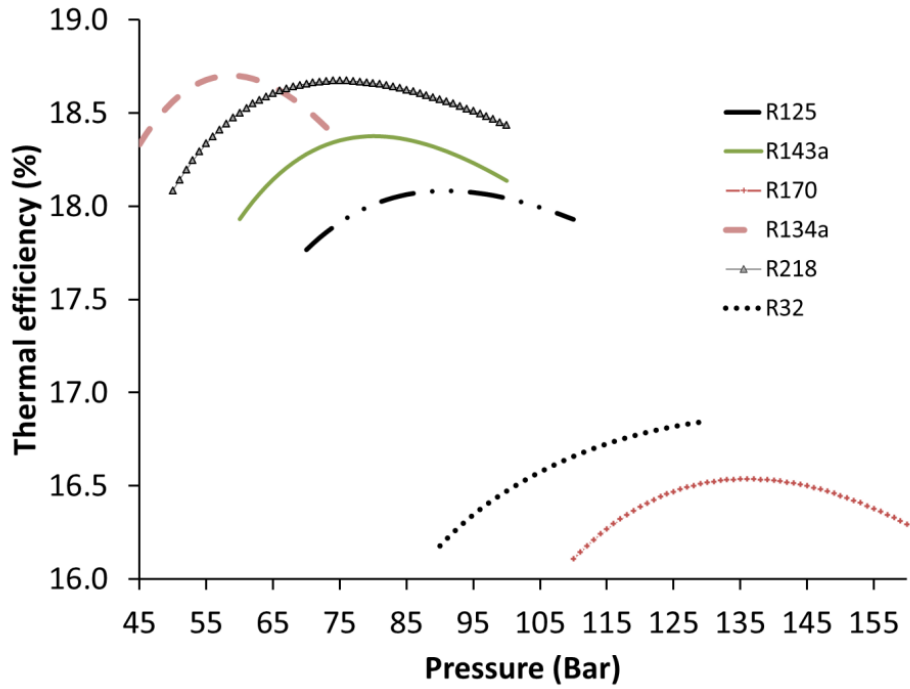
**(a)**
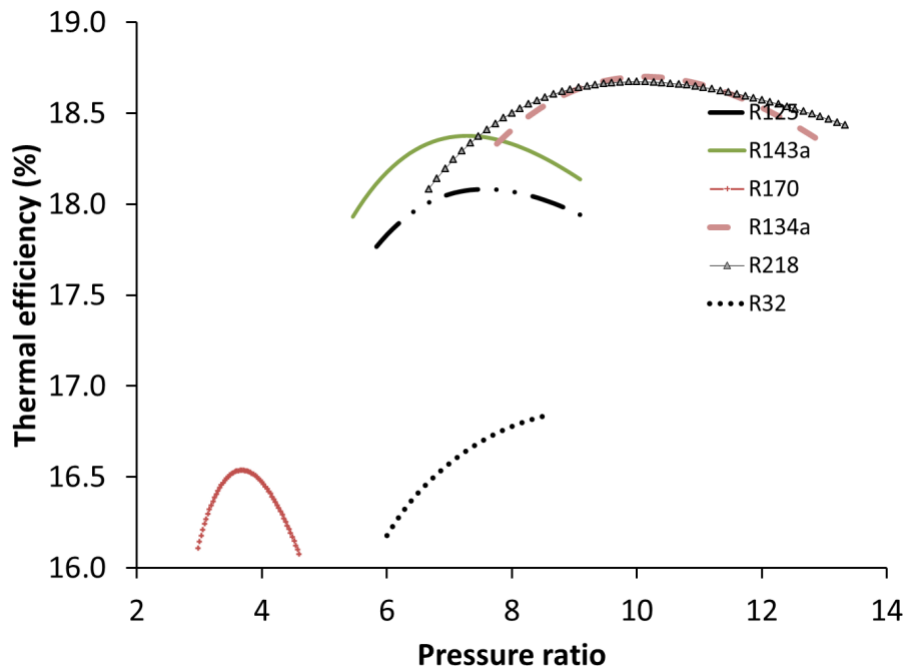


**(b)**

Figure 20. Thermal efficiency of SRC at 175 °C heat source temperature and 10 °C sink temperature.
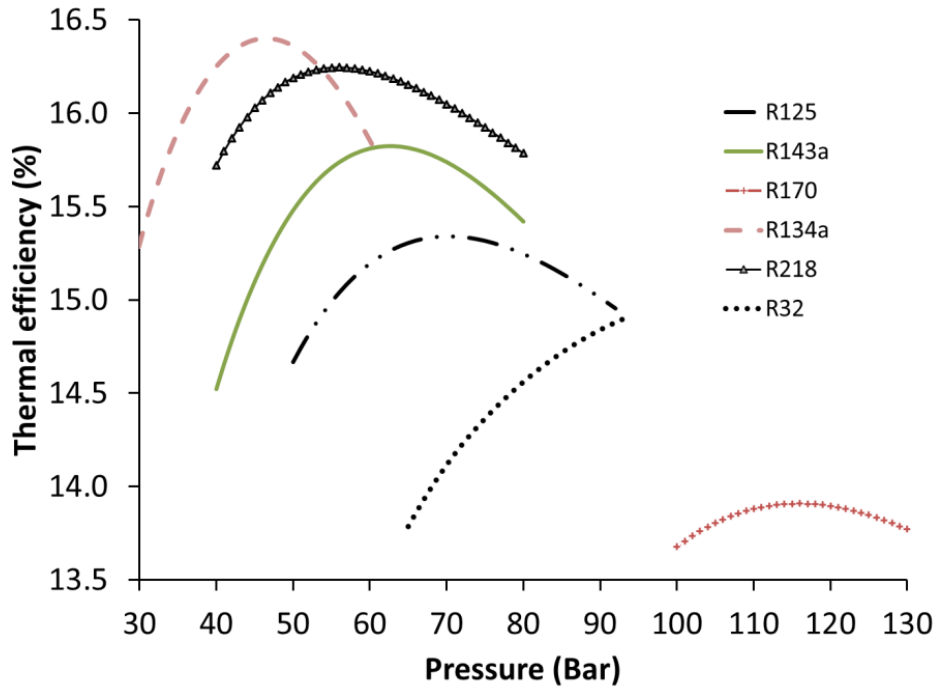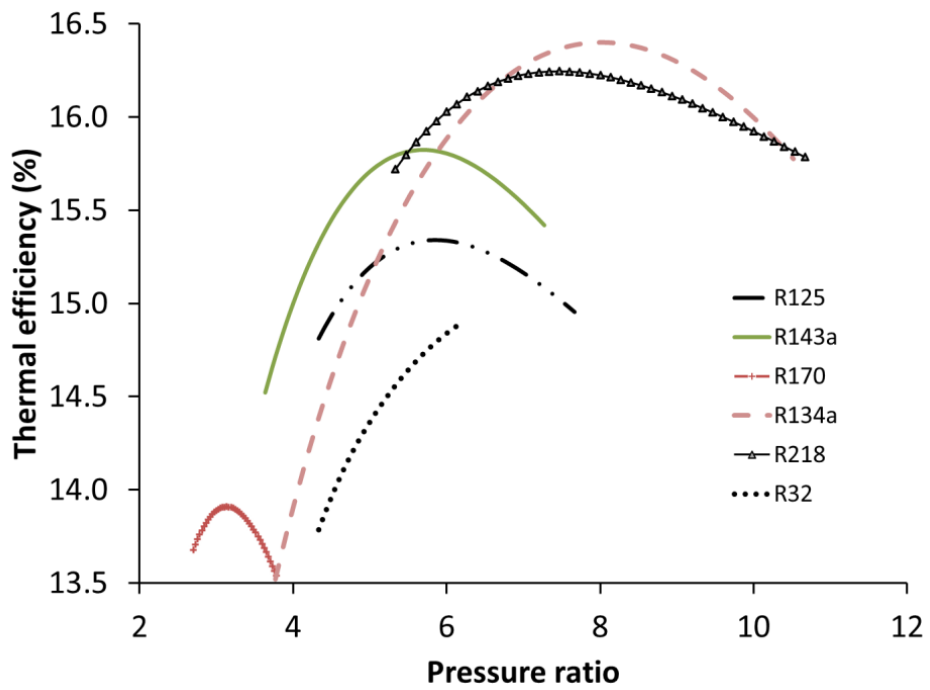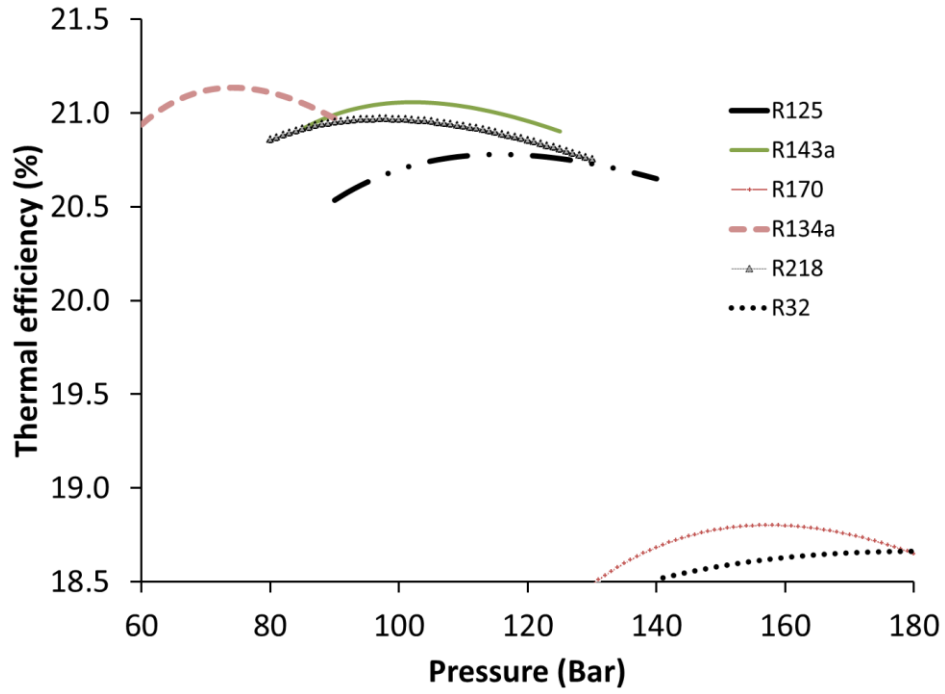
**(a)**
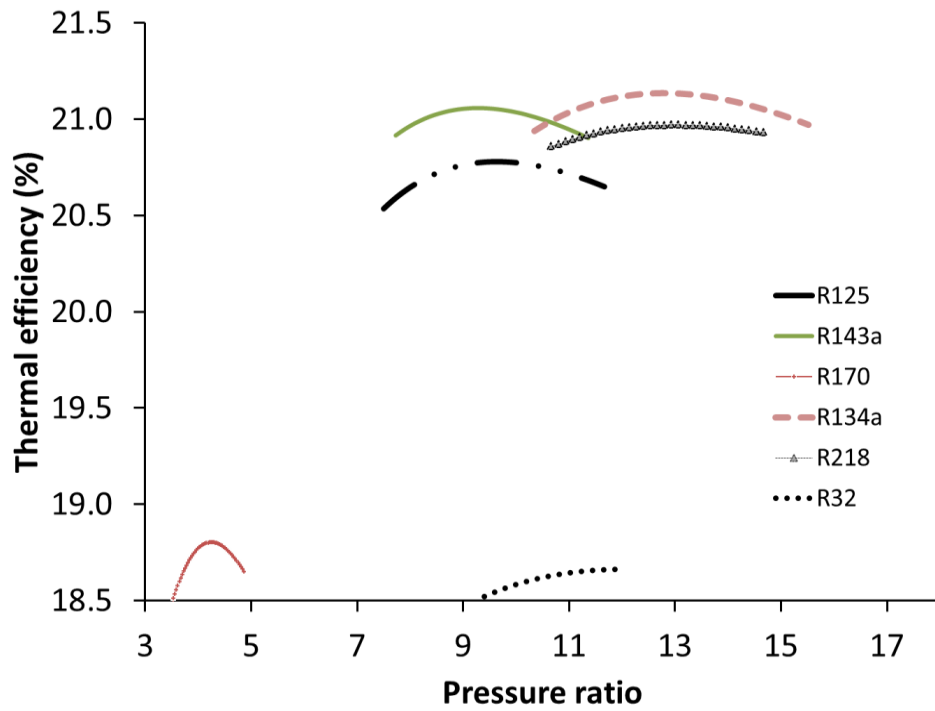


**(b)**

Figure 21. Thermal efficiency of SRC at 200 °C heat source temperature and 10 °C sink temperature.

## 3.7 Effect of Pressure Ratio on Work Output and Input

The existence of optimum pressures for the fluids can be attributed to the fact that the pump work input keeps increasing with increasing pressure while the turbine work output reaches a saturation region where the increase in turbine work output becomes smaller than the increase in the pump work input. This results in a decrease of the net work output. Since the heat input changes very little with the change in pressure, the efficiency starts decreasing when the net work output is reduced. Figure 24 show the turbine work output and pump work input for R134a at 200 °C as a function of the operating pressure. As shown in Figure 22, the power output of the turbine increases with the pressure ratio. However, the rate of increase decreases with the pressure ratio. Over the same pressure ratio, the results shown in Figure 23 indicate a linear increase of the required pump input. It can be observed from Figure 24 that the increase in turbine output decreases with an increase of the pressure ratio while the increase in the pump work input remains constant. The thermal efficiency of the thermodynamic cycle keeps increasing as long as the increase in the turbine work output is greater than the pump work input and achieves its maximum value when the two graphs intersect each other.
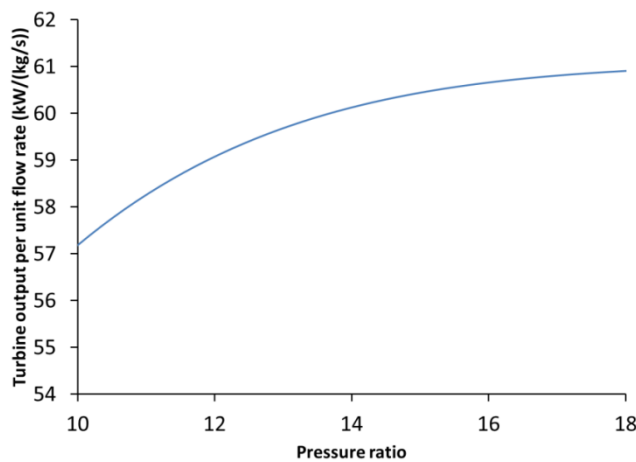


Figure 22. Turbine work output vs. pressure ratio at 200°C heat source temperature for R134a based cycles with flow rate of 1.5 kg/s.
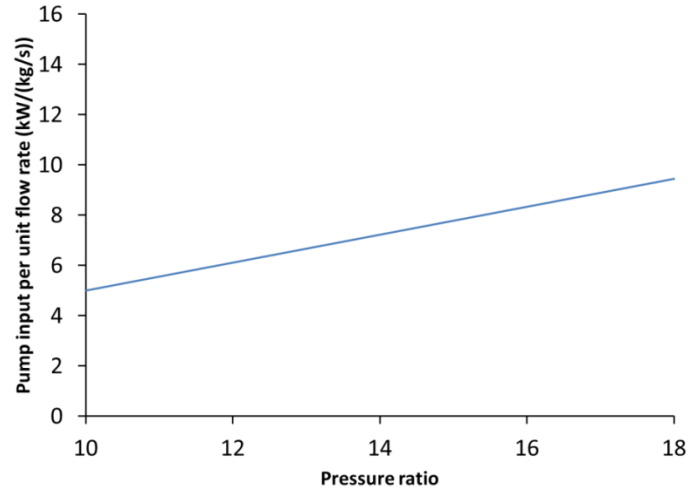
Figure 23. Pump work input vs. pressure ratio at 200°C heat source temperature for R134a based cycles with flow rate of 1.5 kg/s.
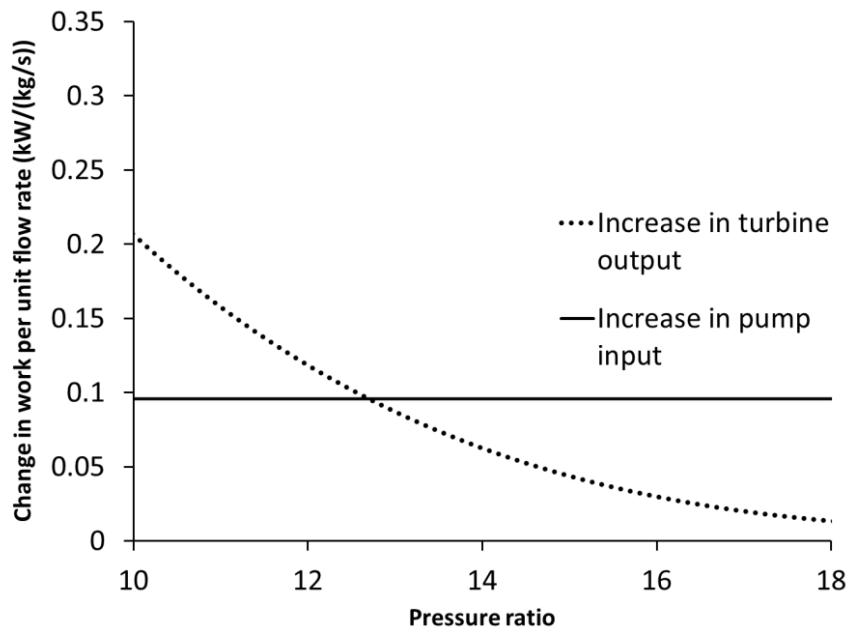


Figure 24. Change in turbine output and pump input as a function of pressure ratio at 200°C heat source temperature and 10 °C sink temperature for R134a based cycles with flow rate of 1.5 kg/s.

## 3.8 Optimum Pressure

Figure 25 shows the variation of optimum pressure with the heat source temperature. It can be observed that for each fluid, the optimum pressure increases with an increase in the heat source temperature. The optimum pressure for R170 (having the lowest critical temperature of all

the fluids considered) is the highest for all the heat source temperatures. This can be attributed to the fact that R170 requires a high condensation pressure at the given cooling conditions resulting in higher operating pressures. R32 has been excluded from this graph because the vapor fraction in the turbine dropped to less than 95% before an optimum point could be achieved. So, the maximum pressure at which it could be operated is considered for further analysis.
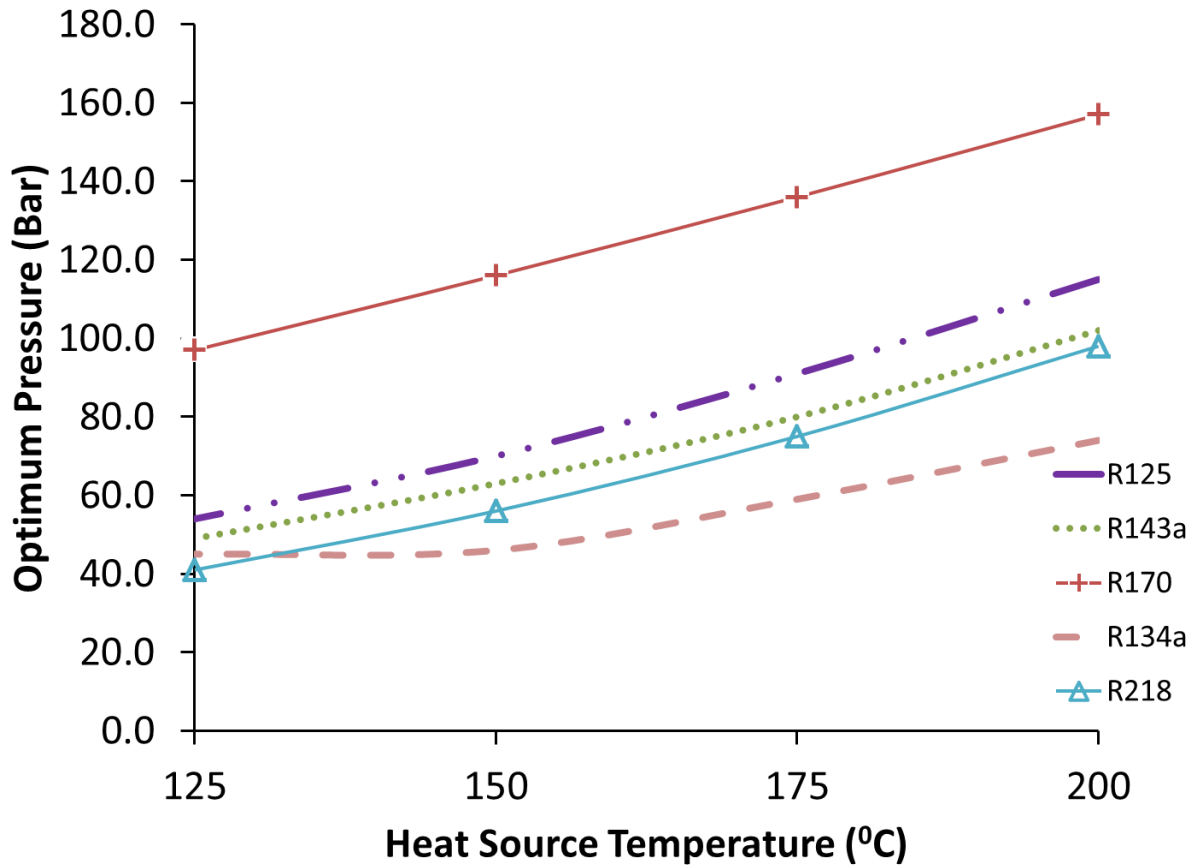


Figure 25. Optimum pressure vs. heat source temperature for the fluids considered at 10 °C heat sink temperature.

## 3.9 Thermal Efficiency at the Optimum Pressure

Figure 26 shows the efficiencies of the cycle at different source temperatures for both a fixed pressure ratio and optimum pressure ratios for R134a. It can be observed that compared to the fixed pressure ratio case, the thermal efficiency of the power cycle increases from 12% to

13.8% when the optimum pressure ratio is used for a heat source temperature of 125°C. The corresponding increase for a heat source temperature of 200°C is from 17.5% to 21.1%. This significant increase suggests the importance of optimizing the operating pressure.
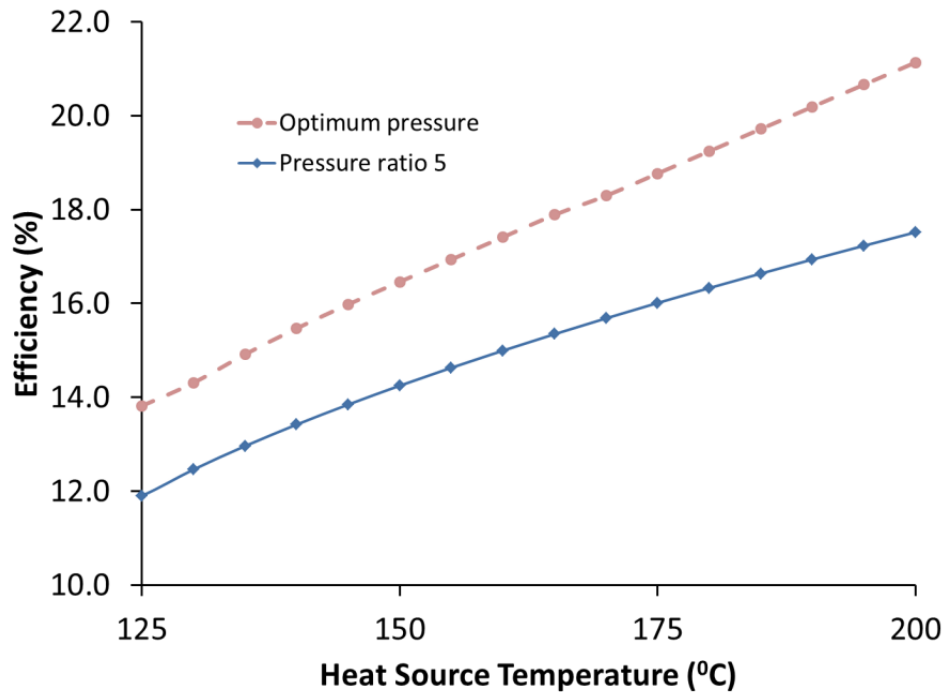


Figure 26. Comparison of thermal efficiency at fixed and optimum pressures for R134a at 10 °C heat sink temperature.

Figure 27 shows the variation of the thermal efficiency as a function of the heat source temperature at optimum pressures for all the fluids considered. Comparing Figure 17 and Figure 27, it can be observed that the relative performance of the fluids changes when the cycle operates at the optimum pressure ratio instead of a pre-determined fixed pressure ratio. For example, among the fluids presented in Figure 17 and Figure 27, R-134a has the highest efficiency when operating at the optimum pressure ratio, while its performance is lower than many other fluids if the pressure ratio is fixed at 5. When operated at optimum pressure ratios, the efficiencies of the R134a, R125, R143a and R218 based cycles are close to each other and higher than the R32 and R170 based power cycles.
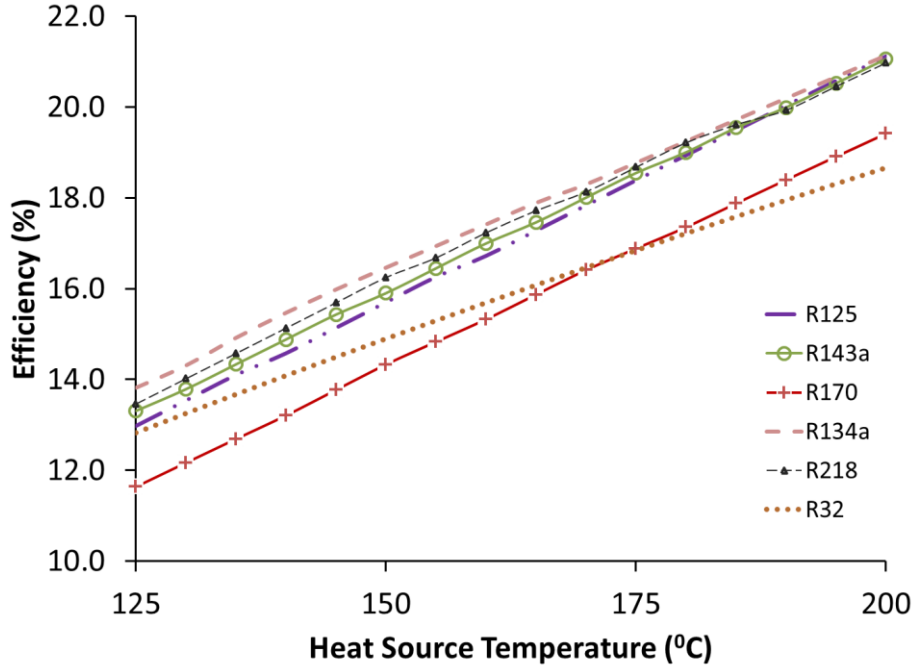
Figure 27. Thermal efficiency of a SRC vs. heat source temperature at optimum pressures at 10°C heat source temperature.

### 3.10 Exergy Efficiency

The exergy efficiency ($\eta_{exergy}$) of the thermodynamic cycle is simulated for the fluids using equation 9.

$$\eta_{exergy} = \frac{\dot{W}_{net}}{\dot{E}_h} = \frac{\dot{E}_{out} - \dot{E}_p}{\dot{E}_h} \tag{11}$$

Only R134a, R143a, R125 and R218 are considered in this section, since these fluids have higher efficiencies among the fluids shown in Figure 27. Figure 28 shows the exergy efficiency obtained for the four fluids as a function of the heat source temperature. The exergy efficiency of the cycle increases with an increase in the source temperature for all the working fluids. It can be inferred from the results that the performance of the R134a based cycle is higher than that of the other three fluids. Though the R143a based cycle has a lower thermal efficiency than the R218, the exergy analysis shows that the exergy efficiency is higher for the R143a.The performance of the R218 can be better or worse than that of the R125, depending on the heat

source temperature, which could be the result of the thermo-physical and critical properties of the fluids.
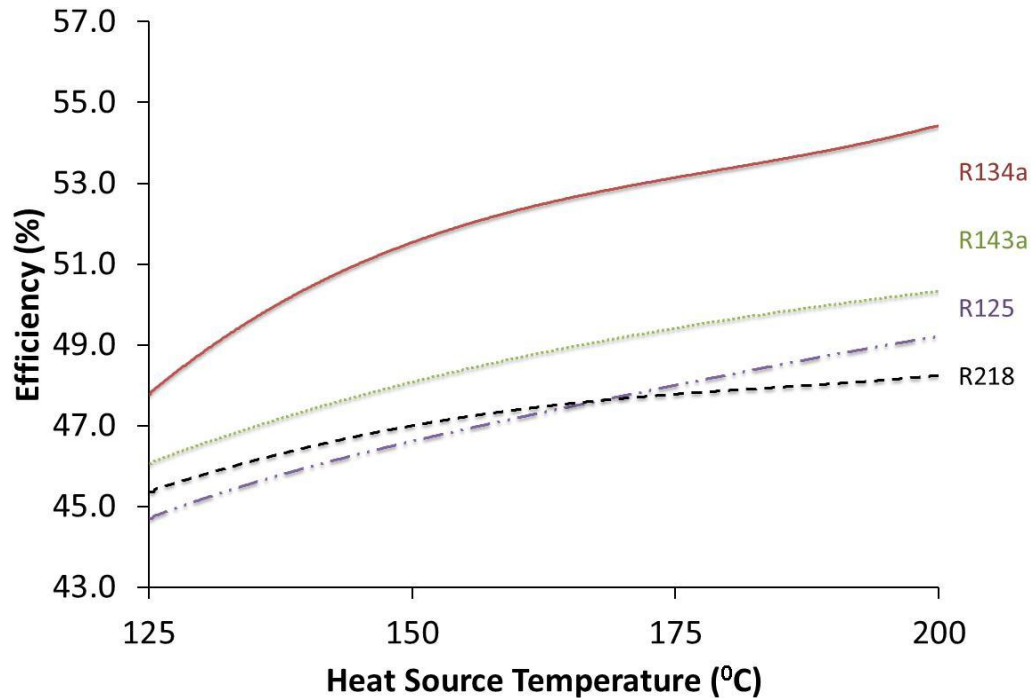


Figure 28. Exergy efficiency of SRC as a function of heat source temperature at 10 °C heat source temperature and optimum operating pressure ratio.

### 3.11 Effect of Cooling Water Temperature

The cooling water temperature was varied from 10°C to 25°C for pressure ratios 10, 12 and 14 when the heat source temperature was 200 °C. It can be observed from Figure 29 that when the cooling water temperature was higher, the power cycle efficiency was greater for a lower pressure ratio. This is because at higher cooling water temperatures, a higher condensation pressure was required. The difference between the cycle high pressure and low pressure becomes larger at the same pressure ratio when the condensation pressure is higher. In order to achieve higher pressure ratios, the required pump work becomes very high while the increase in turbine output is not very significant. So, the net work output is lower for higher pressure ratios and hence, the efficiency is lower.

51
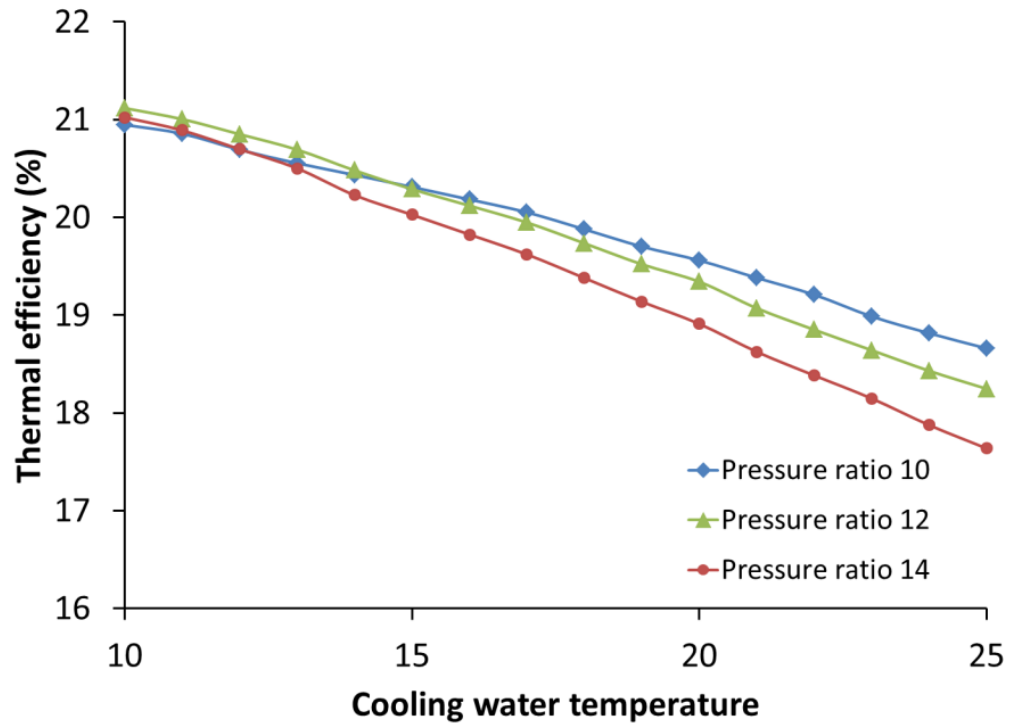
Figure 29. Thermal efficiency for R134a as a function of cooling water temperature at a heat source temperature of 200 °C.

# CHAPTER 4: SUPERCRITICAL RANKINE CYCLE USING ORGANIC MIXTURES

## 4.1 Introduction

Use of mixtures of organic fluids reduces exergy destruction in the heat exchange process because of non-isothermal condensation. So, a thermal glide is obtained in the condensation process that reduces the irreversibilities during heat exchange. Figure 30 shows the thermal glide obtained in the condensation process for a mixture of 50% R134a and 50% R143a (composition by mass) as compared to isothermal condensation of R134a and R143a. [2]



Figure 30. Condensation process of R134a, R143a and their mixture on a T-S diagram.

---

**4.2 R32 and R125**

Mixtures of R32 and R125 have been studied most widely; in nearly all the compositions and at a broad range of temperatures and pressures[211]. R410A is a predefined mixture of R32 and R125 in a mass ratio of 50/50. The mixtures of R32 and R125 in different compositions were analysed to study the effect of varying composition on the thermal efficiency of the supercritical Rankine cycle at different heat source temperatures. Figure 31 shows the variation of thermal efficiency of the SRC as a function of the mass percentage of R32 in the mixture.
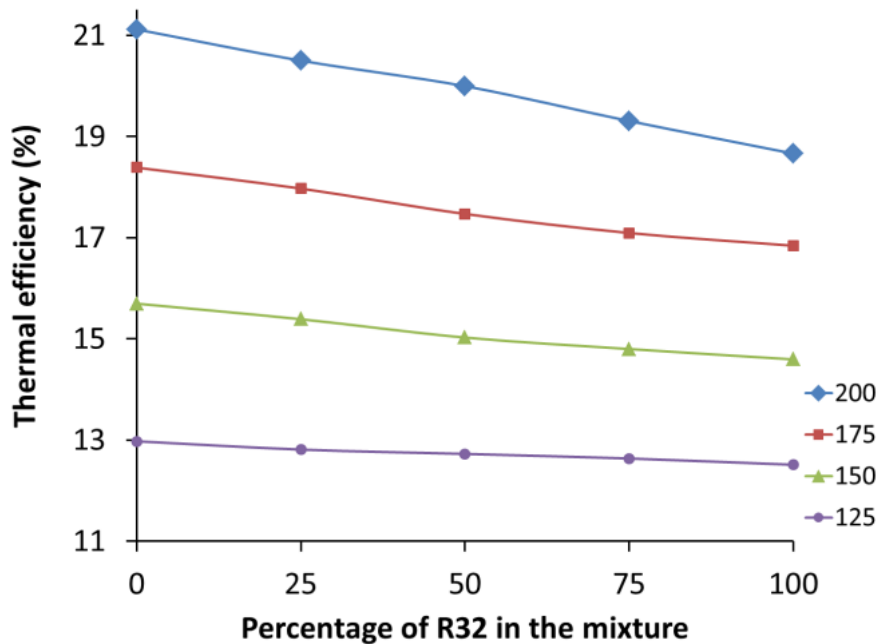


Figure 31. Thermal efficiency as a function of composition of mixture of R32 and R125 at different heat source temperatures (°C); the compositions shown in the figures are in terms of percentage mass of R32 in the mixture.

It can be observed from the graph that the efficiency of the thermodynamic cycle using a mixture was in between the efficiencies for the pure fluids. At higher temperatures, where the difference in the efficiencies for pure R32 and R125 was large, this variation can be easily observed. While at lower heat source temperatures, where the thermal efficiencies for the pure fluids were nearly equal, this variation became less clear.

**4.3 R134a and R143a**

From Figure 27 and Figure 28, we observe that thermodynamic cycles using R134a and R143a as working fluids have high thermal as well as exergy efficiencies in the temperature range considered for this study. Their mixtures in different compositions were analyzed in the thermodynamic cycle as working fluids. Figure 32 shows the effect of varying compositions of the components on the thermal efficiency of the power cycle at different temperatures.
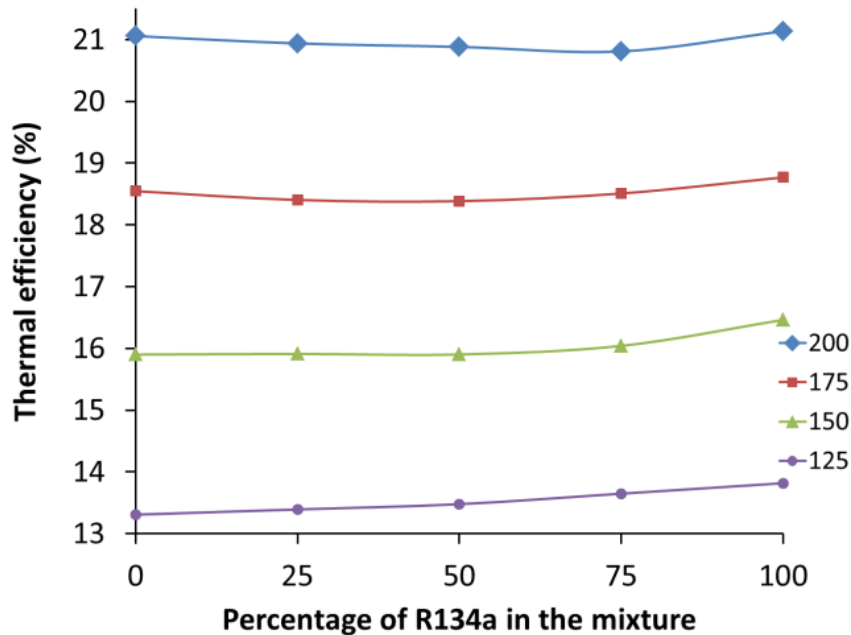


Figure 32. Thermal efficiency as a function of composition of mixture of R134a and R143a at different heat source temperatures (°C); the compositions shown in the figures are in terms of percentage mass of R134a in the mixture.

Thermal efficiencies of the power cycle when pure R134a or pure R143a were used as working fluid were very close. So, a significant difference of using the mixture could not be observed in the thermal analysis of the cycle. The small variation in the thermal efficiency graph for different temperatures could be the result of error in predicted thermo-physical properties of the fluids and their mixtures.

# CHAPTER 5: PASSIVE COOLING

## 5.1 Introduction

Different passive cooling systems and their effects on the efficiency of the SRC have been studied. The ground cooling systems that utilize earth as the heat sink for cooling air (earth-air-heat-exchanger) and water (ground coupled water cooling) have been coupled with an air-cooled-condenser and a double pipe heat exchanger, respectively. A water reservoir cooled using night-sky-radiative cooling system has been coupled with a shell-and-tube type condenser.

## 5.2 Earth-Air-Heat-Exchanger

The condenser of the SRC was coupled with an earth-air-heat-exchanger, using the earth as the heat sink. Figure 33 shows a schematic diagram of an EAHE system. Ambient air is blown through the tunnel buried underground using a blower. As it flows through the tunnel, the air exchanges heat with the soil. Figure 34 shows the annual variation of temperature of the ambient air and soil at various depths for Las Vegas where the yearly average ambient temperature is 19.5°C. As can be seen from the figure, the temperature at a depth of 4 m does not vary much during the year and has a phase lag of about 90 days. In the summer, when the ground temperature is lower than the ambient, heat is rejected into the ground. However, in the winter season, the ambient air temperature is lower than the soil temperature. In this case, the ambient air is directly used in the condenser for cooling the working fluids.[3]

---

[3] Part of this section was published in Energy Procedia. It is open access journal.
Rachana Vidhi, D. Yogi Goswami, E.K. Stefanakos, "Parametric study of Supercritical Rankine cycle and Earth-Air-Heat-Exchanger for low temperature power generation". *Energy Procedia,* 2014. **49**(0): p. 1228-1237

Figure 33. Schematic of an EAHE.
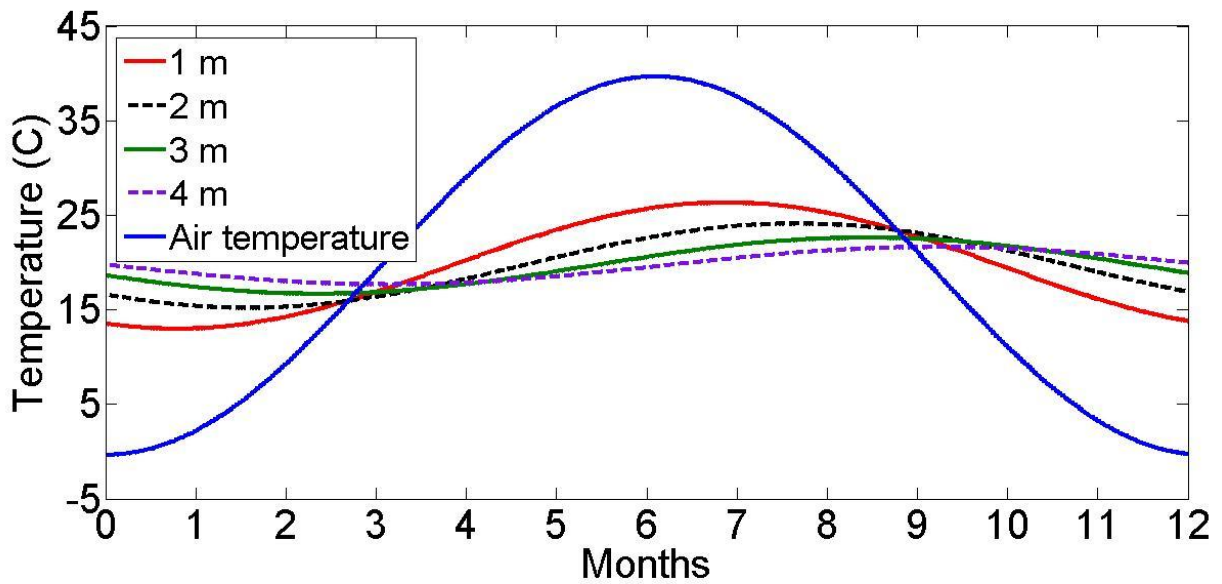


Figure 34. Annual variation of ambient air and soil temperature.

The effect of various system parameters on the performance of the SRC was investigated. Since R134a was found to have the maximum efficiency for the temperature range considered above, it was chosen for further analysis with the EAHE.

## 5.2.1 Methodology

Several different models have been proposed and verified with reasonable accuracy by a number of researchers [27, 31, 35, 91, 102, 118-121, 124, 133, 212-216]. For this study, a two

dimensional model developed by Dhaliwal and Goswami was used to study heat transfer between the air and soil [99-101]. The tunnel length was divided into small segments as shown in Figure 35 and energy balance was performed on each segment.
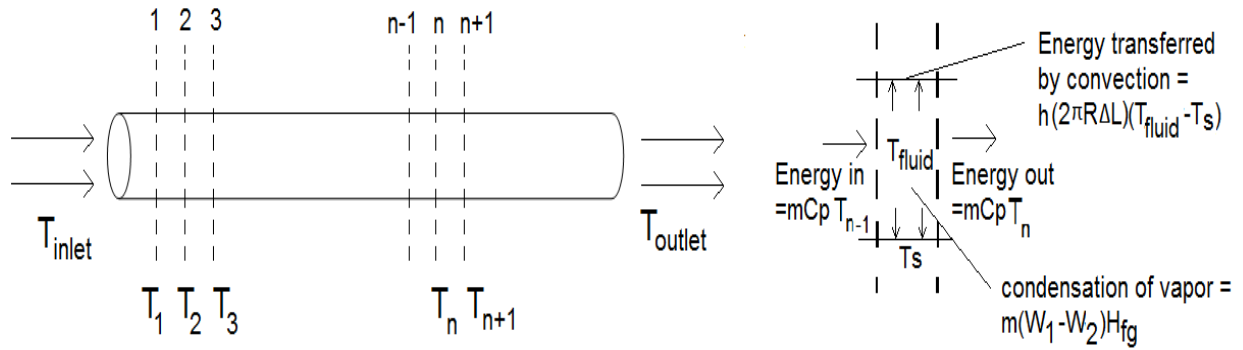


Figure 35. The buried pipe is divided into small segements and energy balance is applied to each segment.

- Heat transfer in air

The inlet temperature was specified and was used to find the temperature of the air leaving the first element. This value was then used as the inlet for the second element and so on. The temperature of the air leaving the nth element is given by equation 12.

$$
T_n = \begin{cases} \dfrac{[(1-U/2)T_{n-1} + UT_s]}{1+U/2} & \text{If the air is unsaturated} \\[4mm] \dfrac{\left[(1-U/2)T_{n-1} + \dfrac{(W_{n-1} - W_n)}{C_p}H_{fg} + UT_s\right]}{1+U/2} & \text{If the air is saturated} \end{cases} \tag{12}
$$

where,

$$
U = \frac{Ah}{mC_p}
$$

- Heat transfer in soil

The temperature of the soil can be obtained using equation 13, where r is the radial distance from the center of the tunnel and t is the time.

58

$$\frac{\partial^2 T(r,t)}{\partial r^2} + \frac{1}{r}\frac{\partial T(r,t)}{\partial r} = \frac{1}{\alpha}\frac{\partial T(r,t)}{\partial t} \tag{13}$$

The solution for equation 13 was obtained using an integral method [99-101] and is given in equation 14,

$$T(r,t) = T_e(t) - \frac{q'R/k}{\delta/R}\left(1+\frac{\delta}{R}-\frac{r}{R}\right)^2 \left(\frac{1}{\delta/R+2\ln(1+\delta/R)}\right)\ln\left(\frac{r/R}{1+\delta/R}\right) \tag{14}$$

where, Te is the bulk earth temperature and $\delta$ is the penetration depth in the soil given by equation 15. The temperature of the soil remains unchanged beyond this length.

$$\delta = \sqrt{8\alpha t} \tag{15}$$

- Ambient air temperature

The diurnal and annual variations of average ambient air temperature are sinusoidal. A sinusoidal profile close to practical conditions was used for yearly variations; while the Erbs Model (equation 16) was selected for the variation over a day.

$$T(t) = T_{avg} + A_T[0.4632\cos(\alpha - 3.805)\,0.0984 + \cos(2\alpha - 0.360)$$

$$+\, 0.0168\cos(3\alpha - 0.822) + 0.0138\cos(4\alpha - 3.513)] \tag{16}$$

$$\text{where } \alpha = \frac{2\pi(t-1)}{24}, \text{and t is the hour}$$

### 5.2.2 Improvement with EAHE

Figure 36 shows the inlet and outlet temperatures for 10 days of operation. It can be observed that the change in outlet temperature is much smaller than the inlet temperature, which suggests that we not only obtain a lower sink temperature for the power cycle, but also a more stable temperature profile with lower fluctuations. Such performance can be used to ensure that the power generation system operates at near optimum condition at all time.
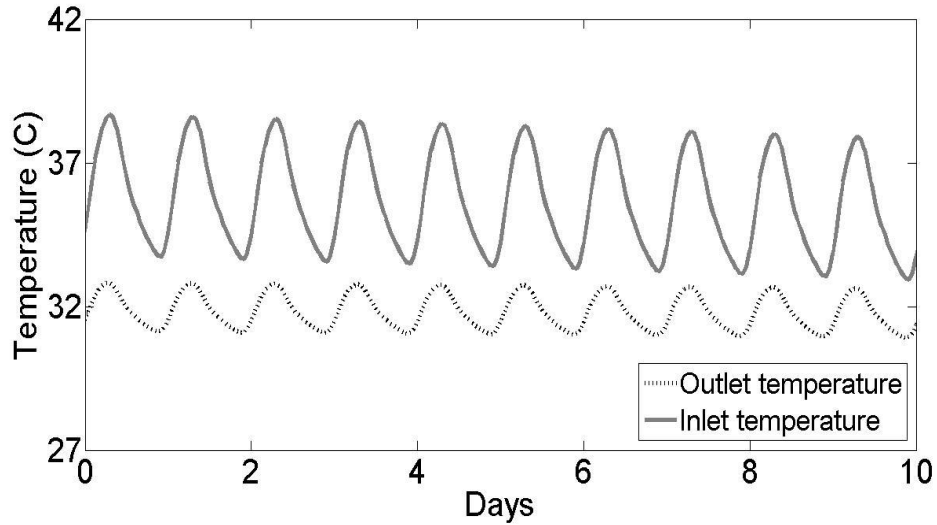
Figure 36. Inlet and outlet temperature for 10 days in June for a 25 m long pipe buried at 2 m.

The outlet air was used for cooling the working fluid in the power cycle. As the temperature of the air inlet to the EAHE increased, the outlet temperature also increased. Since higher sink temperatures resulted in lower efficiency of the power cycle, the trend of variation of efficiency was opposite to the trend of the temperature. Figure 37 shows the variation in efficiency of the power cycle with and without the EAHE for 10 days. We observe that an efficiency increase of about 1% was obtained when EAHE was used for the condenser.
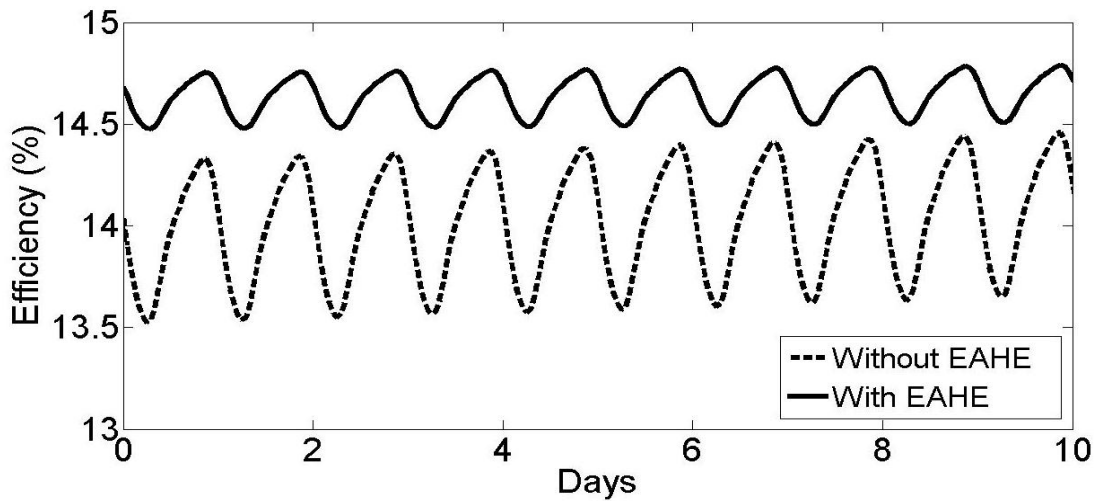


Figure 37. Efficiency of SRC with and without EAHE for 10 days in June for Las Vegas when source temperature is 150°C.

**5.2.3 Effect of Depth**

The depth of EAHE was varied from 1m to 4m. Figure 38 shows the annual variation of outlet temperature for different depths.
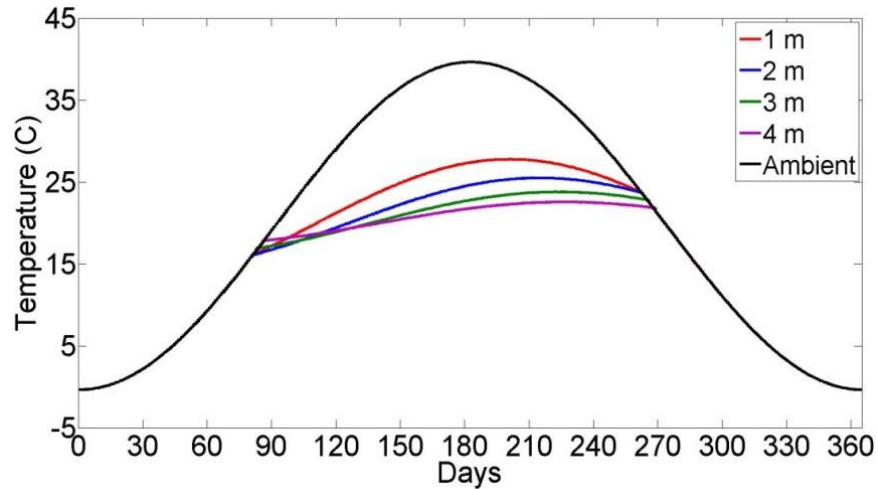


Figure 38. Outlet air temperature for different depths at Las Vegas.

The effect of depth on the efficiency of the SRC can be observed in Figure 39. The efficiency is better for larger depths in the summer season. During colder weather, the ambient air is used directly for cooling the working fluid.
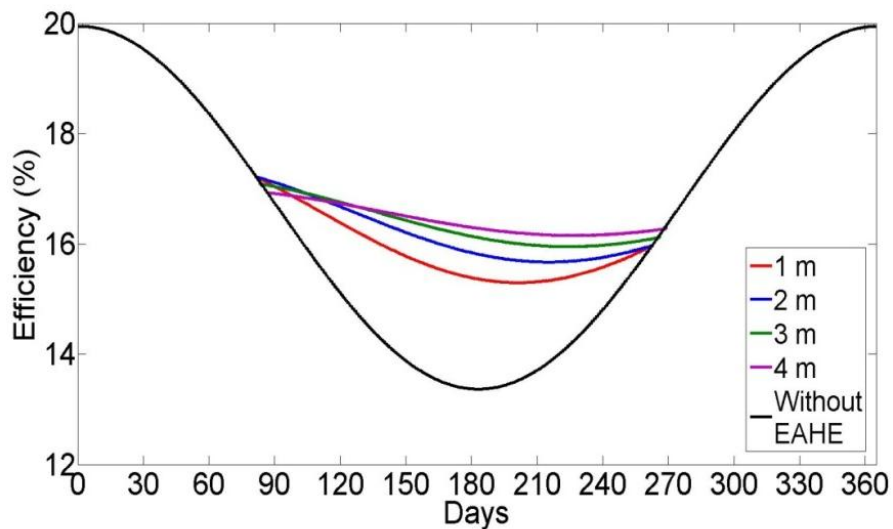


Figure 39. Efficiency of SRC with a heat source of 150°C for different depths of EAHE.

**5.2.4 Effect of Length**

Four different lengths of the underground tunnel, 10, 25, 50 and 100 m, were analyzed for a pipe radius of 25 cm and a depth of 4 m. With increasing length, the outlet temperature of the air was lower. However, this decrease becomes negligible after 50 m. Figure 40 shows the variation of the air temperature for different tunnel lengths. As the length of the pipe increases, the variation in the temperature of the air at the EAHE outlet decreases. The outlet air temperature approaches the undisturbed soil temperature and so, it can be observed that, the annual profile of the outlet air follows that of the soil. As seen in Figure 40, the time lag between the inlet air temperature and the outlet air temperature profiles increases with the pipe length as the outlet air starts to follow the soil temperature profile more closely. This behavior has direct influence on the cycle efficiency which increases when pipe length is increased but no significant improvement is observed after 50m.
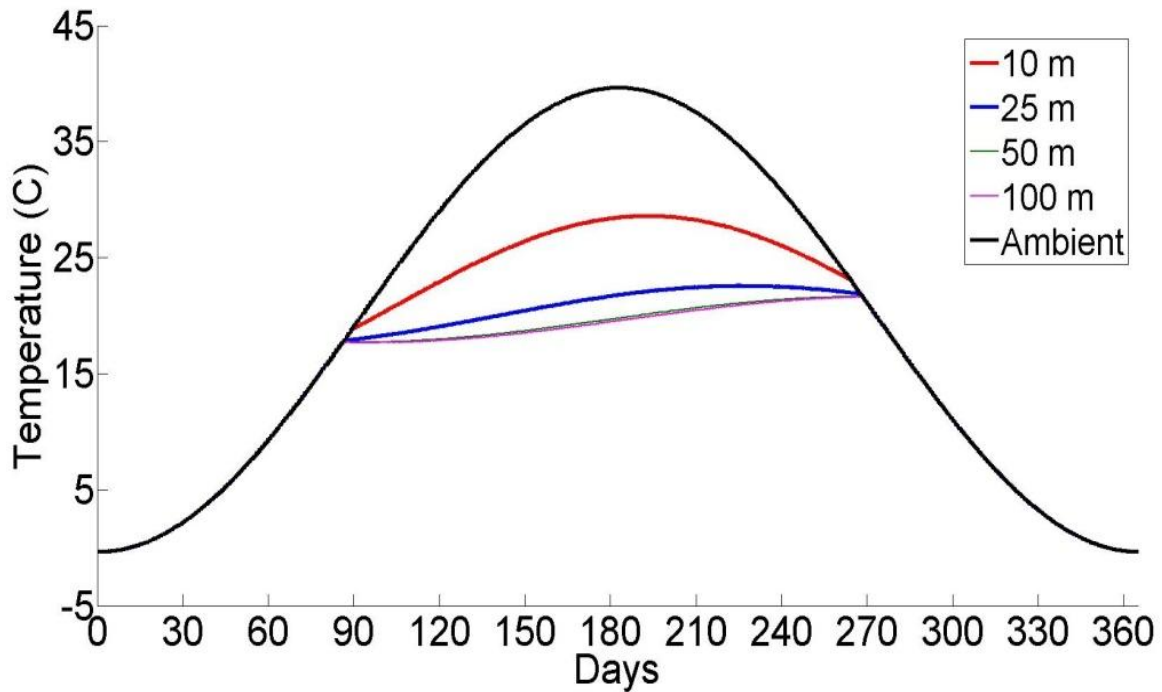


Figure 40. Annual variation of inlet and outlet temperatures for different lengths.
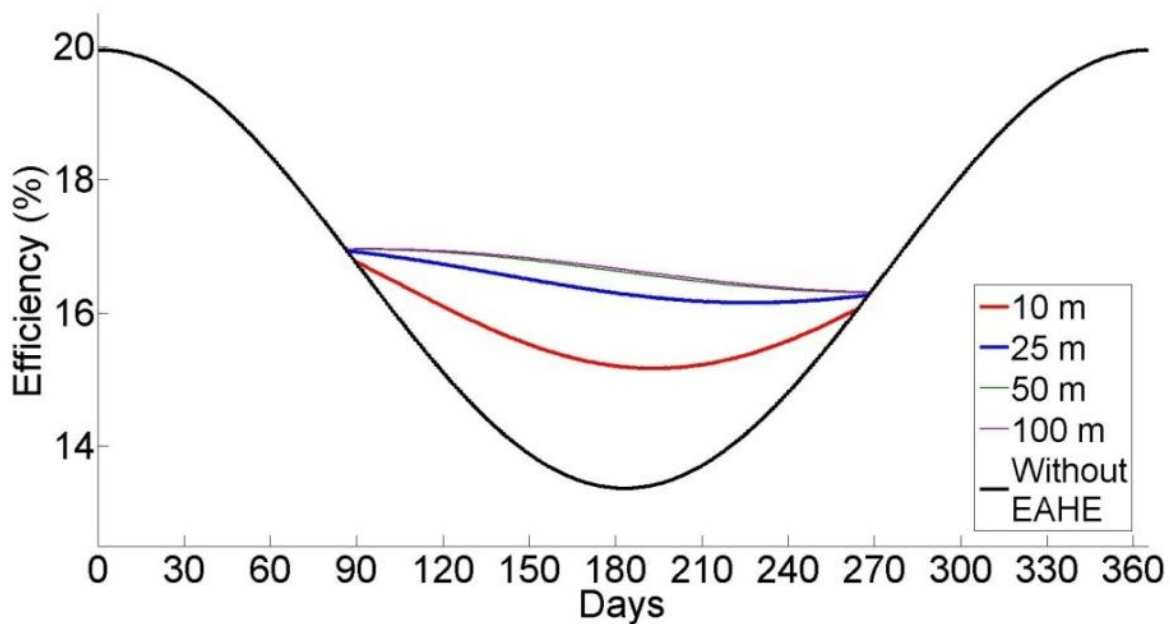
Figure 41. Annual variation of SRC efficiency with 150°C source temperature for different pipe lengths.

### 5.2.5 Underground Temperature

The heat transfer from the air affects the temperature of soil around the underground pipe. As expected, the temperature of soil very close to the pipe varies more and follows a profile similar to the air temperature.

#### 5.2.5.1 Effect of Time and Distance from the Surface

As the distance from the pipe increases, the variation in soil temperature reduces and the profile gets closer to that of the bulk soil temperature. Figure 42 shows the variation of temperature of two points located at a horizontal distance of 0.1 m and 0.5 m from the surface, half way from the inlet of the tunnel. It can be observed that the temperature of soil 0.1 m from the surface of the pipe increases by almost 0.5°C at end of 1 month and 2°C at the end of 3 months above the bulk temperature, while the increase in soil temperature 0.5 m from the surface

is negligible and was less than 0.5°C.  As time increases, the thermal penetration inside the soil

increases and so the effect of heat transfer on the temperature of soil becomes more prominent.
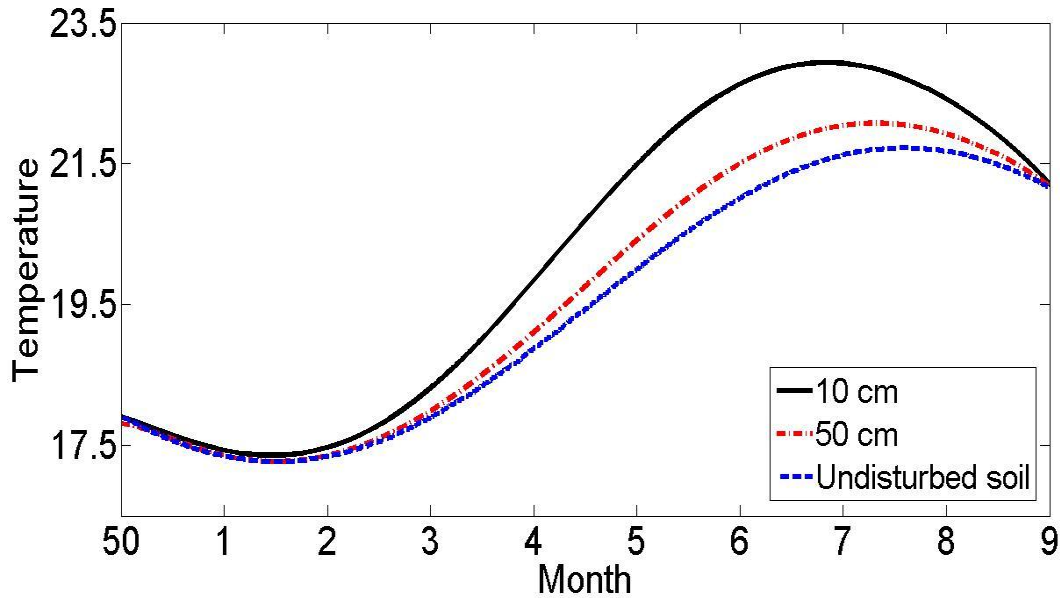


Figure 42. Variation of soil temperature over 3 months at 0.5 m and 2 m from the surface.

### 5.2.5.2 Effect of Position from Inlet

The temperature of air inside the tunnel decreases at a faster rate in the beginning as the

temperature gradient with the soil temperature is higher. So, the temperature of soil increases

more in the initial portion of the pipe and starts decreasing as the heat transfer from the air

decreases along the length. Figure 43 shows the variation in soil temperature as function of

distance from the surface, for four corresponding positions at the pipe. It can be observed that the

soil temperature at the close to the pipe surface decreases as the position is moved farther from

the inlet. Also, the difference between the graphs for 5 m and 10 m points is more compared to

the difference between 15 m and 20 m graphs. It can also be noticed that the temperature of soil

approximately 2 m from the surface converges to the bulk temperature for all positions from the

inlet.
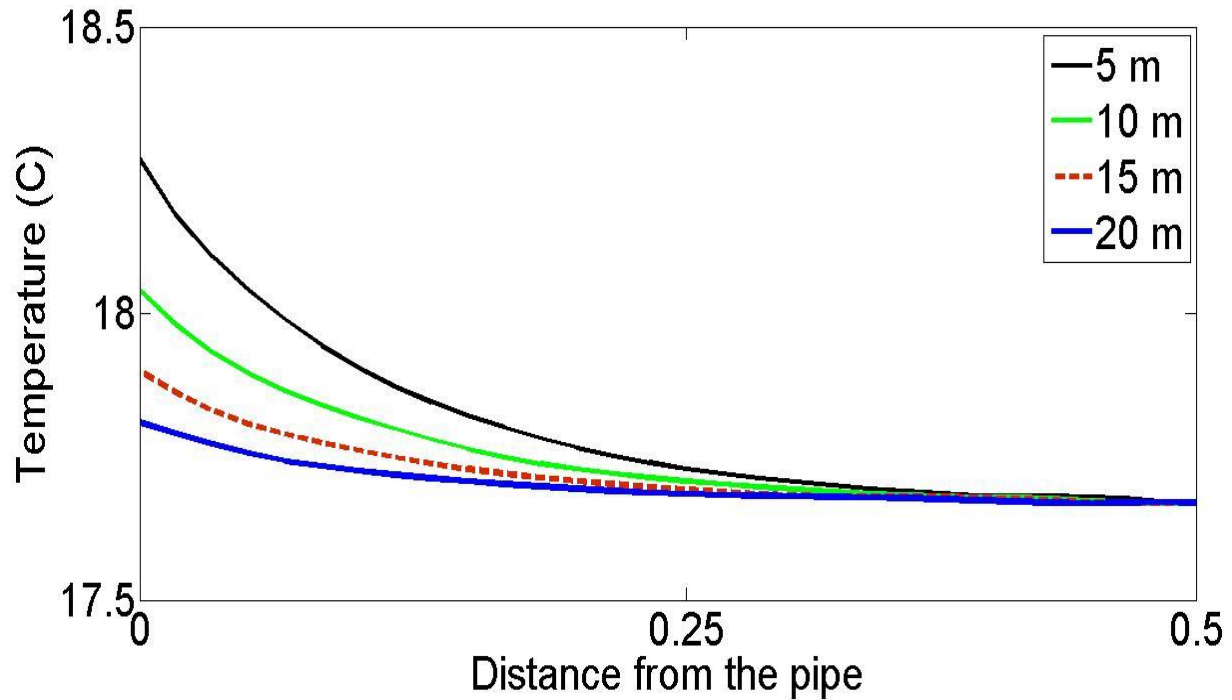
Figure 43. Soil temperature variation with distance from the surface for different locations from the inlet at the end of 3 months.

## 5.3 Ground Coupled Water Cooling

Underground water cooling systems work on the same principle as the EAHE, but water is used instead of air in the heat exchanger. The underground pipes can be vertical or horizontal depending upon the area available. The horizontal systems not only require larger area, but the effect of season change is also more pronounced as the depth is lower. While the vertical systems have much larger depths and hence, the surrounding soil stays at the average annual temperature, throughout the operation. In this study, an underground heat exchanger with vertical boreholes was analyzed for cooling water that may be used in the condenser of the SRC. Figure 44 shows a schematic of a U-shaped vertical ground heat exchanger (VGHX). Warm water coming out of the condenser is passed through the pipes, where it cools down by rejecting heat to the soil and then re-circulates to the condenser.
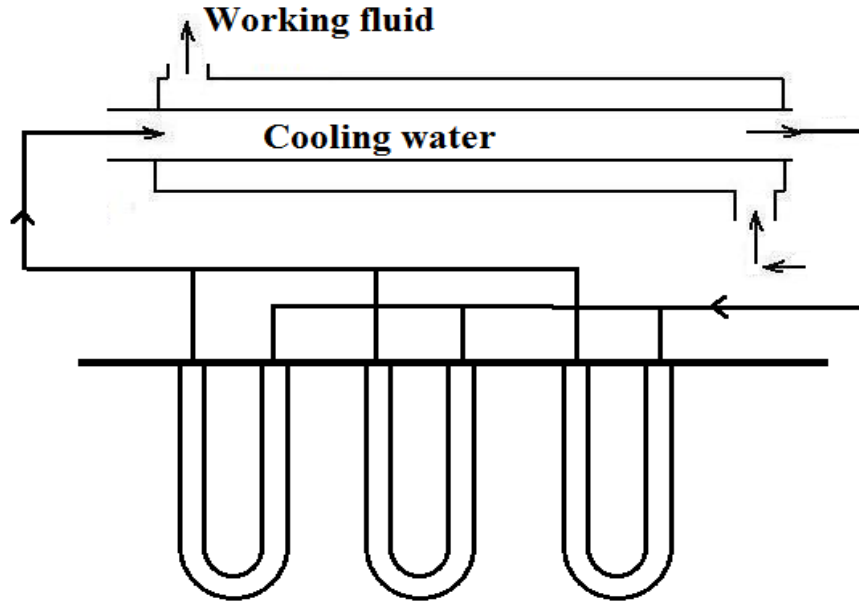
Figure 44. Schematic of ground coupled heat exchanger with condenser.

### 5.3.1 Methodology

The mathematical model proposed by Sanaye et al. [81, 141] is used for studying the VGHX. The model uses the heat transfer rate, inlet and outlet temperature of water and thermal resistance to obtain the length of boreholes needed. Table 8 lists the parameters used for the current study.

Table 8. Parameters of ground coupled water cooling.

| S. no | Parameter | Value |
|-------|-----------|-------|
| 1. | Pipe internal diameter | 2.0-2.5 cm |
| 2. | Pipe external diameter | 2.5-3.0 cm |
| 3. | Inlet temperature | 35°C |
| 4. | Outlet temperature | 30°C |
| 5. | Heat transfer rate | 4.96 W |
| 6. | Soil thermal conductivity | 2.4 W/m-K |

- Thermal resistances

The total thermal resistance for the heat flow was calculated by combining the resistance caused by water flow, pipe wall and the soil (equation 17).

$$R_{total} = R_w + R_p + R_s \tag{17}$$

where

$$R_w = \frac{1}{h_w \pi D_i 2L}$$

$$R_p = \frac{\ln\left(\frac{D_o}{D_i}\right)}{2\pi k_p 2L}$$

$$R_s = \frac{F}{U_s \pi D_o 2L}$$

- Length of pipe

The thermal resistances can be used to calculate the heat transfer rate using equation 18.

$$Q = \frac{\Delta T}{R_{total}} = \frac{\Delta T}{R_w + R_p + R_S} \tag{18}$$

If the heat transfer rate is known, this equation can be used to obtain the length of the pipe needed for a given temperature difference (equation 19).

$$L = \frac{Q}{\Delta T}\left(\frac{1}{2h_w \pi D_i} + \frac{\ln(D_o/D_i)}{4\pi k_p} + \frac{1}{2U_s \pi D_o}\right) \tag{19}$$

**5.3.2 Effect on Efficiency**

The above model has been used to calculate outlet temperature from the pipe of a given length for different temperatures. The soil temperature determines the lowest temperature of the thermodynamic cycle and hence the efficiency of the cycle, for a given source temperature. Since the underground pipe rejects the heat to the soil at a higher rate than it can be dissipated,

temperature around the soil increases. This results in an increase in the outlet temperature of the water cooling system and a decrease in the efficiency of the cycle. Figure 45 and Figure 46 show the variation in outlet temperature and cycle efficiency at a heat source temperature of 175°C for four months of operation.
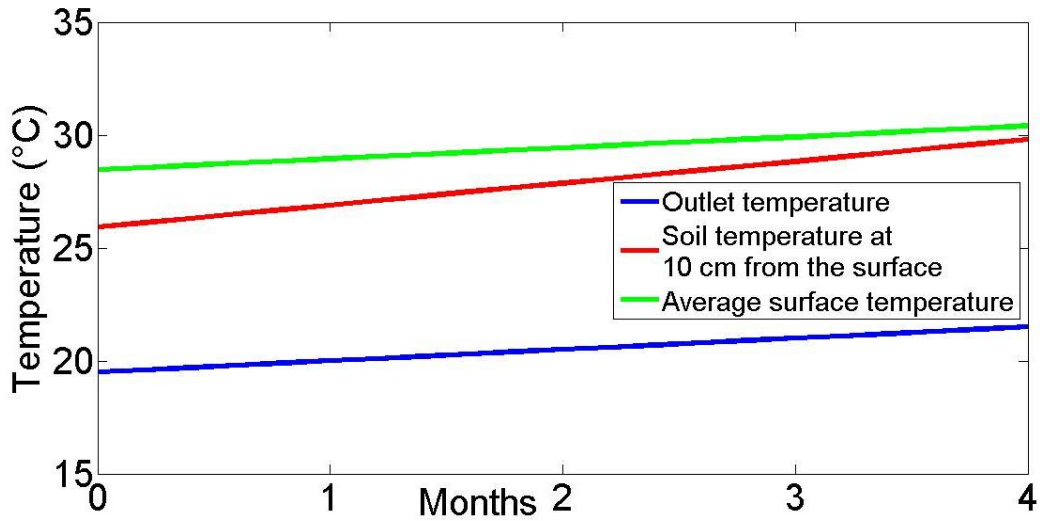


Figure 45. Increase in soil and outlet temperature over four months from April to August.
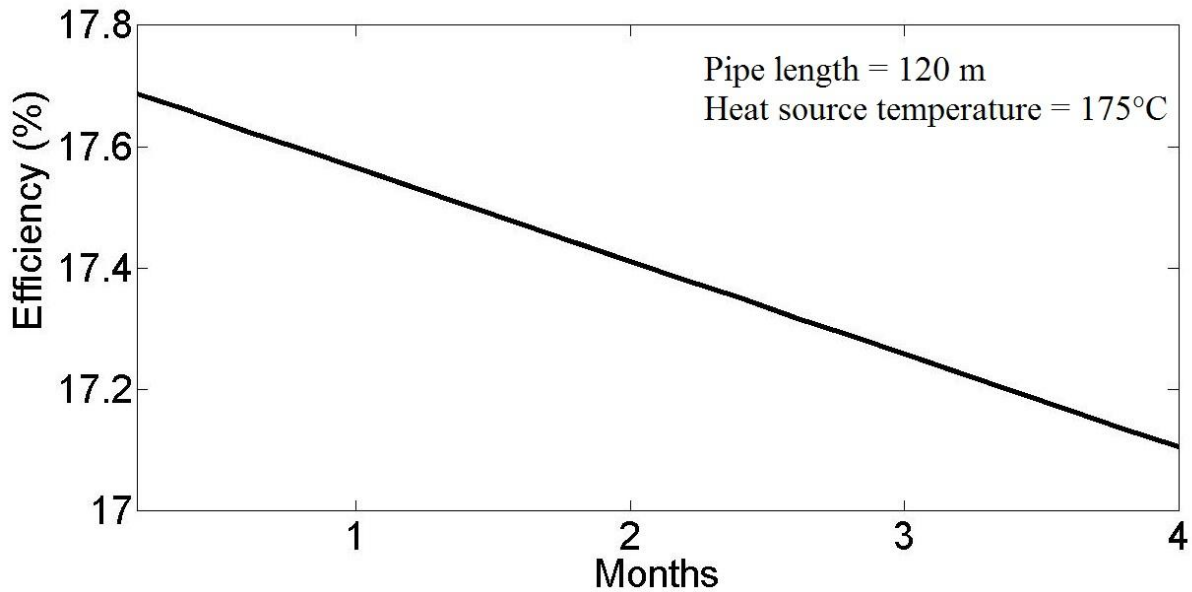


Figure 46. Efficiency of SRC vs. soil temperature for heat source temperature of 175°C.

68

### 5.3.3 Area of Underground Pipes Required

The amount of heat that needs to be removed and the temperature of water and soil determine the length of the underground pipe. In order to handle a larger heat load, a greater number of pipes may be needed to keep the depth within reasonable limits. In this study, the amount of heat rejected in the condenser per kW of net power produced by the R134a based cycle at the heat source temperature of 175°C is obtained and that value is then used to calculate the pipe area needed. The heat transfer area obtained for water cooling system was about an order of magnitude lower compared to that for air cooling system. This is due to the high specific heat and thermal conductivity and viscosity of water. Figure 47 shows the total area of the underground pipes as the number of boreholes is increased for different pipe diameters when the soil temperature is at the annual average at the two locations and the water inlet temperature is 35°C. It can be observed that the total area increases with the number of pipes, even though the length of the boreholes reduces, as shown in Figure 48; however it may not be economically viable to use multiple bores. A detailed economic analysis is needed to determine the optimum number of pipes.
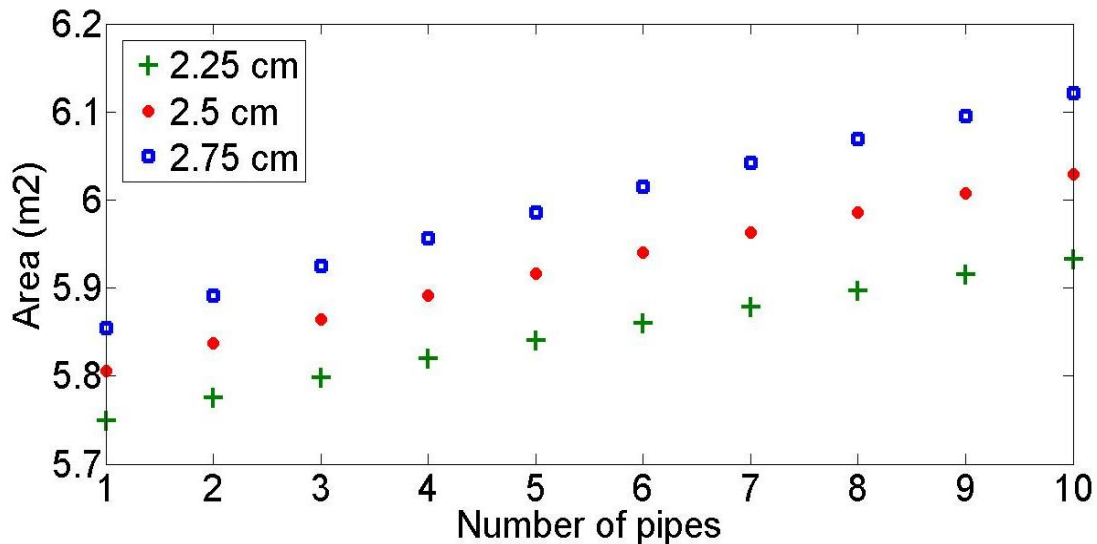


Figure 47. Total area vs. number of pipes.
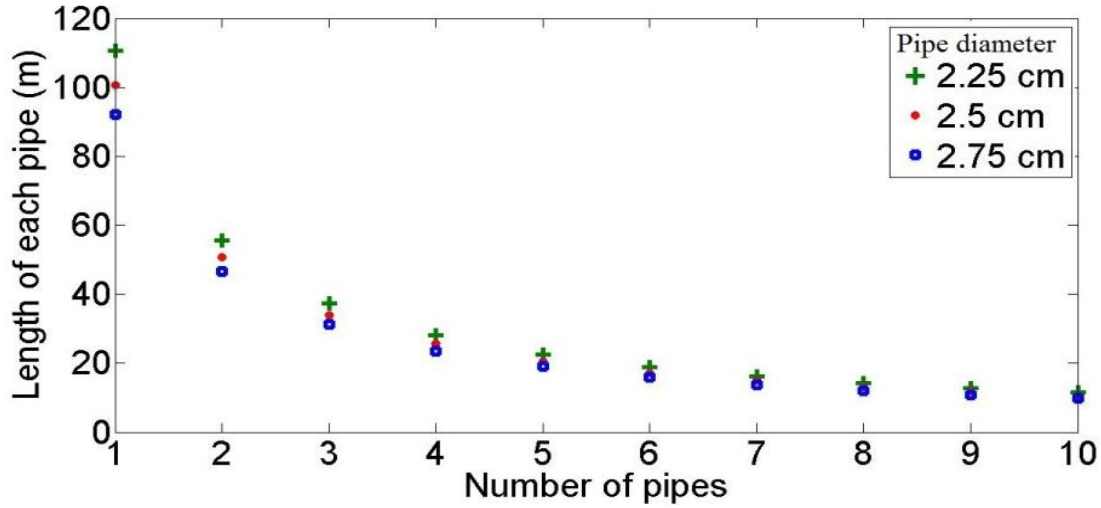
Figure 48. Length of each pipe vs. number of pipes.

### 5.3.4 Water-Cooled Condenser

A counter current double pipe heat exchanger was considered to be used as the condenser for the power cycle where the cooling water, returning from the underground pipes, goes through the inner tube while the working fluid passes through the outer annulus. The length of the condenser was estimated by equation 20 [81] for various values of heat exchanger effectiveness.

$$ L = \frac{Q}{\Delta T_{LMTD}} \times \left( \frac{1}{h_f \pi D_i} + \frac{\ln\left(\frac{D_o}{D_i}\right)}{2\pi k_{cond}} + \frac{1}{h_w \pi D_o} \right) \tag{20} $$

where $h_f$ is the condensation heat transfer coefficient for the working fluid [217] and $h_w$ is the convective heat transfer coefficient for the cooling water. Table 9 shows various parameters used for the calculations and Figure 49 shows the variation in the condenser length as a function of the heat exchanger effectiveness for different diameters of the tube. As expected the length of the condenser decreased for increasing effectiveness. A larger diameter increases the thermal resistance and lowers the velocity and turbulence, thus requiring a larger length of the condenser. Other types of heat exchangers, shell-and-tube or brazed plate heat exchanger, may provide

70

better performance and a comparative thermal and economic analysis is needed to select the most suitable configuration.
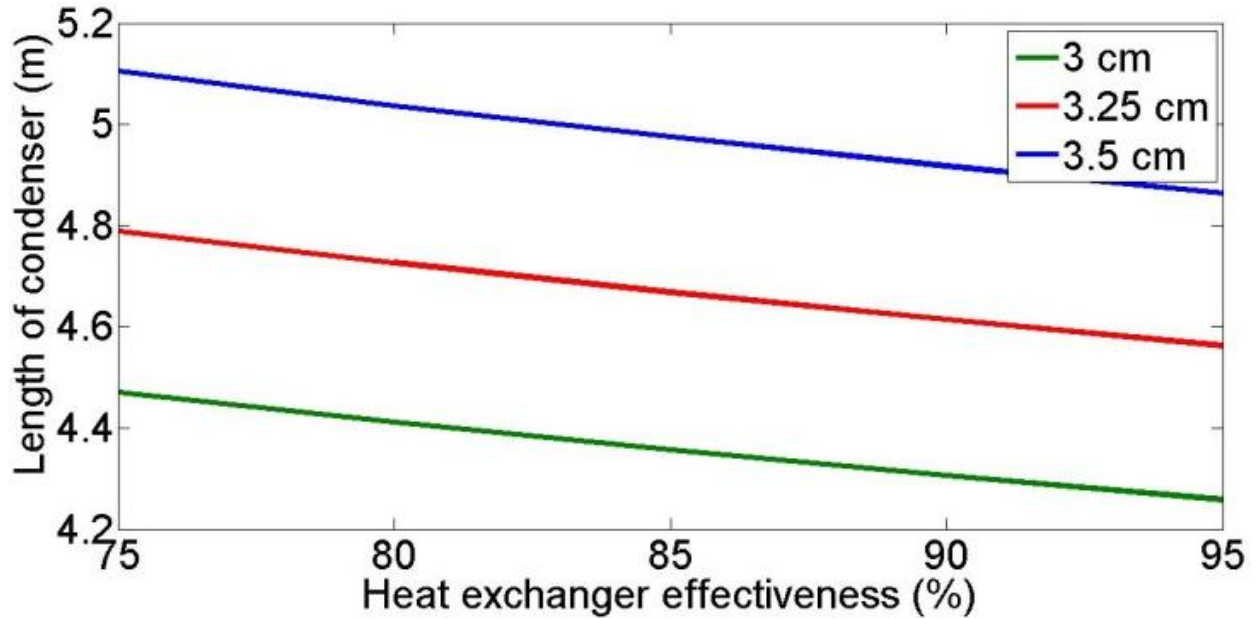


Figure 49. Condenser length vs. heat exchanger effectiveness for different tube diameters.

Table 9. Design parameters for the condenser.

| S. no | Parameter | Value |
|-------|-----------|-------|
| 1. | Inner diameter of the tube | 3-3.5 cm |
| 2. | Outer diameter of the tube | 3.25-3.75 cm |
| 3. | Thermal conductivity | 398 W/m/K |
| 4. | Heat exchanger effectiveness | 75-95% |

### 5.4 Night Sky Radiative Cooling

Water stored in a tank can be cooled at night using radiative cooling and the cooler water can then be used in the condenser heat exchanger of the SRC. The heat transfer occurs by radiation, convection and evaporation as shown in Figure 50. The temperature of water in the

71

reservoir is lower at the bottom and higher at the top due to natural convection. However, bulk assumption is generally made for modeling such systems and has been proven to give accurate results [38, 45, 168, 169, 171, 173, 182, 186, 218].
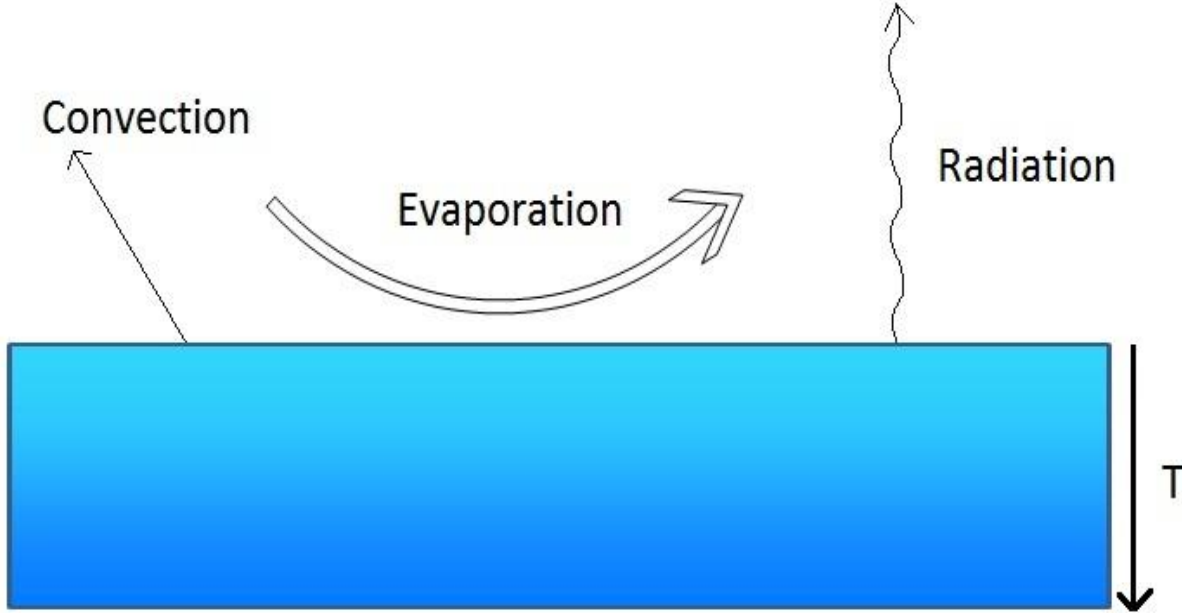


Figure 50. Heat transfer schematic for nocturnal cooling.

### 5.4.1 Methodology

The following heat transfer model was used to analyze the variation in temperature of the stored water. This model has previously been used to calculate the radiative heat transfer between the water storage tank and the sky [43, 45, 186, 187, 197, 219]. The reservoir is assumed to be covered during the day using a movable insulation and is allowed to cool during the night time. Water in the tank is assumed to be perfectly mixed to allow lumped model analysis. Equation 21 shows the energy balance analysis of the water at the night time:

$$h_c(T_a - T_w) - (0.2253 + 0.2464v)(P_w - \emptyset P_a)^{0.82} - \varepsilon_w \sigma\left[(T_w + 273)^4 - T_{sky}^4\right]$$

$$= H_1 \rho_w C p_w \frac{dT_w}{dt} \tag{21}$$

72

Here, the first term signifies the convective heat transfer between the air and the water, the second term accounts for the heat transfer due to the evaporation of water from the free surface and the third term on the left hand side of the equation is the radiative heat transfer term between the water and the sky. $H_l$ is the depth of the water storage tank and $\rho_w$ and $Cp_w$ are the density and specific heat capacity of water, respectively. The convective heat transfer coefficient depends on the wind velocity, $v$ and is given by equation 22 [220].

$$h_c = 2.8 + 3v \tag{22}$$

$\Phi$ is the relative humidity of the air and $P_w$ and $P_a$ are the saturated vapor pressures at the water and ambient temperatures, respectively and can be calculated by equation 23 [220].

$$P = 3385.5 \exp(-8.0929 + 0.97608(T + 42.607)^{0.5}) \tag{23}$$

The effective sky temperature (given in equations 24-27) is calculated using the emissivity expression given by Berdahl and Martin [202]. This model has been verified for several locations in the United States, including locations in Nevada that are similar to Las Vegas, as shown in Table 4.

$$T_{sky} = \varepsilon_{sky}^{0.25}(T_a + 273) \tag{24}$$

$$\varepsilon_{sky} = 0.711 + 0.56\left(\frac{T_{dp}}{100}\right) + 0.73\left(\frac{T_{dp}}{100}\right)^2 \tag{25}$$

Here, the dew point temperature, $T_{dp}$ can be obtained from relative humidity and ambient temperature, which are used to calculate the vapor pressure, Pv and saturation vapor pressure, $P_s$ [221].

$$P_s = \exp\left(\frac{16.78T_a - 116.9}{T_a + 237.3}\right) \tag{26}$$

$$P_v = \frac{RH}{100} \cdot P_s$$

$$So, \exp\left(\frac{16.78T_{dp} - 116.9}{T_{dp} + 237.3}\right) = \frac{RH}{100}\exp\left(\frac{16.78T_a - 116.9}{T_a + 237.3}\right)$$

$$16.78T_{dp} - 116.9 = (T_{dp} + 237.3)\left(\log\left(\frac{RH}{100}\right) + \frac{16.78T_a - 116.9}{T_a + 237.3}\right)$$

Let

$$\log\left(\frac{RH}{100}\right) + \frac{16.78T_a - 116.9}{T_a + 237.3} = \gamma$$

So,

$$16.78T_{dp} - 116.9 = \gamma T_{dp} + \gamma 237.3$$

$$T_{dp} = \frac{\gamma 237.3 + 116.9}{16.78 - \gamma} \tag{27}$$
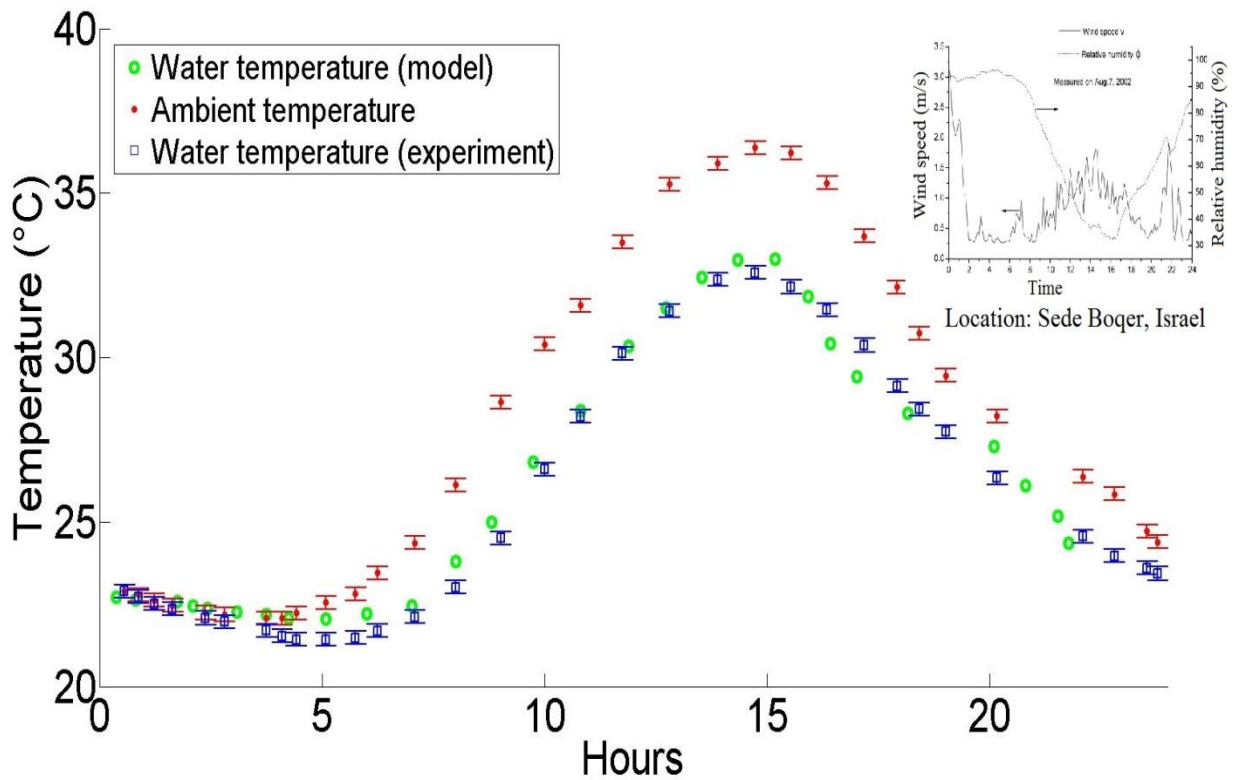


Figure 51. Comparison of the analytical model with experimental data obtained by Tang et al. [43, 186] in Sede Boqer, Israel. The experimentally obtained humidity and wind speed values were obtained from the article. (Copyright persmission in Appendix B.)

Figure 51 shows the comparison of the above model with the experimental data obtained by Tang and Etzion [43, 186]. The experiments were conducted on a shallow reservoir measuring 117x117x22 cm and the temperature sensors were calibrated to <0.1°C. The ambient conditions recorded with the experiment were used as input to the theoretical model. It can be observed that the model results conform to the experimental data with a root mean square error of 1.7 °C. However, since the model was verified with experimental data for a tank with small depth in a humid climate, application to a large body of water in an arid climate has limitations. The validation was done for a humid location but the model would be applied for Las Vegas which has an arid climate. This may cause some error in the final results. Experimental verification of the model for an arid location is needed to verify the accuracy of the results. The results also depend on the aerosol concentration in the atmosphere, cloud cover, humidity and wind speed which vary with the location.

## 5.4.2 Cooling Obtained at Night

The energy equation was solved at elemental time intervals (60 sec) and the temperature of water was obtained as a function of time from 9:00 pm to 5:00 am for a typical summer night (July 1) and a winter night (January 31) at Las Vegas. The relative humidity and wind speed values were obtained from the TMY3 data provided by NREL. Figure 52 and Figure 53 show the results obtained for different values of reservoir depths when the initial temperature of water is assumed to be the same for both cases. It can be observed that the temperatures obtained at the end of 8 hours for both the cases were nearly the same even though the ambient temperatures were very different (5°C and 40°C). This is due to the difference in relative humidity and the wind velocity. For this location, the wind velocity is much higher (4m/s) during the summer

months compared to 2m/s during winter. Hence the cooling obtained by evaporation is higher in the summer.
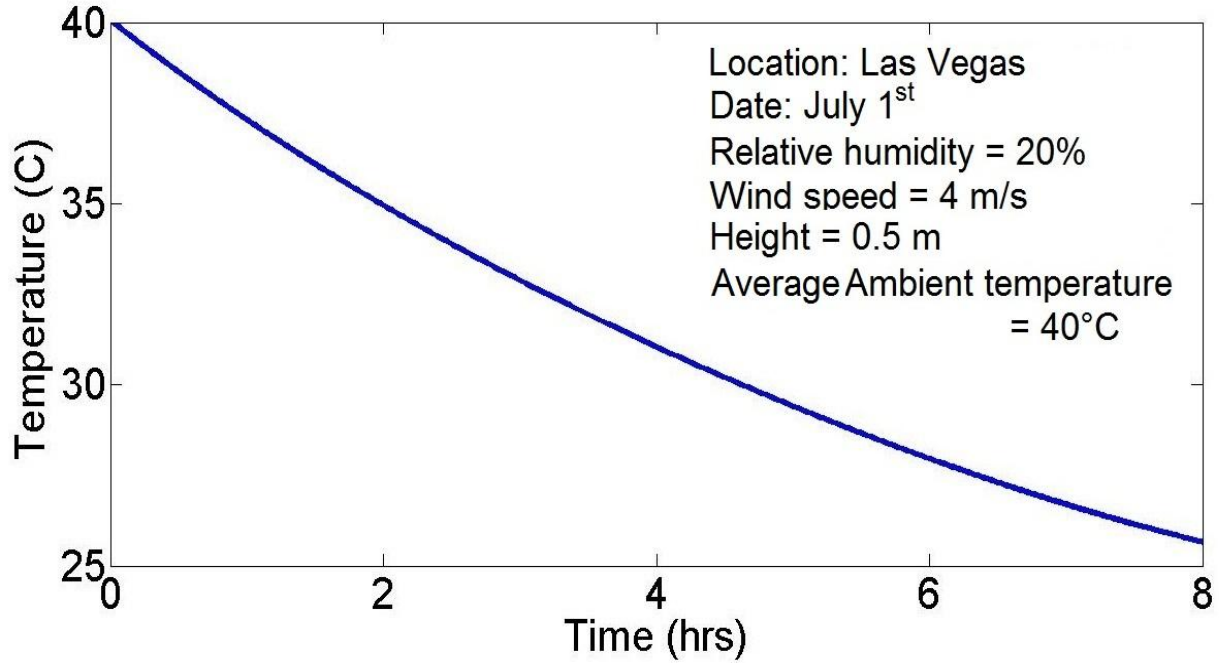


Figure 52. Temperature variation in the summer.
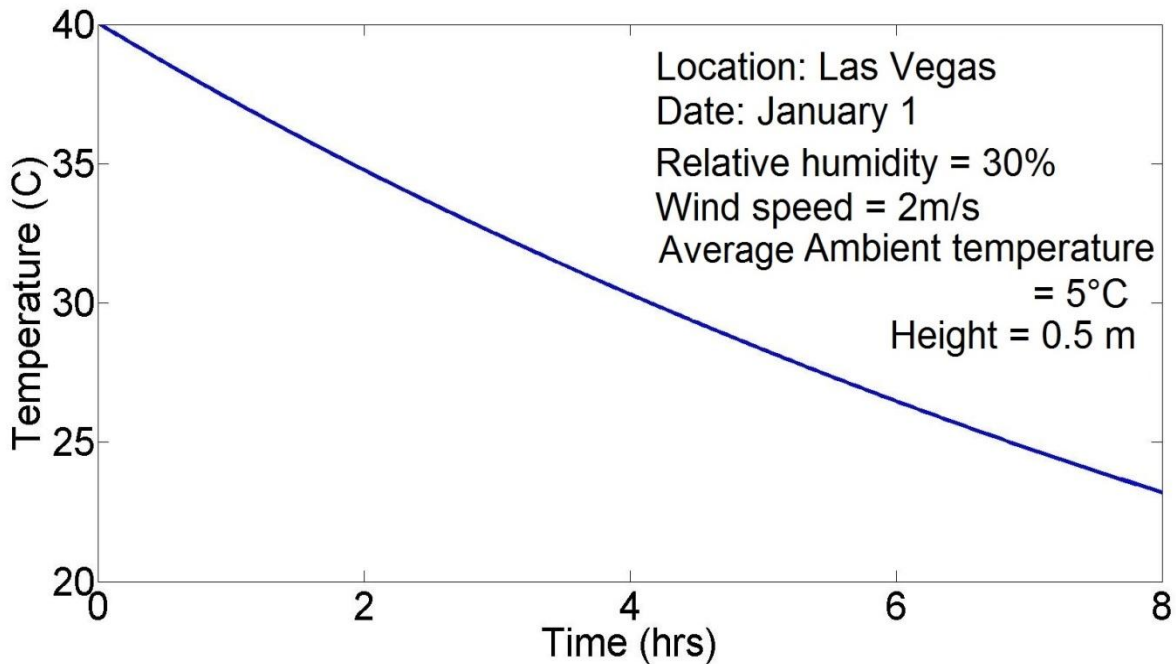


Figure 53. Temperature variation in the winter.

### 5.4.3 Effect of Humidity

Humidity directly affects the evaporative heat transfer rates and the dew point temperature, which in turn affects the effective sky temperature and the radiative heat transfer rate. So, the resulting water temperatures differ for locations with different humidities. The nocturnal cooling model was studied for different values of relative humidities when the ambient temperature and wind speed was fixed. Figure 54 and Figure 55 show two such cases when the ambient temperatures were 15 and 35°C, respectively and the wind speed was 2 m/s. It can be observed that when the ambient temperature is higher, change in humidity affects the water temperature more. For 15°C ambient temperature, the difference in water temperature at the end of 8 hours is only 2°C when the relative humidity changes from 10% to 90%; while for 35°C ambient temperature, the final water temperature is about 5°C higher for 90% relative humidity compared to that at 10%.
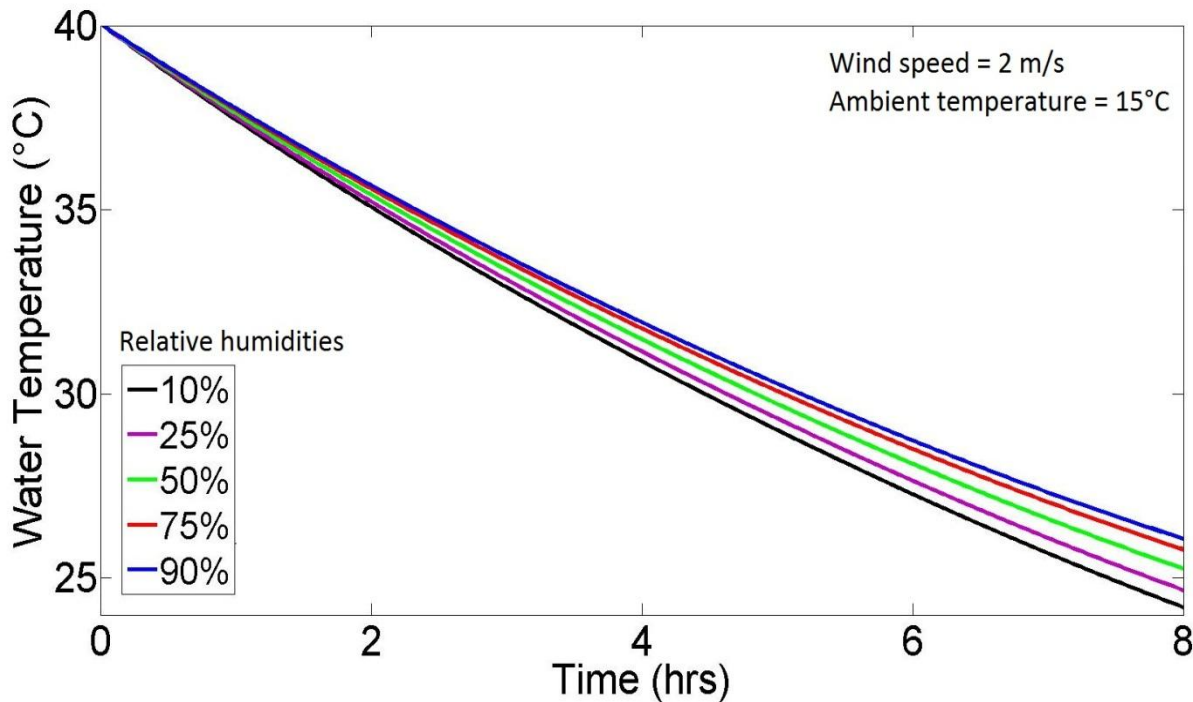


Figure 54. Effect of humidity when ambient temperature is 15°C
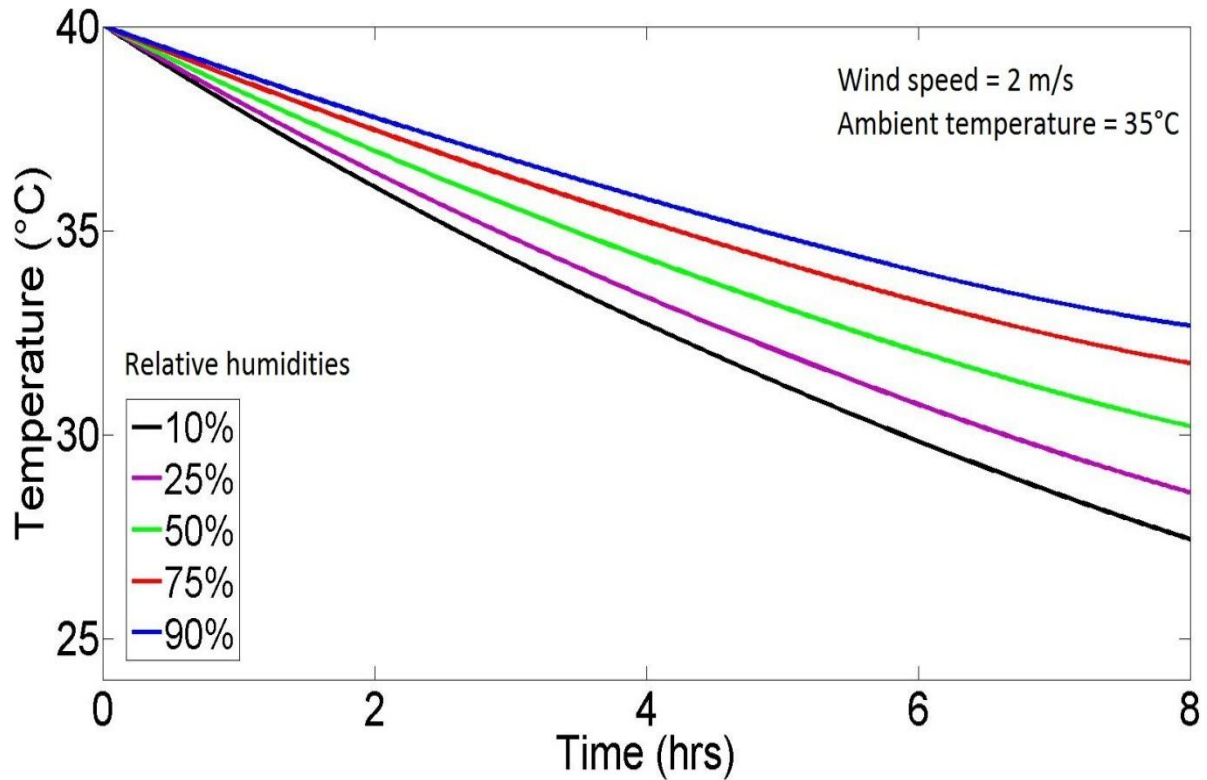
Figure 55. Effect of humidity when ambient temperature is 35°C

### 5.4.4 Effect of Wind Speed

Wind speed is another environmental factor that affects the performance of the nocturnal cooling system. It directly influences the convective and evaporative heat transfer rates. As seen from Figure 52 and Figure 53, higher wind speed and lower humidity in the summer resulted in reservoir temperatures that were comparable to the temperatures obtained in the winter. Figure 56 and Figure 57 show the effect of wind speed on the water temperature when the ambient temperatures were 15 and 35°C, respectively and relative humidity was 30%. It can be observed that the varying wind speeds had a larger impact on the water temperature for lower ambient temperature. When the ambient temperature was 15°C, the difference in temperature for 1m/s and 5 m/s was ~10°C at the end of 8 hours while for 35°C, it was ~5°C.
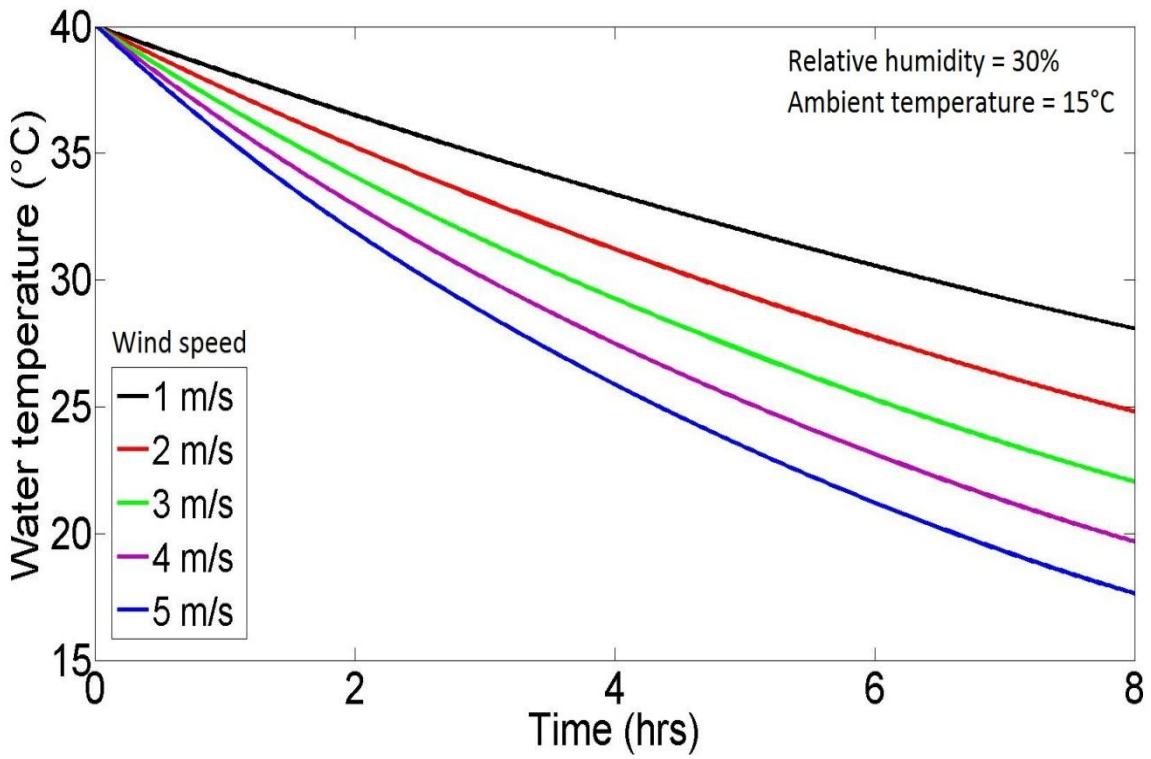
Figure 56. Water temperature for different wind speeds at 15°C ambient temperature
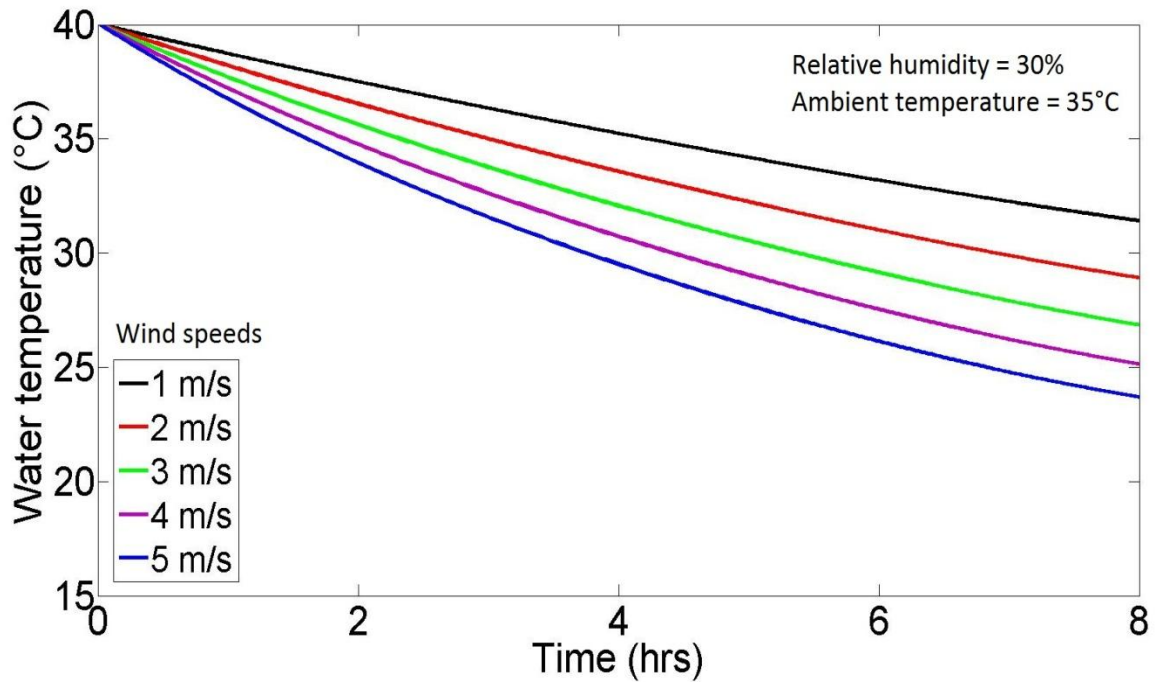


Figure 57. Water temperature for different wind speeds at 35°C ambient temperature

### 5.4.5 Efficiency Improvement

Warm water coming out of the condenser enters the reservoir where it is cooled and the cooler water is then used to condense the working fluid in the thermodynamic cycle. This adds another term in the energy balance equation for the incoming water stream. The effect of nocturnal cooling system on the efficiency of the cycle was analyzed when the heat source temperature was 175°C and R134a was used as the working fluid for approximately 100kW power generation. It was assumed that the reservoir is cooled during the night from 9:00 pm to 5:00 am and is covered during the day. The cooling water from the condenser of the SRC continues to pass through the reservoir, thus increasing its temperature during the day time. Figure 58 shows the water temperature variation over a period of 10 days for different reservoir sizes and Figure 59 shows the corresponding variation in the SRC efficiency. The hourly variation during the second night is shown in Figure 60 and Figure 61. It can be observed that the improvement obtained by increasing the surface area becomes smaller beyond 250 m$^2$ reservoir area. Different input parameters are listed in Table 10.

Table 10. Input parameters for SRC coupled with nocturnal cooling system.

| S. No. | Input parameter | Value |
|--------|-----------------|-------|
| 1. | Pump efficiency | 85% |
| 2. | Turbine efficiency | 85% |
| 3. | Relative humidity | 30% |
| 4. | Wind speed | 2 m/s |
| 5. | Tank height | 0.5 m |
| 6. | Average ambient temperature | 30°C |
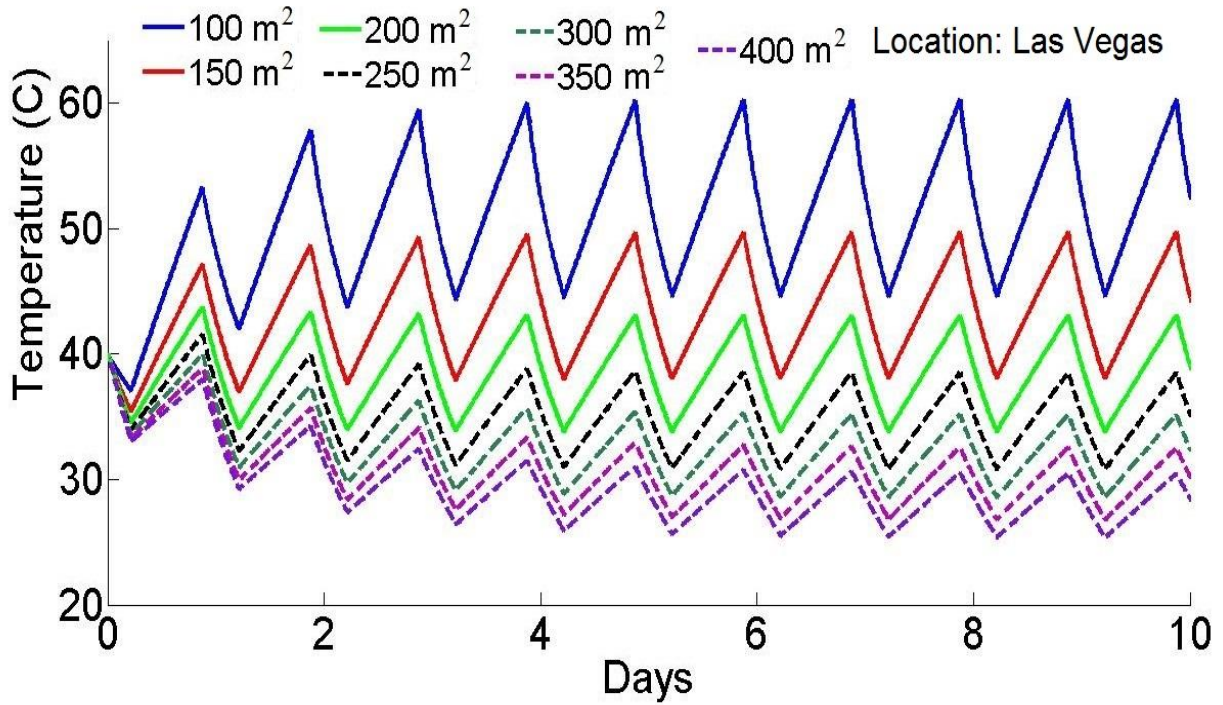
Figure 58. Water temperature variation for different surface area of the reservoir. Input parameters are given in Table 10.
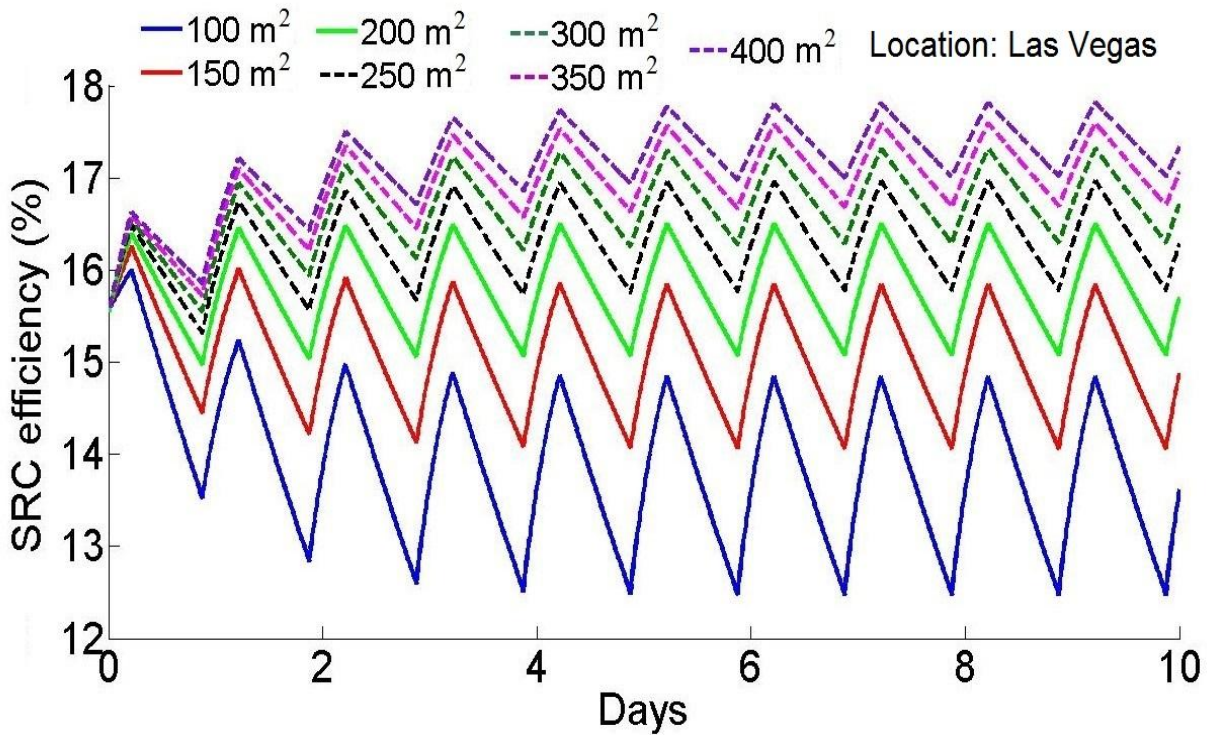


Figure 59. Efficiency variation for different surface area of the reservoir. Input parameters are given in Table 10.
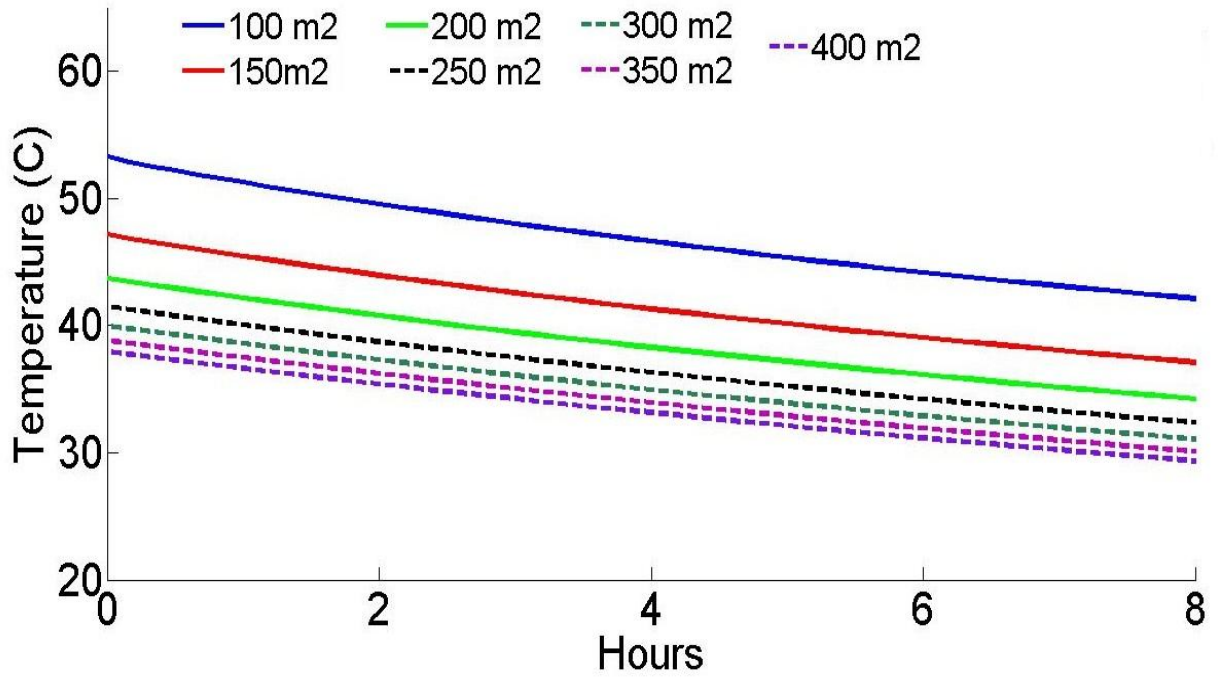
Figure 60. Hourly variation in water temperature for different surface area.
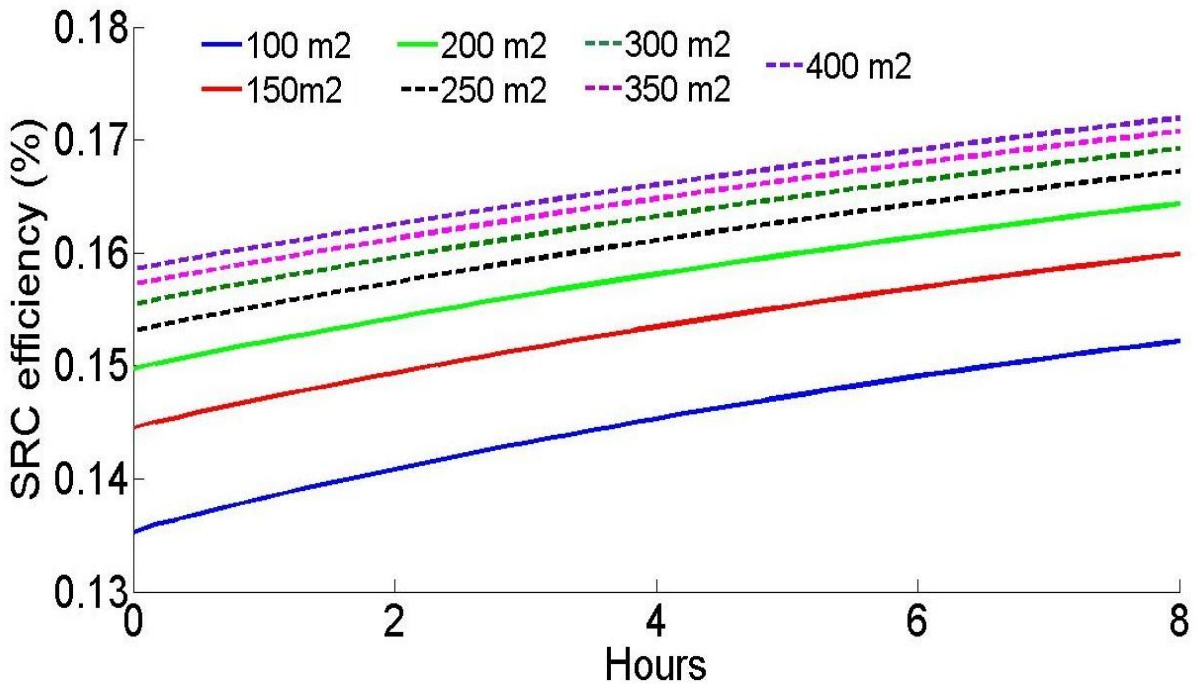


Figure 61. Variation in SRC efficiency during the night for different surface area.

It can be observed from the figures that larger surface area provides more cooling and hence lower reservoir temperatures. For surface area less than 250 m², the cooling obtained at night is not sufficient for the load of ~100 kW power generation and the temperature of the water increases above the starting value of 40°C. This leads to lower values of efficiency as shown in Figure 61. In order to successfully employ nocturnal cooling system in the condenser, the surface area should be at least 250 m² for the given conditions.

### 5.4.5.1 Covered vs. Uncovered

If the ambient temperature is low, the reservoir may not need to be covered during the day as the heat can be rejected even during the day. Figure 62 compares the temperature variation of the reservoir for different values of average ambient temperatures for a 20 m x 10 m surface that stays exposed during the entire time with the case when it is covered during the day. Other conditions remain the same as given in Table 10. It can be observed that for these conditions the nocturnal cooling system performed better when it was left uncovered during the day. The corresponding efficiencies of the SRC are shown in Figure 63.
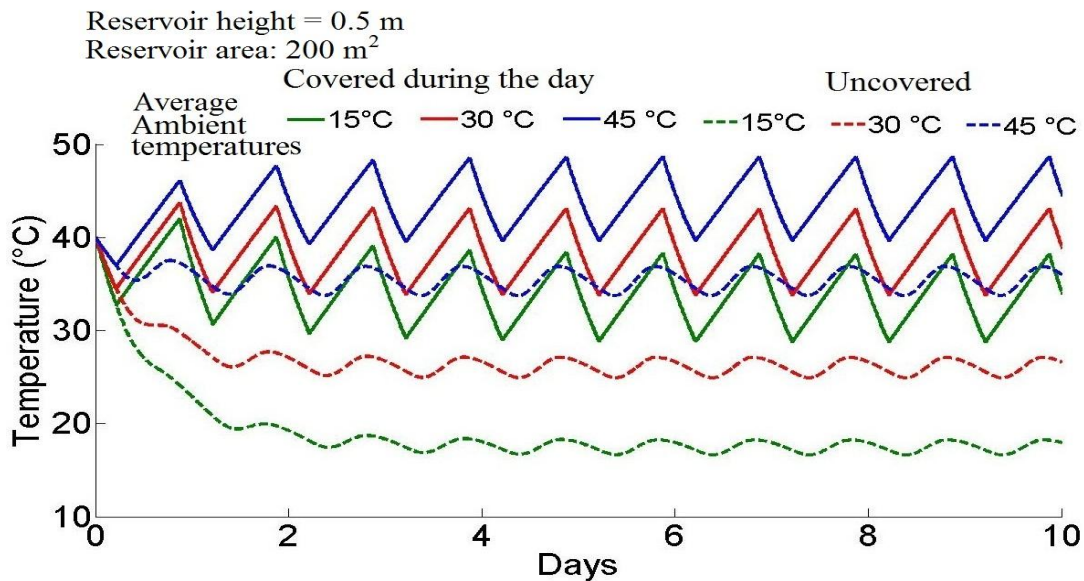


Figure 62. Comparison of water temperature for covered and uncovered cases.
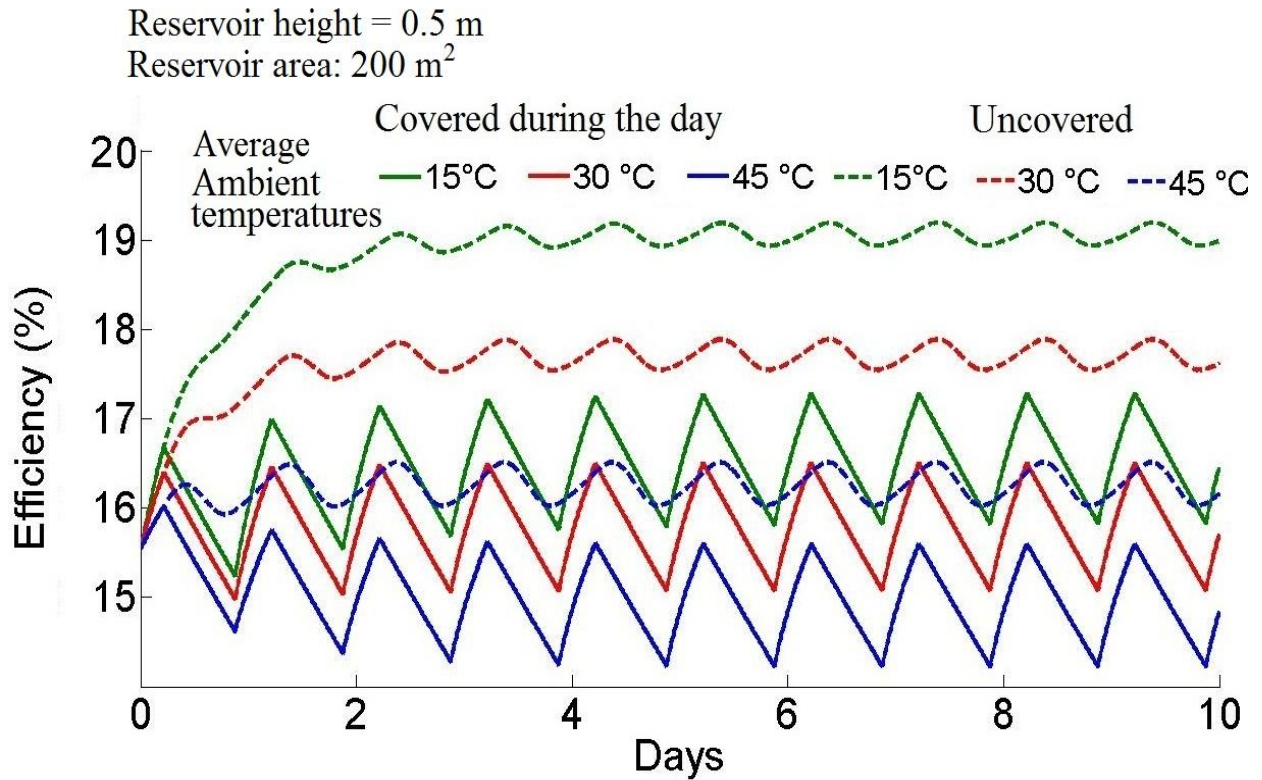
Figure 63. SRC efficiency for covered and uncovered cases.

The reason behind this behaviour is the heat loss due to evaporation. The heat gain during the day is compensated by the evaporative heat loss. However, the evaporative heat loss results in loss of water volume as well. So make up water is needed after the system has been operational for a prolonged period of time. Figure 64 shows the amount of water lost in kg for both covered and uncovered cases when the ambient temperature was 30°C. It can be observed that at night time the water loss from the reservoir which is covered during the day is more than the reservoir which stayed uncovered all the time. This is because the temperature of the covered reservoir was higher than the uncovered reservoir and hence the temperature gradient between the water and the ambient was more. This resulted in greater water loss at night. Nonetheless, the overall water loss was greater for the uncovered reservoir. The total amount of make-up water required for different ambient temperatures is given in Table 11. The area of the reservoir was

kept constant at 200 m$^2$. It can be observed that the water lost is a very small percentage of the total volume.
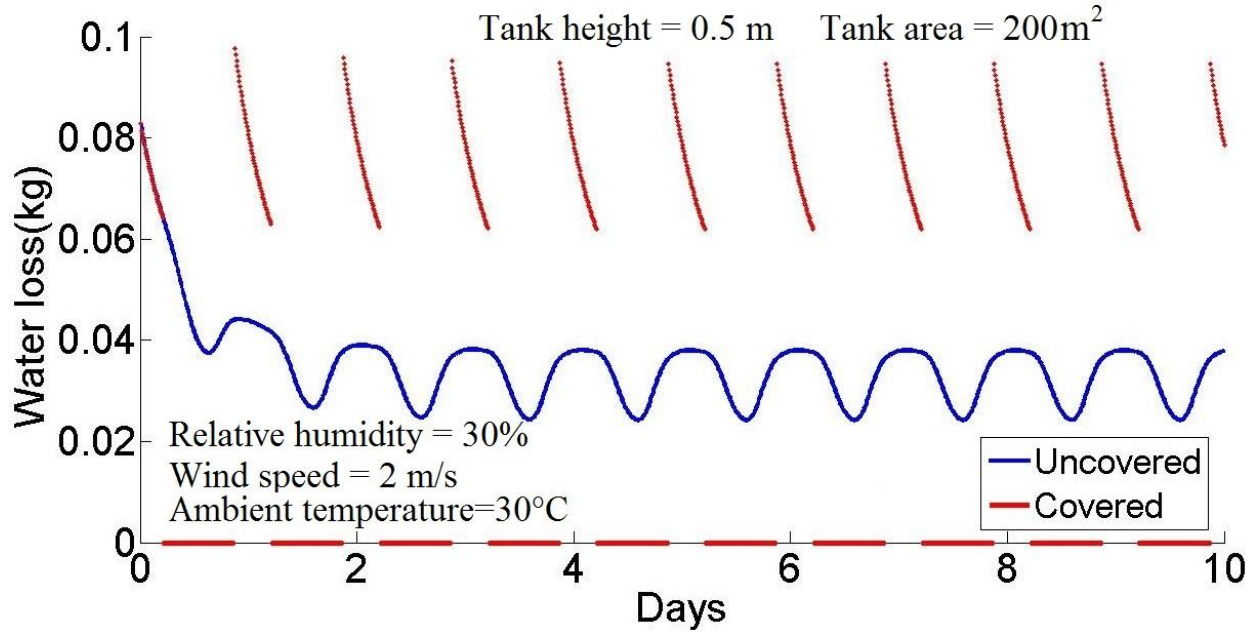


Figure 64. Water loss from the reservoir for covered and uncovered cases.

Table 11. Total water lost over 10 days.

| S. no. | Ambient temperature | Covered/Uncovered during the day | Total water loss over 10 days (kg) | Percentage loss for the whole volume |
|--------|---------------------|----------------------------------|-------------------------------------|--------------------------------------|
| 1 | 15°C | Covered | 33.2 | 0.06 |
| 2 | 15°C | Uncovered | 40.6 | 0.08 |
| 3 | 30°C | Covered | 37.5 | 0.07 |
| 4 | 30°C | Uncovered | 50.4 | 0.10 |
| 5 | 45°C | Covered | 41.5 | 0.08 |
| 6 | 45°C | Uncovered | 61.1 | 0.12 |

# CHAPTER 6: NOVEL CONDENSER DESIGN

## 6.1 Introduction

The different passive cooling techniques described in the previous chapter can be combined together to achieve superior performance of the condenser which affects the efficiency of the SRC much more significantly. In this chapter, two possible configurations of passive cooling systems have been presented that may be used for a novel condenser design and their effects on the SRC efficiency have been analyzed.

## 6.2 Condenser Design 1

In this configuration, the water in the storage tank is cooled by both underground cooling and radiative cooling. A schematic of such a configuration is shown in Figure 65. The reservoir stays uncovered all the time to allow cooling via convective and evaporative methods even during the day time and radiative cooling during the night. During the day, water from the reservoir is passed through underground pipes, if the underground soil temperature is lower than the water temperature, where it rejects heat. If the underground temperature gets higher than the water temperature, the water is not pumped through the underground pipes and only sky/air cooling is used. The cooled water from the reservoir is then directly used in a water cooled condenser for condensing the working fluid in the SRC. This condenser can be a shell-and-tube, double pipe or plate type heat exchanger. Detailed design of the heat exchanger is beyond the scope of this study.
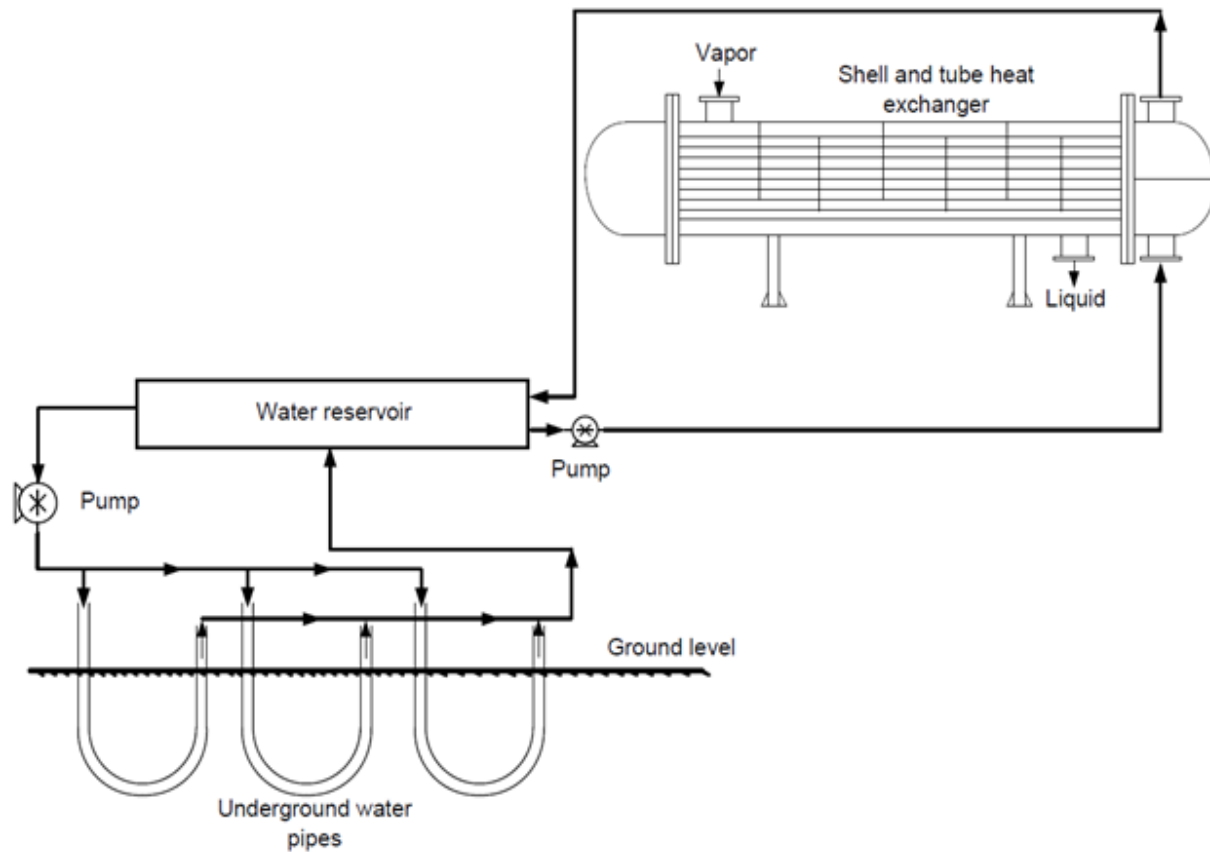
Figure 65. Schematic of configuration 1. Temperature in the shell-and-tube condenser is lowered by using passive cooling.

### 6.2.1 Results

The feasibility of using the configuration shown in Figure 65 was investigated for the condenser of a SRC. The operating parameters were selected based on the analyses of the previous chapters and are summarized in Table 12. The system was studied for an operating period of 5 days in July at Las Vegas when the ambient temperature is approximately 40 °C. The ambient conditions were obtained using the TMY3 data provided by NREL. It was assumed that the underground system was operational for 16 hours during the day and was turned off for 8 hours during the night to allow recharging of the soil temperature similar to the experimental and theoretical analysis by Goswami and Ileslamlou [100, 101]. Figure 66 and Figure 67 show the variation in reservoir temperature and the corresponding variation in the efficiency of the SRC,

87

respectively for different surface area of the reservoir. It can be observed that the efficiency of the system improved by 2-2.5% when the new condenser design with largest surface area was used. In for the smallest area, efficiency improved by 1-1.5%. Figure 68 (a) and (b) show the variation in reservoir temperature for different underground pipe area when the reservoir size was kept constant at 250 m$^2$ and 100 m$^2$. From figure (a), we notice that the effect of underground cooling was negligible when the reservoir size was large. However, for smaller size of the reservoir, cooling obtained by underground pipes became significant. The sudden change in the slope of the curve denotes the time when the ground cooling was turned on or off The corresponding efficiencies of the SRC are shown in Figure 69 (a) and (b). It can be observed that the efficiency improvement for larger reservoir area of 250 m$^2$ was only about 0.1% when the underground pipe area increased from 21 m$^2$ to 106 m$^2$ while it improved by 0.5% for the similar increase in the underground pipe area when the reservoir area was 100 m$^2$.

Table 12. Design and operating parameters used for the condenser.

| S. No. | Input parameter | Value |
|---|---|---|
| 1. | Location | Las Vegas |
| 2. | Average ambient temperature | 40°C |
| 3. | Tank height | 0.5 m |
| 4. | Underground pipe length | 100 m |
| 5. | Pipe diameter | 2.25 cm |
| 6. | Power capacity | 100 kW |
| 7. | Working fluid | R134a |
| 8. | Heat source temperature | 175 °C |
| 9. | Condenser heat exchanger effectiveness | 75% |
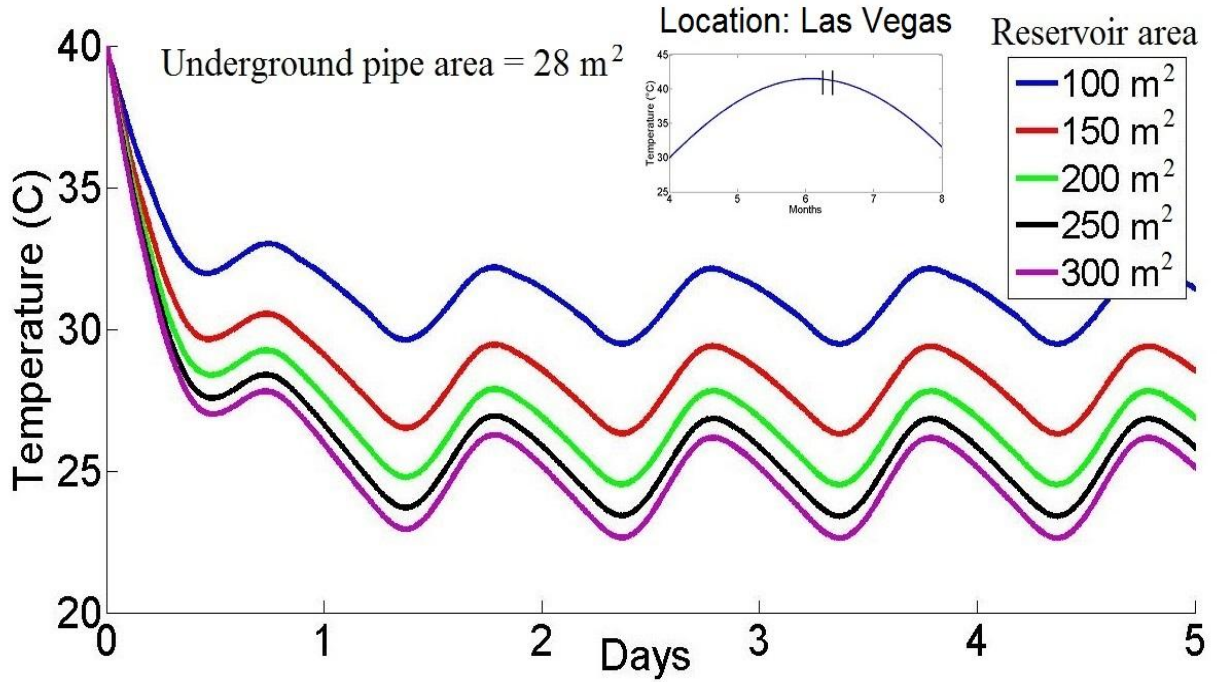
Figure 66. Water temperature variation for different reservoir area.
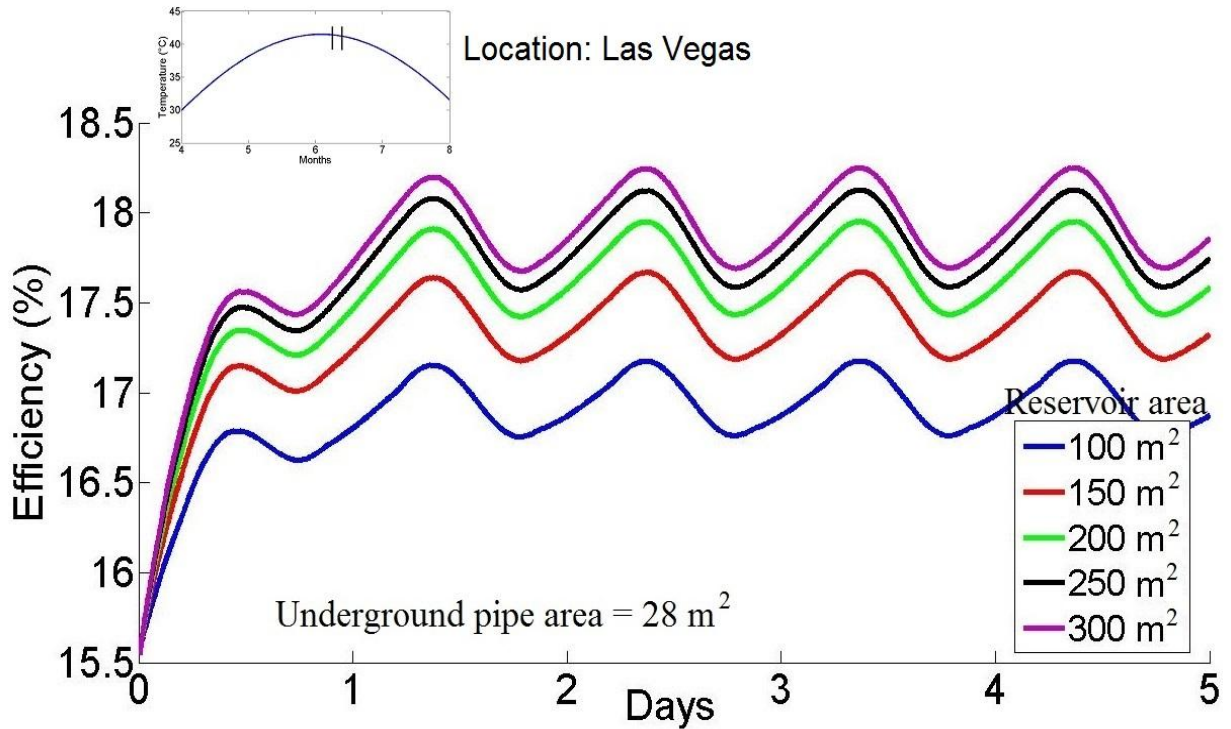


Figure 67. Efficiency of a 100 kW SRC for different reservoir area.
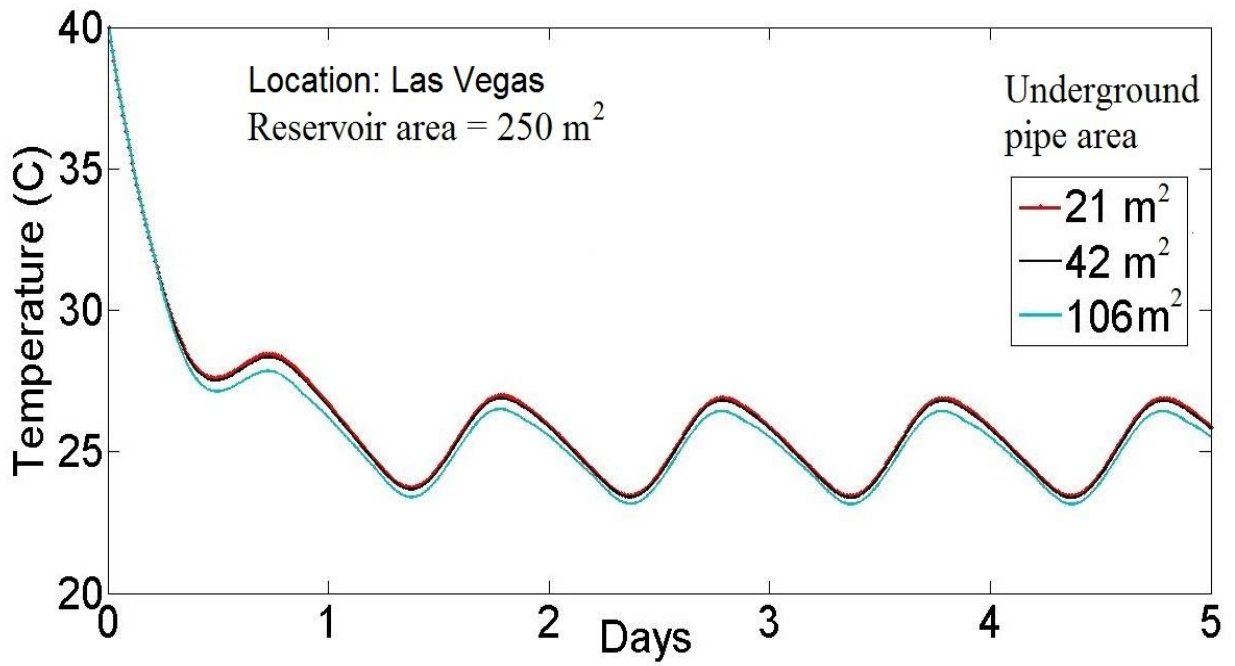
(a)
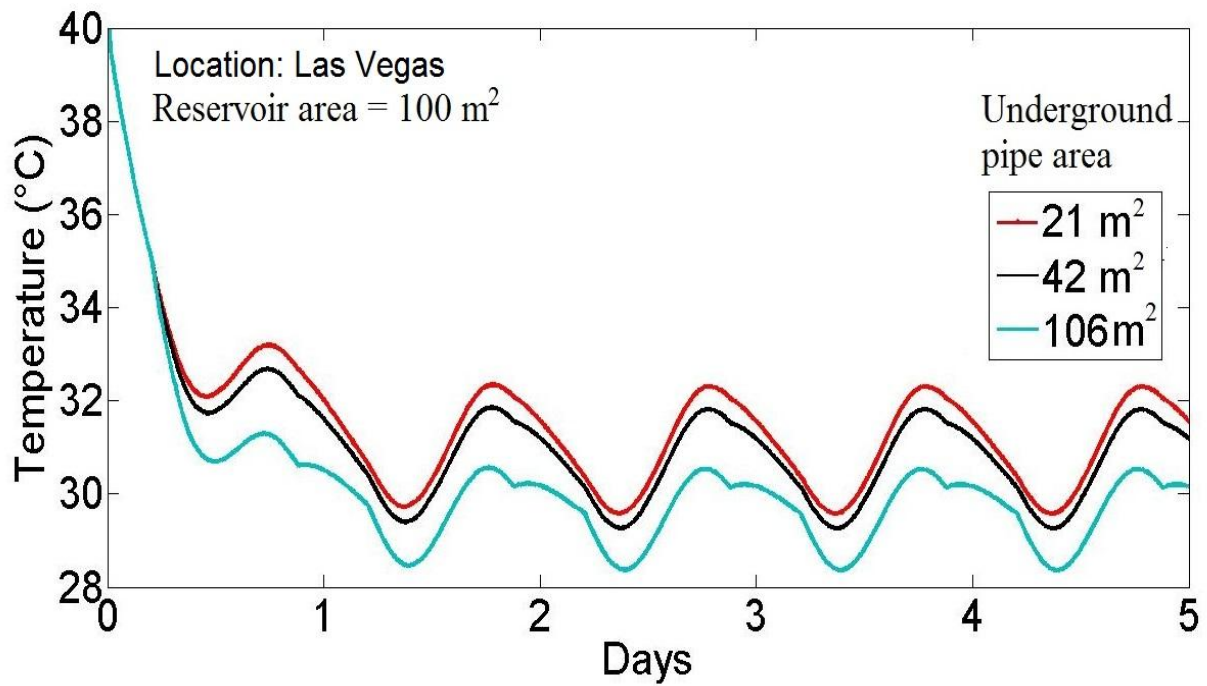


(b)

Figure 68. Effect of underground pipes on the reservoir temperature.
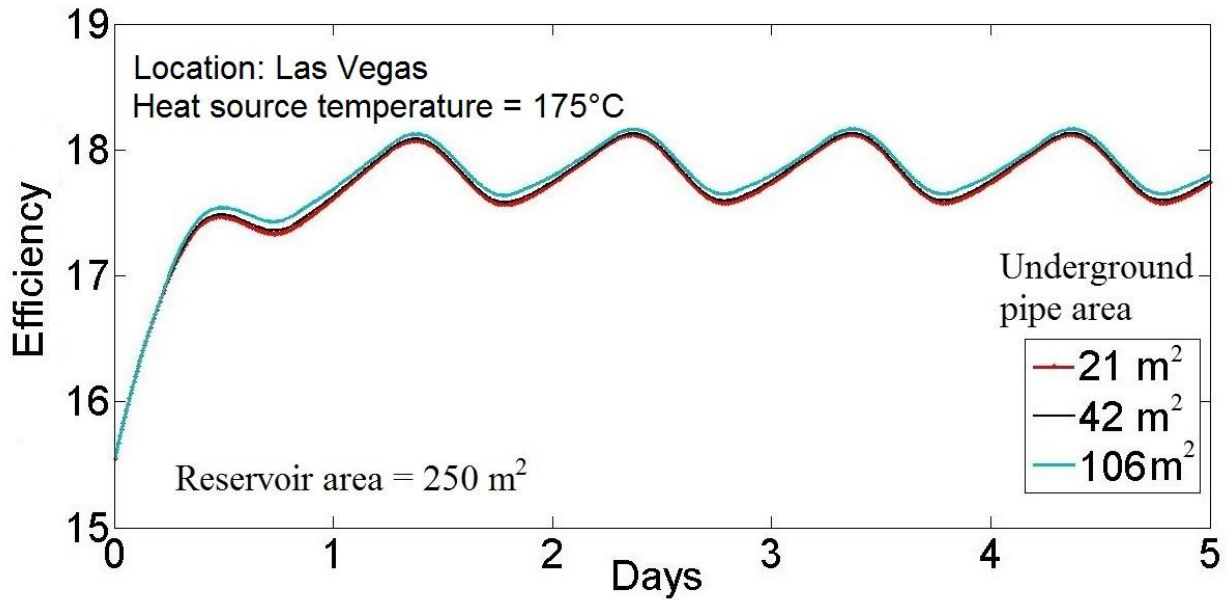
(a)
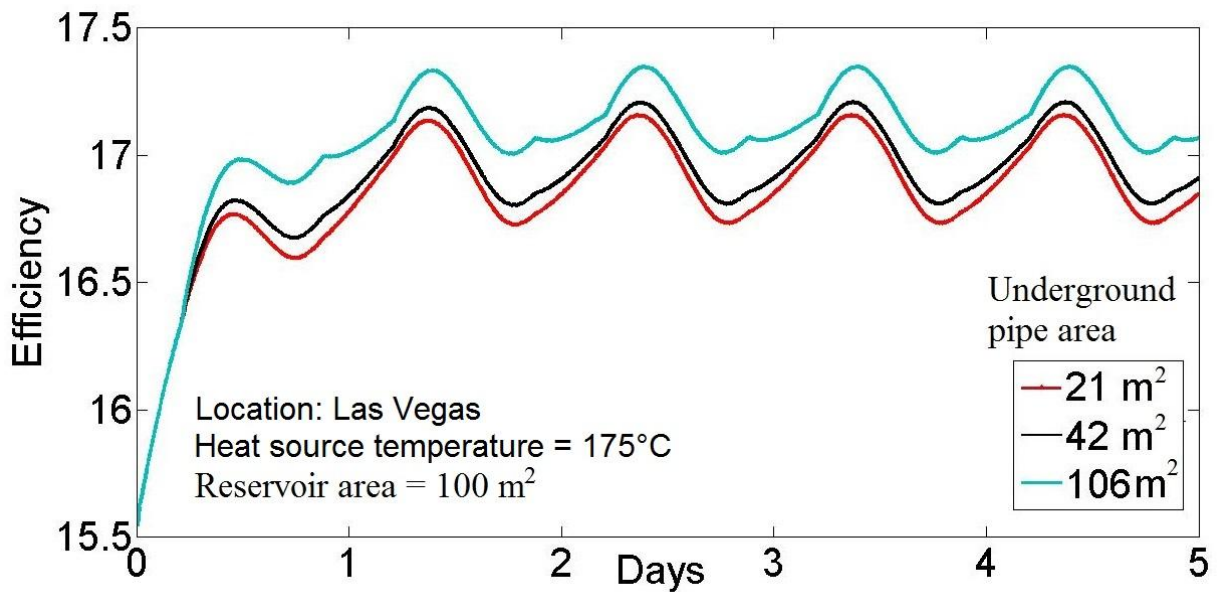


(b)

Figure 69. Effect of underground pipes on the efficiency of a 100 kW SRC.

Figure 70 and Figure 71 show the variation in the reservoir temperature when the system was operational for the whole year. The underground cooling system was used only when the difference in the soil temperature and the reservoir temperature was more than 5°C. The average heat transfer rate per unit power generation per unit area was calculated for both the technologies

91

for the time they were operation. It was 3.15 kW/kWe/m$^2$ due to the radiative cooling system was while for the ground cooling system, the value was 1.4 kW/kWe/m$^2$.
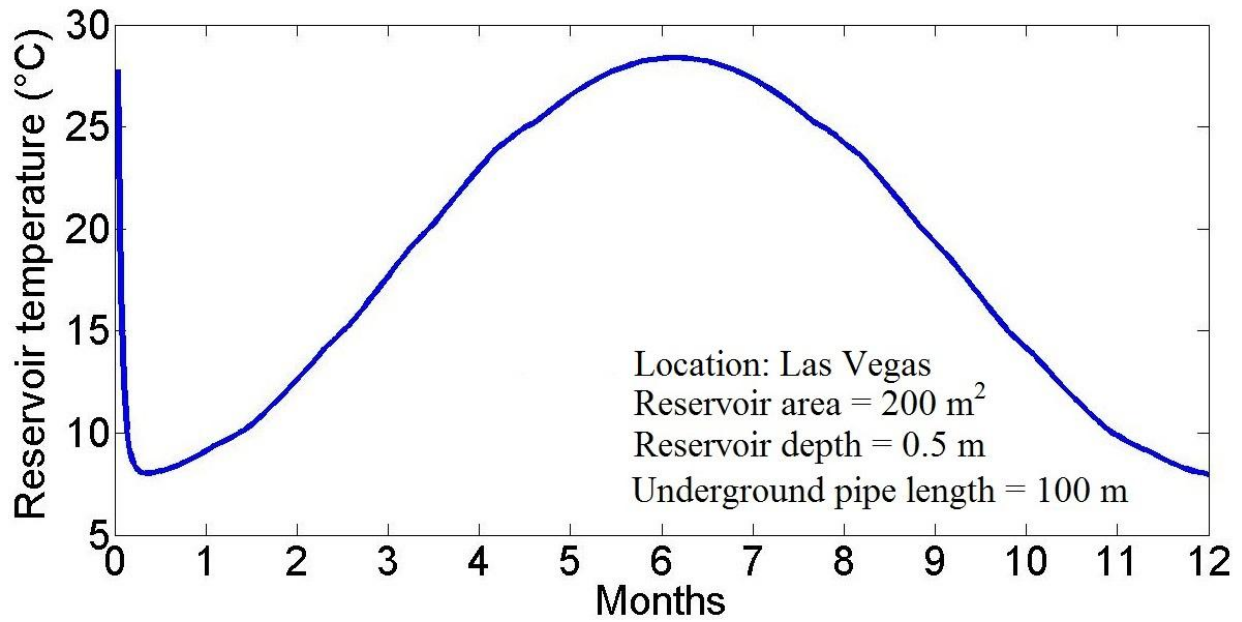


Figure 70. Reservoir temperature variation over a year.
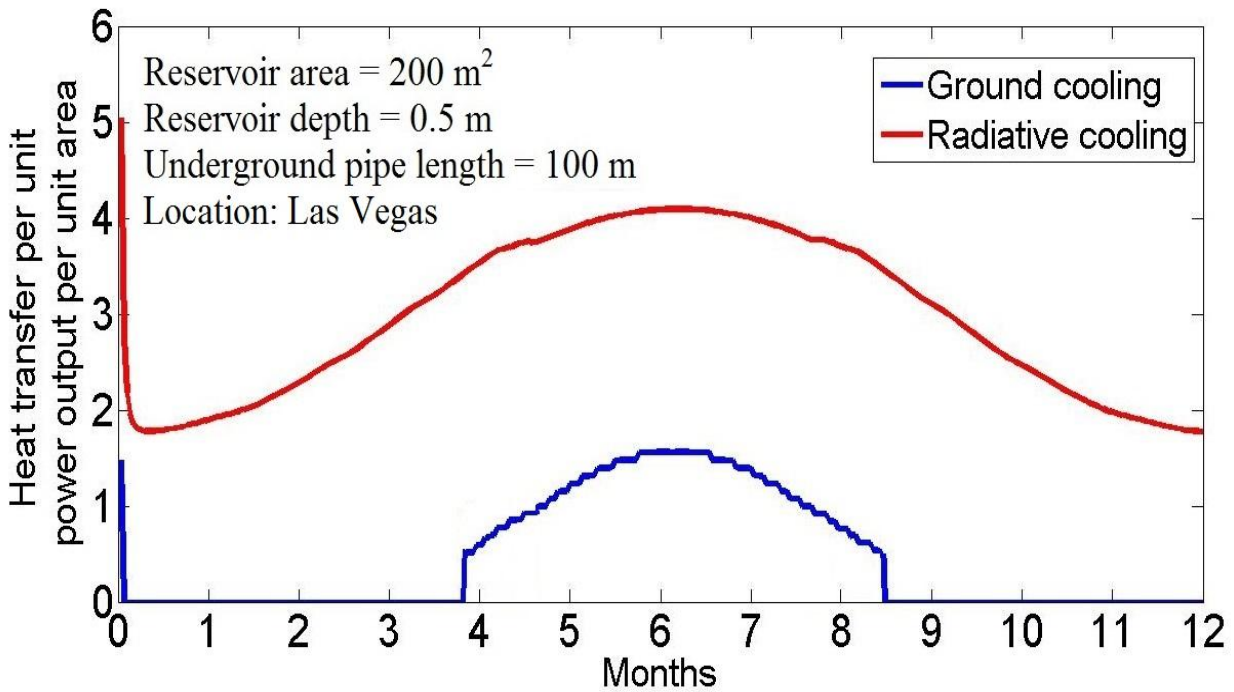


Figure 71. Comparison of heat transfer rate per unit power generation per unit area for ground cooling and radiative cooling over a year.

## 6.3 Condenser Design 2

In this design, the earth-air-heat-exchanger is coupled with an air-cooled condenser where the working fluid in vapor state enters at the top and the leaves from the bottom in liquid state as shown in Figure 72. Air coming out of the underground pipes in blown into the air-cooled condenser from the bottom. This configuration eliminates the use of water for the power plant application. At a location where water is not available, e.g. a solar power plant located in a desert area, or the use of water is not allowed by the local government due to environmental concerns, air-cooled condensers are the only option. So, this configuration can offer a solution by significantly improving the efficiency of the power plant without the need of any water. However, the system cannot be used continuously for a long period of time as the underground soil needs to be recharged. So, it is turned off at night and cooler night air is used directly in the air-cooled condenser.
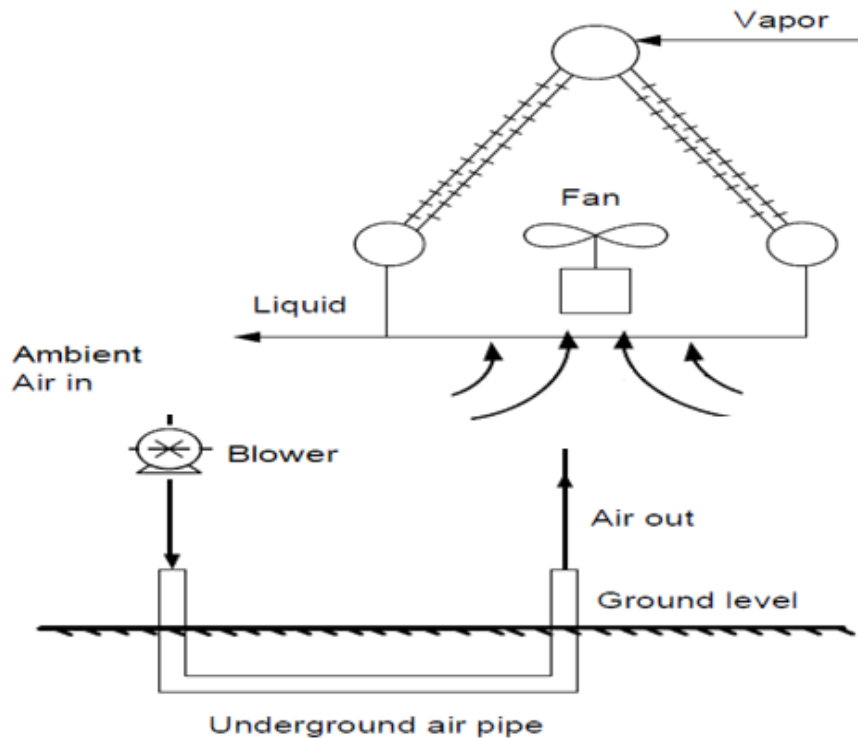


Figure 72. Schematic of configuration 2.

Selecting an efficient air-cooled condenser is also very important for this configuration. Several designs are already in market and more are being investigated. The most common design is a plate and fin type air-cooled condenser as shown in Figure 73[4]. The working fluid enters the condenser at the top and passes through the thin tubes while the cooling air is passed through the finned chambers to increase the contact area between the heat exchanging fluids. The condensed fluid is obtained at the bottom and is sent back to the SRC. The detailed optimization of the ACC depends on a number of factors, such as $X_L$, $X_T$, $X_D$ and fin pitch etc., which is beyond the scope of this study but can be found in a great detail in [222]



(a)



(b)
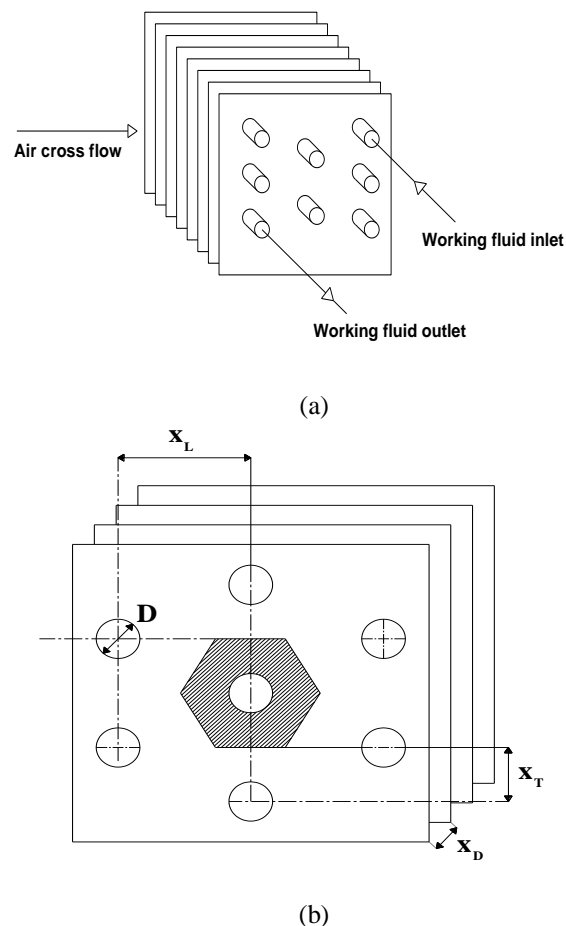
Figure 73. Schematic of a plate-fin-and-tube heat exchanger. (a) overall layout (b) hexagonal layout for a single fin with the description of major geometric aspects (redrawn from [223]).

---

[4] Figures were drawn by Pardeep Garg, Department of Mechanical Engineering, Indian Institute of Science, Bangalore, India.

### 6.3.1 Results

The condenser system was studied for 5 days in July for Las Vegas. It was assumed that the system was operational from 5:00 am to 9:00 am and was turned off for 8 hours during the night for thermal recharge of the underground soil [100, 101]. The ACC then had to use the ambient air directly, which was at relatively higher temperature. So, the efficiency of the SRC was lower during night as shown in Figure 74.
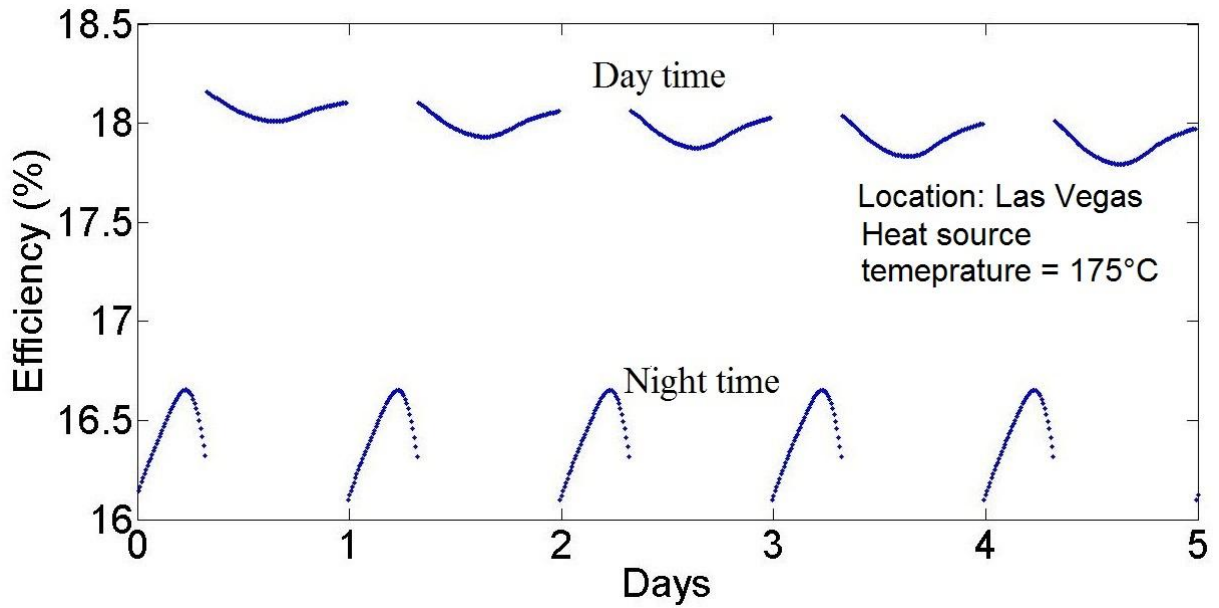


Figure 74. Efficiency of SRC for condenser design 2.

# CHAPTER 7: SUMMARY, CONCLUSIONS AND RECOMMENDATIONS

A supercritical Rankine cycle was analyzed for low temperature power generation and the feasibility of using a condenser coupled with passive cooling system was investigated. Six organic fluids were selected based on a previous study by Chen et al. where potential working fluids were screened for power generation applications and environmental safety. The optimum efficiency for each fluid at the given conditions is reported. Use of earth-air-heat-exchanger, ground coupled water cooling system and night sky radiative cooling and their effects on the SRC efficiency were studied.

The following conclusions can be made from this study:

- The optimum pressure ratio depends on the heat source temperature and increases with temperature.

- Among the working fluids considered in the analysis (R23, R32, R125, R134a, R143a, R170, R218), the highest efficiency was obtained for R134a for the source temperatures of 125-200°C.

- For higher condensation temperatures, the thermal efficiency is higher for lower pressure ratios.

- Use of an EAHE improves the efficiency of the SRC and reduces daily fluctuations.

- Larger depths of the EAHE improve the efficiency of the SRC but the improvement was negligible beyond a depth of 4 m.

- Temperature of soil 10 cm from the ground coupled heat exchanger increased by 2 °C

over four months. The increase in soil temperature resulted in a decrease in efficiency from 17.7% to 17.1%, a 3% decrease.

- Nocturnal cooling can be used to reject heat from a power plant. However, the effectiveness depends on the atmospheric conditions. Because of lack of experimental data, the study is inconclusive.

- When the reservoir was not covered during the day, additional cooling was obtained due to evaporation. However, the improvement in cooling needs to be weighed against the additional water loss associated with evaporation.

- The condensers coupled with the passive cooling systems improved the efficiency of the cycle by 2-2.5%. The average heat transfer rate per unit power generation per unit area due to the radiative cooling system was 3.15 $kW/kWe/m^2$ while for the ground cooling system, it was 1.4 $kW/kWe/m^2$.

- Nocturnal cooling model was validated with experimental data for a tank with a small depth in a humid climate due to lack of experimental data in the literature. So its accuracy for applications with large bodies of water and different climates is questionable. However, the performance for a dry location with less atmospheric pollution might be better than prediction from this model.

- The particulate matter in the atmosphere, such as aerosol, dust particles and other pollutants, that affect the performance were not considered in the model. Even though the experimental data was obtained for a city-based location, the application is expected to be at a low temperature power plant located far away from the city. So the performance will not be affected by the city air pollution. However, if it is located at a desert location, the sand particles will interfere with the overall performance of the cooling system.

## 7.1 Recommendations for Future Work

This study was performed to identify technical feasibility of the various systems. In order to implement the technologies described here, further practical details need to be analyzed including the economic analysis. The author recommends following direction for future work:

- Economic comparison of different working fluids over a long period of time should be done.

- Although mixtures didn't show any improvement compared to the pure working fluid in this study but it was limited to only two sets of mixtures. In order to better answer the question of pure working fluids vs. mixtures, additional mixtures of organic fluids should be investigated for other operating conditions to identify the best working fluid(s) for any given set of source and sink temperatures.

- An integrated model of the air-cooled and the water-cooled condensers with the passive cooling system should be developed for the complete system design.

- An economic analysis should be done to study the viability of using these cooling systems.

- Other configurations for passive cooling systems that have been described in the literature with detailed optimization of the air and water cooled condensers should be studied in the future. An example is shown in Figure 75 where the water in the reservoir is cooled by ground cooling and sky/air cooling. This cold water can then be used to cool the air before it enters an air-cooled condenser.
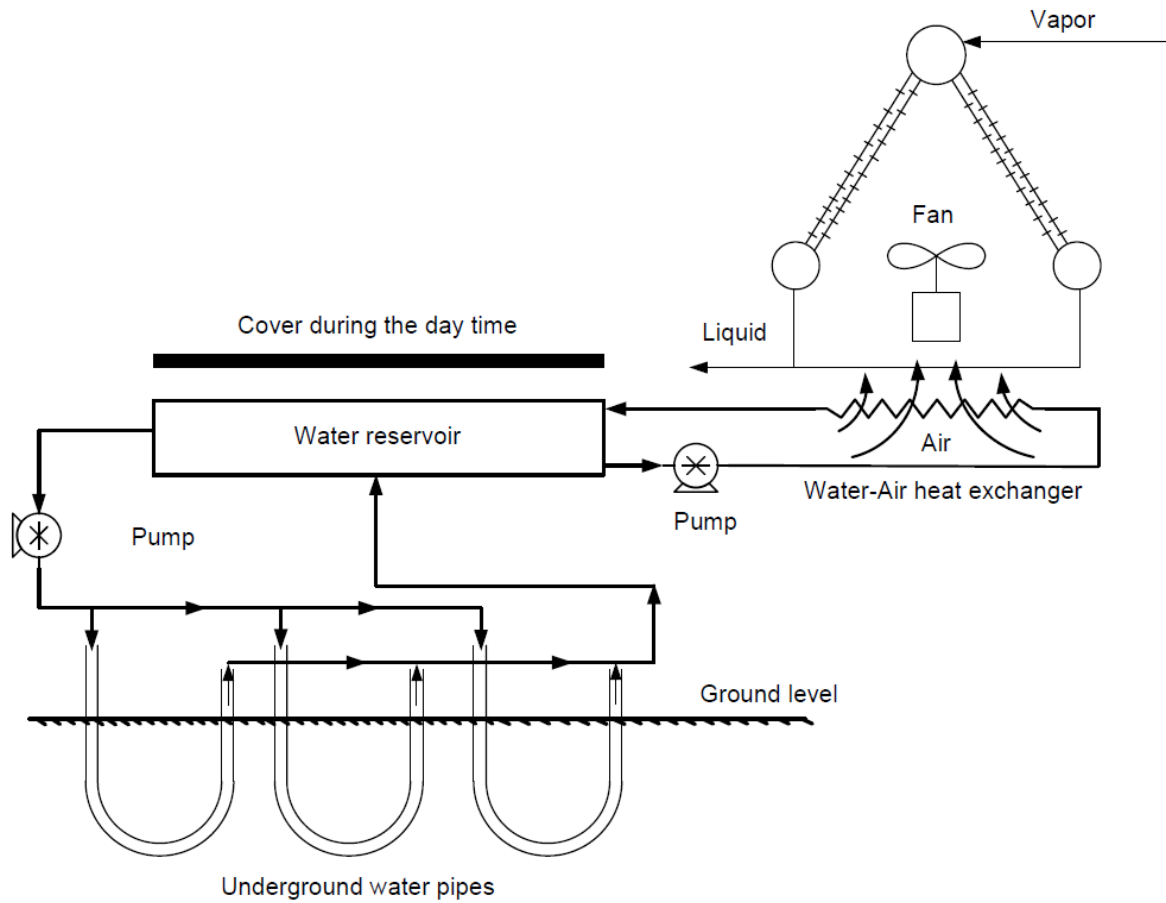
Figure 75. Schematic for configuration 3. Temperature in the air-cooled condenser is lowered by using passive cooling.

# REFERENCES

1.  Renner, J.L., *The future of geothermal energy.* 2006.

2.  Kalina, A.I. *Combined cycle and waste heat recovery power systems based on a novel thermodynamic energy cycle utilizing low-temperature heat for power generation.* 1983.

3.  Lu, S. and D.Y. Goswami, *Optimization of a novel combined power/refrigeration thermodynamic cycle.* Journal of Solar Energy Engineering, Transactions of the ASME, 2003. **125**(2): p. 212-217.

4.  Goswami, D.Y. and F. Xu, *Analysis of a new thermodynamic cycle for combined power and cooling using low and mid temperature solar collectors.* Journal of Solar Energy Engineering, Transactions of the ASME, 1999. **121**(2): p. 91-97.

5.  Vijayaraghavan, S. and D.Y. Goswami, *A combined power and cooling cycle modified to improve resource utilization efficiency using a distillation stage.* Energy, 2006. **31**(8-9): p. 1177-1196.

6.  Steidel, R.F., D.H. Pankow, and K.A. Brown, *The empirical modeling of a Lysholm screw expander.* 18th Intersociety Energy Conversion Engg. Conf. On Energy For The Marketplace, Orlando, U.S.A., 1983. **1**: p. 286-293.

7.  Andersen, W.C. and T.J. Bruno, *Rapid screening of fluids for chemical stability in organic rankine cycle applications.* Industrial and Engineering Chemistry Research, 2005. **44**(15): p. 5560-5566.

8.  Chen, H., D.Y. Goswami, and E.K. Stefanakos, *A review of thermodynamic cycles and working fluids for the conversion of low-grade heat.* Renewable and Sustainable Energy Reviews, 2010. **14**(9): p. 3059-3067.

9.  I.K. Smith, N.S., A. Kovacevic, *Power Recovery from Low Cost Two- Phase Expanders*, in *Expanders GRC Annual Meeting*. 2001.

10. Vidhi, R., et al., *Organic fluids in a supercritical rankine cycle for low temperature power generation.* Journal of Energy Resources Technology, Transactions of the ASME, 2013. **135**(4).

11. Saleh, B., et al., *Working fluids for low-temperature organic Rankine cycles.* Energy, 2007. **32**(7): p. 1210-1221.

12.      Chen, H., et al., *Energetic and exergetic analysis of CO 2- and R32-based transcritical Rankine cycles for low-grade heat conversion.* Applied Energy, 2011. **88**(8): p. 2802-2808.

13.      Borsukiewicz-Gozdur, A. and W. Nowak, *Comparative analysis of natural and synthetic refrigerants in application to low temperature Clausius-Rankine cycle.* Energy, 2007. **32**(4): p. 344-352.

14.      Cayer, E., N. Galanis, and H. Nesreddine, *Parametric study and optimization of a transcritical power cycle using a low temperature source.* Applied Energy, 2010. **87**(4): p. 1349-1357.

15.      Gu, Z. and H. Sato, *Optimization of cyclic parameters of a supercritical cycle for geothermal power generation.* Energy Conversion and Management, 2001. **42**(12): p. 1409-1416.

16.      Chen, H., et al., *A supercritical Rankine cycle using zeotropic mixture working fluids for the conversion of low-grade heat into power.* Energy, 2011. **36**(1): p. 549-555.

17.      Chacartegui, R., et al., *Alternative ORC bottoming cycles FOR combined cycle power plants.* Applied Energy, 2009. **86**(10): p. 2162-2170.

18.      Karellas, S. and A. Schuster, *Supercritical fluid parameters in organic rankine cycle applications.* International Journal of Thermodynamics, 2008. **11**(3): p. 101-108.

19.      Cayer, E., et al., *Analysis of a carbon dioxide transcritical power cycle using a low temperature source.* Applied Energy, 2009. **86**(7-8): p. 1055-1063.

20.      Ochs, T.L.A., OR, US), O'connor, William K. (Lebanon, OR, US), *Energy recovery during expansion of compressed gas using power plant low-quality heat sources*. 2006, The United States of America as represented by the United States Department of Energy (Washington, DC, US): United States.

21.      Augustine, C., et al. *Modeling and analysis of sub- and supercritical binary rankine cycles for low- to mid-temperature geothermal resources*. 2009.

22.      *Geothermal TEchnologies program: The Future of Geothermal Energy.*

23.      Abbaspour-Fard, M.H., A. Gholami, and M. Khojastehpour, *Evaluation of an earth-to-air heat exchanger for the north-east of Iran with semi-arid climate.* International Journal of Green Energy, 2011. **8**(4): p. 499-510.

24.      Santamouris, M., et al., *Use of buried pipes for energy conservation in cooling of agricultural greenhouses.* Solar Energy, 1995. **55**(2): p. 111-124.

25.      Trombe, A. and L. Serres, *Air-earth exchanger study in real site experimentation and simulation.* Energy and Buildings, 1994. **21**(2): p. 155-162.

26.     Said, S.A.M., et al., *Feasibility of using ground-coupled condensers in A/C systems.* Geothermics, 2010. **39**(2): p. 201-204.

27.     Bansal, N.K. and M.S. Sodha, *An earth-air tunnel system for cooling buildings.* Tunnelling and Underground Space Technology incorporating Trenchless, 1986. **1**(2): p. 177-182.

28.     Bansal, V., et al., *Performance analysis of earth-pipe-air heat exchanger for winter heating.* Energy and Buildings, 2009. **41**(11): p. 1151-1154.

29.     Bansal, V., et al., *Performance analysis of earth-pipe-air heat exchanger for summer cooling.* Energy and Buildings, 2010. **42**(5): p. 645-648.

30.     Ghosal, M.K., G.N. Tiwari, and N.S.L. Srivastava, *Thermal modeling of a greenhouse with an integrated earth to air heat exchanger: An experimental validation.* Energy and Buildings, 2004. **36**(3): p. 219-227.

31.     Sodha, M.S., et al., *Evaluation of an earth-air tunnel system for cooling/heating of a hospital complex.* Building and Environment, 1985. **20**(2): p. 115-122.

32.     Jacovides, C.P. and G. Mihalakakou, *An underground pipe system as an energy source for cooling/heating purposes.* Renewable Energy, 1995. **6**(8): p. 893-900.

33.     Lee, K.H. and R.K. Strand, *The cooling and heating potential of an earth tube system in buildings.* Energy and Buildings, 2008. **40**(4): p. 486-494.

34.     Mihalakakou, G., M. Santamouris, and D. Asimakopoulos, *On the cooling potential of earth to air heat exchangers.* Energy Conversion and Management, 1994. **35**(5): p. 395-402.

35.     Mihalakakou, G., M. Santamouris, and D. Asimakopoulos, *Use of the ground for heat dissipation.* Energy, 1994. **19**(1): p. 17-25.

36.     Santamouris, M., G. Mihalakakou, and D.N. Asimakopoulos, *On the coupling of thermostatically controlled buildings with ground and night ventilation passive dissipation techniques.* Solar Energy, 1997. **60**(3-4): p. 191-197.

37.     Al-Hemiddi, N., *Thermal performance of a roof-pond integrated to a building for heating during cold-winter desert climate conditions in Saudi Arabia.* International Journal of Ambient Energy, 1999. **20**(1): p. 45-52.

38.     Ali, A.H.H., *Passive cooling of water at night in uninsulated open tank in hot arid areas.* Energy Conversion and Management, 2007. **48**(1): p. 93-100.

39.     Al-Jamal, K., et al., *Passive cooling evaluation of roof pond systems.* Solar and Wind Technology, 1988. **5**(1): p. 55-65.

40.     Chávez, J.R.G., B. Givoni, and S. Mundet. *Cooling by roof pond with floating insulation in the hot humid climate of Veracruz, Mexico*. 2007.

41.     Chen, B., et al. *Evaluation and testing of the nebraska modified roof pond for severe heating and cooling environments*. 1986. Montreal, Que, Can: Pergamon Press.

42.     Kharrufa, S.N. and Y. Adil, *Roof pond cooling of buildings in hot arid climates.* Building and Environment, 2007. **43**(1): p. 82-89.

43.     Runsheng, T., Y. Etzion, and E. Erell, *Experimental studies on a novel roof pond configuration for the cooling of buildings.* Renewable Energy, 2003. **28**(10): p. 1513-1522.

44.     Sodha, M.S., et al., *Experimental validation of thermal model of open roof pond.* Building and Environment, 1981. **16**(2): p. 93-98.

45.     Tang, R. and Y. Etzion, *On thermal performance of an improved roof pond for cooling buildings.* Building and Environment, 2004. **39**(2): p. 201-209.

46.     Yellott, J.I., *Solar heating and cooling of homes.* Solar Energy Engineering, 1977: p. 365-383.

47.     Yellott, J.I. and J.P. Manzo, *Comfort cooling with solar energy.* Specif Eng, 1978. **39**(2): p. 94-99.

48.     DiPippo, R., *Geothermal Power Plants: Principles, Applications, Case Studies and Envirometnal Impact*. 2008: Elsevier Science & Technology.

49.     Zhang, X.R., H. Yamaguchi, and D. Uneno, *Experimental study on the performance of solar Rankine system using supercritical CO2.* Renewable Energy, 2007. **32**(15): p. 2617-2628.

50.     Zhang, X.R., et al. *Experimental performance analysis of supercritical CO2 thermodynamic cycle powered by solar energy*. 2006. Sendai.

51.     Zhang, X.R., et al., *Analysis of a novel solar energy-powered Rankine cycle for combined power and heat generation using supercritical carbon dioxide.* Renewable Energy, 2006. **31**(12): p. 1839-1854.

52.     Zhang, X.R., et al., *A feasibility study of CO2-based rankine cycle powered by solar energy.* JSME International Journal, Series B: Fluids and Thermal Engineering, 2006. **48**(3): p. 540-547.

53.     Mines, G.L., W.D. Swank, and C.J. Bliem, *Geothermal heat cycle research: Supercritical cycle with horizontal counterflow condenser*. 1987. OSTI ID: 6103409; DE87014878.

54.     Bliem, C.J. and G.L. Mines, *Advanced binary geothermal power plants: Limits of performance*. 1991. p. OSTI ID: 5982472; DE91010065.

55.     Bliem, C.J., Demuth, O.J., Mines, G.L., Whitbeck, J.F., et al., *Heat Cycle Research Experimental Program, FY-1985*. OSTI ID: 6414575; DE86003219.

56.     Mines, G.L. and C.J. Bliem, *Improving the efficiency of binary cycles*. 1988. OSTI ID: 6833071; DE88015108.

57.     Bliem, C.J., Mines, G.L., et al., *Initial results for supercritical cycle experiments using pure and mixed-hydrocarbon working fluids*. OSTI ID: 6562256; DE84017008.

58.     Bliem, C.J., Mines, G.L., et al., *Overview of recent activities in the Heat Cycle Research Program*. OSTI ID: 5657133; DE88005544.

59.     Bliem, C.J., Mines, G.L., et al., *Overview of the Heat Cycle Research project*. OSTI ID: 5627324; DE91014072.

60.     Bliem, C.J., *Performance and operability study of the Raft River 5 MW(e) pilot geothermal power plant steady-state behavior*. 1979. p. OSTI ID: 5814498.

61.     Bliem, C.J., Mines, G.L., et al., *Second law analysis of advanced power generation systems using variable temperature heat sources*. OSTI ID: 6390558; DE91001818.

62.     Bliem, C.J., Mines, G.L., et al., *Supersaturated Turbine Expansions for Binary Geothermal Power Plants*. OSTI ID: 891896.

63.     Bliem, C.J., Demuth, O.J., Mines, G.L., Swank, W.D., et al., *Vaporization at supercritical pressures and counterflow condensing of pure and mixed-hydrocarbon working fluids for geothermal power plants*. OSTI ID: 5641225; DE86011034.

64.     Bliem, C.J., Mines, G.L., et al., *Advanced binary geothermal power plants working fluid property determination and heat exchanger design*. OSTI ID: 6303098; DE89011144.

65.     Bliem, C.J., Mines, G.L., et al., *Geothermal heat cycle research supercritical cycle with counterflow condenser in different orientations*. OSTI ID: 5453385; DE90002014.

66.     Heberle, F. and D. Brüggemann, *Exergy based fluid selection for a geothermal Organic Rankine Cycle for combined heat and power generation.* Applied Thermal Engineering, 2010. **30**(11-12): p. 1326-1332.

67.     Guo, T., H. Wang, and S. Zhang, *Working fluids of a low-temperature geothermally-powered Rankine cycle for combined power and heat generation system.* Science China Technological Sciences, 2010. **53**(11): p. 3072-3078.

68.     Guo, T., H.X. Wang, and S.J. Zhang, *Fluids and parameters optimization for a novel cogeneration system driven by low-temperature geothermal sources.* Energy, 2011. **36**(5): p. 2639-2649.

69.     Guo, T., H.X. Wang, and S.J. Zhang, *Selection of working fluids for a novel low-temperature geothermally-powered ORC based cogeneration system.* Energy Conversion and Management, 2011. **52**(6): p. 2384-2391.

70.     Lakew, A.A. and O. Bolland, *Working fluids for low-temperature heat source.* Applied Thermal Engineering, 2010. **30**(10): p. 1262-1268.

71.     Maizza, V. and A. Maizza, *Working fluids in non-steady flows for waste energy recovery systems.* Applied Thermal Engineering, 1996. **16**(7): p. 579-590.

72.     Gawlik, K. and V. Hassani. *Advanced binary cycles: optimum working fluids*. 1997.

73.     Maizza, V. and A. Maizza, *Unconventional working fluids in organic Rankine-cycles for waste energy recovery systems.* Applied Thermal Engineering, 2001. **21**(3): p. 381-390.

74.     Angelino, G. and P. Colonna Di Paliano, *Multicomponent working fluids for organic Rankine cycles (ORCs).* Energy, 1998. **23**(6): p. 449-463.

75.     Wang, X.D. and L. Zhao, *Analysis of zeotropic mixtures used in low-temperature solar Rankine cycles for power generation.* Solar Energy, 2009. **83**(5): p. 605-613.

76.     Radermacher, R., *Thermodynamic and heat transfer implications of working fluid mixtures in Rankine cycles.* International Journal of Heat and Fluid Flow, 1989. **10**(2): p. 90-102.

77.     Bliem, C.J.M., G.L. Mines, *Supercritical binary geothermal cycle experiments with mixed-hydrocarbon working fluids and a near-horizontal in-tube condenser.* 1989. p. OSTI ID: 6532956; DE91001815.

78.     Vidhi, R., D.Y. Goswami, and E.K. Stefanakos, *Parametric Study of Supercritical Rankine cycle and Earth-Air-Heat-Exchanger for Low Temperature Power Generation*. Energy Procedia: SolarPACES, September, 2013.

79.     Vidhi, R., D.Y. Goswami, and E.K. Stefanakos, *Supercritical Rankine cycle coupled with ground cooling for low temperature power generation*. Energy Procedia: Solar World Congress, November, 2013.

80.     Yumrutaş, R. and M. Ünsal, *Energy analysis and modeling of a solar assisted house heating system with a heat pump and an underground energy storage tank.* Solar Energy, 2012. **86**(3): p. 983-993.

81.     Sanaye, S. and B. Niroomand, *Thermal-economic modeling and optimization of vertical ground-coupled heat pump.* Energy Conversion and Management, 2009. **50**(4): p. 1136-1147.

82.     Sanaye, S. and B. Niroomand, *Horizontal ground coupled heat pump: Thermal-economic modeling and optimization.* Energy Conversion and Management, 2010. **51**(12): p. 2600-2612.

83. Wang, H. and C. Qi, *Performance study of underground thermal storage in a solar-ground coupled heat pump system for residential buildings.* Energy and Buildings, 2008. **40**(7): p. 1278-1286.

84. Camdali, U. and E. Tuncel, *An Economic Analysis of Horizontal Ground Source Heat Pumps (GSHPs) For Use in Heating and Cooling in Bolu, Turkey.* Energy Sources, Part B: Economics, Planning, and Policy, 2013. **8**(3): p. 290-303.

85. Ally, M.R., et al., *Exergy analysis and operational efficiency of a horizontal ground-source heat pump system operated in a low-energy test house under simulated occupancy conditions.* International Journal of Refrigeration, 2012. **35**(4): p. 1092-1103.

86. Sanner, B., et al., *Current status of ground source heat pumps and underground thermal energy storage in Europe.* Geothermics, 2003. **32**(4–6): p. 579-588.

87. Mustafa Omer, A., *Ground-source heat pumps systems and applications.* Renewable and Sustainable Energy Reviews, 2008. **12**(2): p. 344-371.

88. Florides, G. and S. Kalogirou, *Ground heat exchangers—A review of systems, models and applications.* Renewable Energy, 2007. **32**(15): p. 2461-2478.

89. Ozgener, O. and L. Ozgener, *Exergoeconomic analysis of an underground air tunnel system for greenhouse cooling system.* International Journal of Refrigeration, 2010. **33**(5): p. 995-1005.

90. Ascione, F., L. Bellia, and F. Minichiello, *Earth-to-air heat exchangers for Italian climates.* Renewable Energy, 2011. **36**(8): p. 2177-2188.

91. Thiers, S. and B. Peuportier, *Thermal and environmental assessment of a passive building equipped with an earth-to-air heat exchanger in France.* Solar Energy, 2008. **82**(9): p. 820-831.

92. Ahmed, A., et al. *Thermal performance of earth-air heat exchanger for reducing cooling energy demand of office buildings in the United Kingdom*. 2009.

93. Al-Ajmi, F., D.L. Loveday, and V.I. Hanby, *The cooling potential of earth-air heat exchangers for domestic buildings in a desert climate.* Building and Environment, 2006. **41**(3): p. 235-244.

94. Ramírez-Dávila, L., et al., *Numerical study of earth-to-air heat exchanger for three different climates.* Energy and Buildings, 2014. **76**(0): p. 238-248.

95. Vaz, J., et al., *An experimental study on the use of Earth-Air Heat Exchangers (EAHE).* Energy and Buildings, 2014. **72**(0): p. 122-131.

96. Vaz, J., et al., *Experimental and numerical analysis of an earth-air heat exchanger.* Energy and Buildings, 2011. **43**(9): p. 2476-2482.

97.     Sinha, R.R., D.Y. Goswami, and D.E. Klett. *Theoretical and experimental analysis of cooling technique using underground air pipe*. 1982.

98.     Dhaliwal, A.S. and D.Y. Goswani. *Heat transfer analysis in environmental control using an underground air tunnel.* 1984. Las Vegas, NV, USA: ASME.

99.     Goswami, D.Y. and A.S. Dhaliwal, *Heat transfer analysis in environmental control using an underground air tunnel.* Journal of Solar Energy Engineering, Transactions of the ASME, 1985. **107**(2): p. 141-145.

100.    Goswami, D.Y. and S. Ileslamlou, *Performance analysis of a closed-loop climate control system using underground air tunnel.* Trans. ASME J. Solar Energy Engineering, 1990. **112**(2 , May, 1990): p. 76-81.

101.    Ileslamlou, S. and D.Y. Goswami. *Performance analysis of a closed-loop climate control system for residential and agricultural buildings using underground air tunnel*. 1987.

102.    Mihalakakou, G., M. Santamouris, and D. Asimakopoulos, *Modelling the earth temperature using multiyear measurements.* Energy and Buildings, 1992. **19**(1): p. 1-9.

103.    Mihalakakou, G., et al., *Impact of ground cover on the efficiencies of earth-to-air heat exchangers.* Applied Energy, 1994. **48**(1): p. 19-32.

104.    Mihalakakou, G., M. Santamouris, and D. Asimakopoulos, *Modelling the thermal performance of earth-to-air heat exchangers.* Solar Energy, 1994. **53**(3): p. 301-305.

105.    Mihalakakou, G., et al., *Parametric prediction of the buried pipes cooling potential for passive cooling applications.* Solar Energy, 1995. **55**(3): p. 163-173.

106.    Mihalakakou, G., J.O. Lewis, and M. Santamouris, *The influence of different ground covers on the heating potential of earth-to-air heat exchangers.* Renewable Energy, 1996. **7**(1): p. 33-46.

107.    Mihalakakou, G., et al., *On the application of the energy balance equation to predict ground temperature profiles.* Solar Energy, 1997. **60**(3-4): p. 181-190.

108.    Santamouris, M., et al., *On the performance of buildings coupled with earth to air heat exchangers.* Solar Energy, 1995. **54**(6): p. 375-380.

109.    Trombe, A., M. Pettit, and B. Bourret, *Air cooling by earth tube heat exchanger: Experimental approach.* Renewable Energy, 1991. **1**(5-6): p. 699-707.

110.    Eicker, U., *Cooling strategies, summer comfort and energy performance of a rehabilitated passive standard office building.* Applied Energy, 2010. **87**(6): p. 2031-2039.

111.    Eicker, U., et al., *Passive and low energy cooling of office buildings.* International Journal of Ventilation, 2005. **4**(3): p. 203-214.

112. Eicker, U., et al., *Limits and potentials of office building climatisation with ambient air.* Energy and Buildings, 2006. **38**(6): p. 574-581.

113. Ghosal, M.K. and G.N. Tiwari, *Modeling and parametric studies for thermal performance of an earth to air heat exchanger integrated with a greenhouse.* Energy Conversion and Management, 2006. **47**(13-14): p. 1779-1798.

114. Ghosal, M.K. and G.N. Tiwari, *Parametric studies for heating performance of an earth to air heat exchanger coupled with a greenhouse.* International Journal of Energy Research, 2005. **29**(11): p. 991-1005.

115. Goswami, J., *Dry Cooling in Solar Thermal Power Plants.* ASME Conference Proceedings, 2011. **2011**(54686): p. 663-670.

116. Kaushik, S.C. and G.S. Kumar, *Performance evaluation of an earth air tunnel for space heating of a non air-conditioned building.* International Journal of Ambient Energy, 1994. **15**(4): p. 205-218.

117. Mihalakakou, G., J.O. Lewis, and M. Santamouris, *On the heating potential of buried pipes techniques - Application in Ireland.* Energy and Buildings, 1996. **24**(1): p. 19-25.

118. Kumar, R., S. Ramesh, and S.C. Kaushik, *Performance evaluation and energy conservation potential of earth-air-tunnel system coupled with non-air-conditioned building.* Building and Environment, 2003. **38**(6): p. 807-813.

119. Kumar, R., S.C. Kaushik, and S.N. Garg, *Heating and cooling potential of an earth-to-air heat exchanger using artificial neural network.* Renewable Energy, 2006. **31**(8): p. 1139-1155.

120. Kumar, R., S.C. Kaushik, and A.R. Srikonda, *Cooling and heating potential of earth-air tunnel heat exchanger (EATHE) for non-air-conditioned building.* International Journal of Global Energy Issues, 2003. **19**(4): p. 373-386.

121. Puri, V.M., *Heat and mass transfer analysis and modeling in unsaturated ground soils for buried tube systems.* Energy in Agriculture, 1987. **6**(3): p. 179-193.

122. Badescu, V., *Simple and accurate model for the ground heat exchanger of a passive house.* Renewable Energy, 2007. **32**(5): p. 845-855.

123. Jacovides, C.P., et al., *On the ground temperature profile for passive cooling applications in buildings.* Solar Energy, 1996. **57**(3): p. 167-175.

124. Mihalakakou, G., *On estimating soil surface temperature profiles.* Energy and Buildings, 2002. **34**(3): p. 251-259.

125. Ozgener, L., *A review on the experimental and analytical analysis of earth to air heat exchanger (EAHE) systems in Turkey.* Renewable and Sustainable Energy Reviews, 2011. **15**(9): p. 4483-4490.

126.   Bisoniya, T.S., A. Kumar, and P. Baredar, *Experimental and analytical studies of earth-air heat exchanger (EAHE) systems in India: A review.* Renewable and Sustainable Energy Reviews, 2013. **19**: p. 238-246.

127.   Hamada, Y., et al., *Improved underground heat exchanger by using no-dig method for space heating and cooling.* Renewable Energy, 2007. **32**(3): p. 480-495.

128.   Zhang, J. and F. Haghighat, *Development of Artificial Neural Network based heat convection algorithm for thermal simulation of large rectangular cross-sectional area Earth-to-Air Heat Exchangers.* Energy and Buildings, 2010. **42**(4): p. 435-440.

129.   Kumar, R., et al., *A design optimization tool of earth-to-air heat exchanger using a genetic algorithm.* Renewable Energy, 2008. **33**(10): p. 2282-2288.

130.   Cucumo, M., et al., *A one-dimensional transient analytical model for earth-to-air heat exchangers, taking into account condensation phenomena and thermal perturbation from the upper free surface as well as around the buried pipes.* International Journal of Heat and Mass Transfer, 2008. **51**(3-4): p. 506-516.

131.   Sharan, G. and R. Jadhav, *Performance of Single Pass Earth-Tube Heat Exchanger: An Experimental Study*. 2003. Vol. 40. 2003.

132.   Tzaferis, A., et al., *Analysis of the accuracy and sensitivity of eight models to predict the performance of earth-to-air heat exchangers.* Energy and Buildings, 1992. **18**(1): p. 35-43.

133.   Gauthier, C., M. Lacroix, and H. Bernier, *Numerical simulation of soil heat exchanger-storage systems for greenhouses.* Solar Energy, 1997. **60**(6): p. 333-346.

134.   Liu, X., et al., *A fast and simple numerical model for a deeply buried underground tunnel in heating and cooling applications.* Applied Thermal Engineering, 2014. **62**(2): p. 545-552.

135.   Hollmuller, P. and B. Lachal, *Cooling and preheating with buried pipe systems: monitoring, simulation and economic aspects.* Energy and Buildings, 2001. **33**(5): p. 509-518.

136.   Hollmuller, P. and B. Lachal. *Buried pipe systems with sensible and latent heat exchange: Validation of numerical simulation against analytical solution and long-term monitoring*. 2005.

137.   Braud, H.J., H. Klimkowski, and F.E. Baker. *Earth-coupled heat pump and refrigeration design and applications*. 1986.

138.   Yoshino, H., et al. *Measurement of thermal performance of earth tube and its application to heat pump system*. 1992.

139.    Ozgener, O., A. Hepbasli, and L. Ozgener, *A parametric study on the exergoeconomic assessment of a vertical ground-coupled (geothermal) heat pump system.* Building and Environment, 2007. **42**(3): p. 1503-1509.

140.    Wu, H., S. Wang, and D. Zhu, *Modelling and evaluation of cooling capacity of earth-air-pipe systems.* Energy Conversion and Management, 2007. **48**(5): p. 1462-1471.

141.    Sanaye, S. and B. Niroomand, *Vertical ground coupled steam ejector heat pump; Thermal-economic modeling and optimization.* International Journal of Refrigeration, 2011. **34**(7): p. 1562-1576.

142.    *Geosource heat pump handbook. 2nd edition.* 1993, Econar Energy Systems.

143.    Eskilson, P., *Thermal Analysis of Heat Extraction Boreholes.* 1987: Lund University Press.

144.    Ozgener, O. and A. Hepbasli, *Performance analysis of a solar-assisted ground-source heat pump system for greenhouse heating: an experimental study.* Building and Environment, 2005. **40**(8): p. 1040-1050.

145.    Kavanaugh, S. *Optimization of vertical ground-coupled heat pumps.* 1984.

146.    Kavanaugh, S. *Design and performance of vertical ground coupled heat pump systems.* 1986.

147.    Kavanaugh, S. *Design method for commercial ground-coupled heat pumps.* 1995.

148.    Kavanaugh, S., *Water loop design for ground-coupled heat pumps.* ASHRAE Journal, 1996. **38**(5): p. 43-47.

149.    Kavanaugh, S., *Ground source heat pumps.* ASHRAE Journal, 1998. **40**(10): p. 31-36.

150.    Fujii, H., et al., *Numerical simulation and sensitivity study of double-layer Slinky-coil horizontal ground heat exchangers.* Geothermics, 2013. **47**(0): p. 61-68.

151.    Chong, C.S.A., et al., *Simulation of thermal performance of horizontal slinky-loop heat exchangers for ground source heat pumps.* Applied Energy, 2013. **104**(0): p. 603-610.

152.    Zarrella, A., A. Capozza, and M. De Carli, *Performance analysis of short helical borehole heat exchangers via integrated modelling of a borefield and a heat pump: A case study.* Applied Thermal Engineering, 2013. **61**(2): p. 36-47.

153.    Claesson, J. and P. Eskilson, *Conductive heat extraction to a deep borehole: Thermal analyses and dimensioning rules.* Energy, 1988. **13**(6): p. 509-527.

154.    Eskilson, P. and J. Claesson, *Simulation model for thermally interacting heat extraction boreholes.* Numerical heat transfer, 1988. **13**(2): p. 149-165.

155. Bertagnolio, S., M. Bernier, and M. Kummert, *Comparing vertical ground heat exchanger models.* Journal of Building Performance Simulation, 2012. **5**(6): p. 369-383.

156. Pasquier, P., et al. *Simulation of ground-coupled heat pump systems using a spectral approach*. 2013.

157. Zeng, H., N. Diao, and Z. Fang, *Heat transfer analysis of boreholes in vertical ground heat exchangers.* International Journal of Heat and Mass Transfer, 2003. **46**(23): p. 4467-4481.

158. Yang, H., P. Cui, and Z. Fang, *Vertical-borehole ground-coupled heat pumps: A review of models and systems.* Applied Energy, 2010. **87**(1): p. 16-27.

159. Bose, J.E., et al., *Design/data Manual for Closed-loop Ground-coupled Heat Pump Systems*. 1985: American Society of Heating, Refrigerating, and Air-Conditioning Engineers.

160. Hart, D.P. and R. Couvillion, *Earth-coupled Heat Transfer: Offers Engineers and Other Practitioners of Applied Physics the Information to Solve Heat Transfer Problems as They Apply to Earth-coupling*. 1986: National Water Well Association.

161. Lee, C.K. and H.N. Lam, *Computer simulation of borehole ground heat exchangers for geothermal heat pump systems.* Renewable Energy, 2008. **33**(6): p. 1286-1296.

162. Muraya, N.K., *Numerical modeling of the transient thermal interference of vertical U-tube heat exchangers*. 1994, Texas A&M University.

163. Li, Z. and M. Zheng, *Development of a numerical model for the simulation of vertical U-tube ground heat exchangers.* Applied Thermal Engineering, 2009. **29**(5–6): p. 920-924.

164. Li, Z., et al., *Experimental study of a ground sink direct cooling system in cold areas.* Energy and Buildings, 2009. **41**(11): p. 1233-1237.

165. Cimmino, M. and M. Bernier, *A semi-analytical method to generate g-functions for geothermal bore fields.* International Journal of Heat and Mass Transfer, 2014. **70**: p. 641-650.

166. Trillat-Berdal, V., B. Souyri, and G. Fraisse, *Experimental study of a ground-coupled heat pump combined with thermal solar collectors.* Energy and Buildings, 2006. **38**(12): p. 1477-1484.

167. Cui, P., H. Yang, and Z. Fang, *Numerical analysis and experimental validation of heat transfer in ground heat exchangers in alternative operation modes.* Energy and Buildings, 2008. **40**(6): p. 1060-1066.

168. Hamza H. Ali, A., I.M.S. Taha, and I.M. Ismail, *Cooling of water flowing through a night sky radiator.* Solar Energy, 1995. **55**(4): p. 235-253.

169.	Parker, D.S., *Theoretical evaluation of the night cool nocturnal radiation cooling concept. 2005*, *Submitted to U.S Department of Energy*, no. FSEC Contract 20126003.

170.	Sabbagh, J.A., A.M.A. Khalifa, and I.A. Olwi, *Development of passive dry cooling system for power plants in arid land.* Solar Energy, 1993. **51**(6): p. 431-447.

171.	Al-Nimr, M.A., Z. Kodah, and B. Nassar, *A theoretical and experimental investigation of a radiative cooling system.* Solar Energy, 1998. **63**(6): p. 367-373.

172.	Mahdavinia, M. and A. Molla Ebrahim, *The analysis of passive cooling strategies in Iranian traditional architecture: A case study in a hot and arid climate.* International Journal of Environmental Sustainability, 2013. **8**(3): p. 47-59.

173.	Erell, E. and Y. Etzion, *Radiative cooling of buildings with flat-plate solar collectors.* Building and Environment, 2000. **35**(4): p. 297-305.

174.	Khedari, J., et al., *Field investigation of night radiation cooling under tropical climate.* Renewable Energy, 2000. **20**(2): p. 183-193.

175.	Hay, H.R., Yellott John I., *International aspects of air conditioning with movable insulation.* 1969, Solar Energy. p. 427-438.

176.	Smith, G.B. and C.G.S. Granqvist, *Green Nanotechnology: Solutions for Sustainability and Energy in the Built Environment*. 2013: Taylor & Francis.

177.	Olwi, I.A., J.A. Sabbagh, and A.M.A. Khalifa, *Mathematical modeling of passive dry cooling for power plants in arid land.* Solar Energy, 1992. **48**(5): p. 279-286.

178.	Samuel, D.G.L., S.M.S. Nagendra, and M.P. Maiya, *Passive alternatives to mechanical air conditioning of building: Areview.* Building and Environment, 2013. **66**: p. 54-64.

179.	Meir, M.G., J.B. Rekstad, and O.M. LØvvik, *A study of a polymer-based radiative cooling system.* Solar Energy, 2002. **73**(6): p. 403-417.

180.	Martin, M. and P. Berdahl, *Characteristics of infrared sky radiation in the United States.* 1984, Solar Energy. p. 321-336.

181.	Molineaux, B., B. Lachal, and O. Guisan, *Thermal analysis of five outdoor swimming pools heated by unglazed solar collectors.* Solar Energy, 1994. **53**(1): p. 21-26.

182.	Erell, E. and Y. Etzion, *Analysis and experimental verification of an improved cooling radiator.* Renewable Energy, 1999. **16**(1-4 -4 pt 2): p. 700-703.

183.	Etzion, Y. and E. Erell, *Low-cost long-wave radiators for passive cooling of buildings.* Architectural Science Review, 1999. **42**(2): p. 79-86.

184.    Martin, M. and P. Berdahl, *The radiative cooling resource.* Proceedings of the passive and hybrid solar energy update, Washington, DC, 1983, (MCC Associates Inc., Silver Spring, MD), 1983: p. 39-46.

185.    Martin, M. and P. Berdahl, *Summary of results from the spectral and angular sky radiation measurement program.* 1984, Solar Energy. p. 241-252.

186.    Tang, R. and Y. Etzion, *Cooling performance of roof ponds with gunny bags floating on water surface as compared with a movable insulation.* Renewable Energy, 2005. **30**(9): p. 1373-1385.

187.    Tang, R., Y. Etzion, and I.A. Meir, *Estimates of clear night sky emissivity in the Negev Highlands, Israel.* Energy Conversion and Management, 2004. **45**(11-12): p. 1831-1843.

188.    Sodha, M.S., S.P. Singh, and A. Kumar, *Thermal performance of a cool-pool system for passive cooling of a non-conditioned building.* Building and Environment, 1985. **20**(4): p. 233-240.

189.    Clus, O., et al. *Computational fluid dynamic (CFD) applied to radiative cooled dew condensers.* 2006. Corte-Ajaccio.

190.    Jain, D., *Modeling of solar passive techniques for roof cooling in arid regions.* Building and Environment, 2006. **41**(3): p. 277-287.

191.    JH, W., C. WWs, and P. D., *Solar and wind induced external coefficient for solar collectors.* 1999, Comples.

192.    A., W., *Design factors influencing solar collectors, low temperature engineering application of solar energy.* 1967, American Society of Heating, Refrigerating and Airconditioning Engineers.: New York.

193.    Duffie, J.A. and W.A. Beckman, *Solar engineering of thermal process.* 1991, New York: Wiley.

194.    Rincón, J., N. Almao, and E. González, *Experimental and numerical evaluation of a solar passive cooling system under hot and humid climatic conditions.* Solar Energy, 2001. **71**(1): p. 71-80.

195.    Ito, S. and N. Miura, *Studies of radiative cooling systems for storing thermal energy.* Journal of Solar Energy Engineering, Transactions of the ASME, 1989. **111**(3): p. 251-256.

196.    Ito, S., N. Miura, and T. Takahashi, *Studies of a sky radiative thermosyphon cooling system for storing thermal energy.* Nippon Kikai Gakkai Ronbunshu, B Hen/Transactions of the Japan Society of Mechanical Engineers, Part B, 1987. **53**(487): p. 1102-1107.

197.    Spanaki, A., et al., *Theoretical and experimental analysis of a novel low emissivity water pond in summer.* Solar Energy, 2012. **86**(11): p. 3331-3344.

198. Dobson, R.T., *Thermal modelling of a night sky radiation cooling system.* Journal of Energy in Southern Africa, 2005. **16**(2): p. 56-67.

199. A.F., M., *Heat transfer.* 2001: Prentice Hall, Upper Saddle River, NJ.

200. Erell, E. and Y. Etzion, *Heating experiments with a radiative cooling system.* Building and Environment, 1996. **31**(6): p. 509-517.

201. Berdahl, P. and R. Fromberg, *The thermal radiance of clear skies.* 1982, Solar Energy. p. 299-314.

202. Berdahl, P. and M. Martin, *Emissivity of clear skies.* 1984, Solar Energy. p. 663-664.

203. Martin, M. and P. Berdahl, *Characteristics of infrared sky radiation in the United States.* Solar Energy, 1984. **33**(3-4): p. 321-336.

204. Centeno V, M., *New formulae for the equivalent night sky emissivity.* Solar Energy, 1982. **28**(6): p. 489-498.

205. Berger, X., D. Buriot, and F. Garnier, *About the equivalent radiative temperature for clear skies.* Solar Energy, 1984. **32**(6): p. 725-733.

206. Chen, B., et al. *Determination of the clear sky emissivity for use in cool storage roof and roof pond applications* in *Proceedings of the American Solar Energy Society.* 1991. Denver, CO.

207. Chen, B., et al., *Measurement of night sky emissivity in determining radiant cooling from cool storage roofs and roof ponds*, in *Proceedings of the National Passive Solar Conference*. 1995. p. 310-313.

208. National Renewable Energy Lab, S.R.R.L. *http://www.nrel.gov/midc/srrl_bms/*.

209. Wark, K., *Thermodynamics*. New York: McGraw-Hill.

210. Brown, J.S., *Predicting performance of refrigerants using the Peng-Robinson Equation of State.* International Journal of Refrigeration, 2007. **30**(8): p. 1319-1328.

211. Lemmon, E.W. and R.T. Jacobsen, *Equations of state for mixtures of R-32, R-125, R-134a, R-143a, and R-152a.* Journal of Physical and Chemical Reference Data, 2004. **33**(2): p. 593-620.

212. De Paepe, M. *3D unstructured finite volume technique for modelling earth air heat exchangers*. 2002.

213. Levit, H.J., R. Gaspar, and R.D. Piacentini, *Simulation of greenhouse microclimate produced by earth tube heat exchangers.* Agricultural and Forest Meteorology, 1989. **47**(1): p. 31-47.

214. Mihalakakou, G., et al., *On the ground temperature below buildings.* Solar Energy, 1995. **55**(5): p. 355-362.

215. Hollmuller, P., *Analytical characterisation of amplitude-dampening and phase-shifting in air/soil heat-exchangers.* International Journal of Heat and Mass Transfer, 2003. **46**(22): p. 4303-4317.

216. Chel, A. and G.N.Tiwari, *Performance evaluation and life cycle cost analysis of earth to air heat exchanger integrated with adobe building for New Delhi composite climate.* Energy and Buildings, 2009. **41**(1): p. 56-66.

217. Kakaç, S., H. Liu, and A. Pramuanjaroenkij, *Heat Exchangers: Selection, Rating, and Thermal Design, Second Edition*. 2002: Taylor & Francis.

218. Farmahini-Farahani, M. and G. Heidarinejad, *Increasing effectiveness of evaporative cooling by pre-cooling using nocturnally stored water.* Applied Thermal Engineering, 2012. **38**: p. 117-123.

219. Spanaki, A., T. Tsoutsos, and D. Kolokotsa, *On the selection and design of the proper roof pond variant for passive cooling purposes.* Renewable and Sustainable Energy Reviews, 2011. **15**(8): p. 3523-3533.

220. Tang, R. and Y. Etzion, *Comparative studies on the water evaporation rate from a wetted surface and that from a free water surface.* Building and Environment, 2004. **39**(1): p. 77-86.

221. Ward, A.D. and S.W. Trimble, *Environmental Hydrology, Second Edition*. 2003: Taylor & Francis.

222. K., I.M., *Dynamic Modeling and Control Strategies for a Micro-CSP Plant with Thermal Storage Powered by the Organic Rankine Cycle*. Masters thesis submiited in Massachusetts Institute of Technology, February 2014.

223. Wright, M.F., *Plate-Fin-And-Tube condenser performance and design for a refrigerant R-410 A air-conditioner*. 2000.

**APPENDICES**

## Appendix A: MATLAB Codes

### A.1 Thermodynamic Cycle

A MATLAB code was developed to model the thermodynamic cycle shown in Figure 15. This section shows the code that was used to analyze different components of the system. It was modified from the code first developed by Saeb M. Besarati[5].

```
clc
clear all

fluid = 'R134a.fld';              %Working Fluid

eta_p = 0.85;
eta_t = 0.85;
T0 = 0+273.15;                    % Reference temperature for exergy analysis (K)
Tsink = 30+273.15;                % Cooling water input temperature (K)
Tsinkout = Tsink+5;               % Cooling water output temperature (K)
Ts_out = 80+273.15;               % Source output temperature (K)
m = 1;                            % Mass flow rate of the working fluid (kg/sec)
eta_HX = 0.75;                    % Recuperator heat exchanger effectiveness

Pl = refpropm('P','T',Tsink+10,'Q',0,fluid);        % Cycle low pressure
Tcrit = refpropm('T','C',0,'',0,fluid);             % Critical Temperature
Pcrit = refpropm('P','C',0,'',0,fluid);             % Critical Pressure

i=1;
for(Ts_in = 125:5:175)                  % Source inlet temperature (C)

  Ts(i) = Ts_in+273.15;                 % Conversion to K
  j=1;

  for (Ph = 3000:100:7500)              % Cycle high pressure (kPa)

    % Pump inlet
    P1(j) = Pl;                         % kPa
    H1(j) = refpropm('H','P',Pl,'Q',0,fluid);       % J/kg
    S1(j) = refpropm('S','P',Pl,'Q',0,fluid);       % J/kg/K
    T1(j) = refpropm('T','P',Pl,'Q',0,fluid);       % K

    % Pump outlet
    P2(j) = Ph;
```

[5] Doctoral candidate in Chemical Engineering, University of South Florida, Tampa, FL.

```
S2(j) = S1(j);
H21(j) = refpropm('H','P',Ph,'S',S1(j),fluid);
H2(j) = H1(j)+((H21(j)-H1(j))/eta_p);
T2(j) = refpropm('T','P',Ph,'H',H2(j),fluid);
W_p(j) = (H2(j)-H1(j))/1000;              % kJ/kg


% Turbine input
P4(j) = Ph;
T4(j) = Ts(i)-10;
H4(j) = refpropm('H','T',T4(j),'P',Ph,fluid);
S4(j) = refpropm('S','T',T4(j),'P',Ph,fluid);


% Turbine output
S5(j) = S4(j);
P5(j) = Pl;
H51(j) = refpropm('H','P',P5(j),'S',S5(j),fluid);
H5(j) = H4(j)-eta_t*(H4(j)-H51(j));
T5(j) = refpropm('T','P',P5(j),'H',H5(j),fluid);
Hf = refpropm('H','P',P5(j),'Q',0,fluid);
Hg = refpropm('H','P',P5(j),'Q',1,fluid);
x5(j) = (H5(j)-Hf)/(Hg-Hf);

if (x5(j)<0.95)
        fprintf('Vapor quality at turbine outlet is low at pressure %0.2f \n',Ph);
end


P3(j) = Ph;
P6(j) = P5(j);


% Recuperator heat exchanger
if((T5(j)-T2(j))<5)
   T3(j) = T2(j);
   S3(j) = S2(j);
   H3(j) = H2(j);
   T6(j) = T5(j);
   S6(j) = S5(j);
   H6(j) = H5(j);

else
   H31(j) = refpropm('H','T',T5(j),'P',Ph,fluid);
   H61(j) = refpropm('H','T',T2(j),'P',Pl,fluid);
   Q1(j) = H31(j)-H2(j);
   Q2(j) = H5(j)-H61(j);
   Q(j) = min(Q1(j),Q2(j));

   H3(j) = H2(j)+eta_HX*Q(j);
```

```matlab
        T3(j) = refpropm('T','P',Ph,'H',H3(j),fluid);
        S3(j) = refpropm('S','P',Ph,'H',H3(j),fluid);

        H6(j) = H5(j)-eta_HX*Q(j);
        T6(j) = refpropm('T','P',Pl,'H',H6(j),fluid);
        S6(j) = refpropm('S','P',Pl,'H',H6(j),fluid);
        x6(j) = (H6(j)-Hf)/(Hg-Hf);

    end

    % Heat source
    T7(j) = Ts(i);
    P7(j) = refpropm('P','T',T7(j),'Q',0,'water');
    H7(j) = refpropm('H','T',T7(j),'Q',0,'water');
    S7(j) = refpropm('S','T',T7(j),'Q',0,'water');

    T8(j) = Ts_out;
    P8(j) = P7(j);
    H8(j) = refpropm('H','T',T8(j),'P',P8(j),'water');
    S8(j) = refpropm('S','T',T8(j),'P',P8(j),'water');
    m_hot(j) = m*(H4(j)-H3(j))/(H7(j)-H8(j));

    % Heat sink
    T9(j) = Tsink;
    H9(j) = refpropm('H','T',T9(j),'P',100,'water');
    S9(j) = refpropm('S','T',T9(j),'P',100,'water');
    Tcond(j) = refpropm('T','P',Pl,'Q',1,fluid);          % Temperature at    which working fluid
starts condensing
    Qw(j) = m*(H5(j)-H6(j));     % Heat taken out from the working fluid
    eta_cond = 0.8;              % Condenser heat exchanger effectiveness
    Qs(j) = eta_cond*Qw(j);
    T10(j) = Tsinkout;
    H10(j) = refpropm('H','T',T10(j),'P',100,'water');
    S10(j) = refpropm('S','T',T10(j),'P',100,'water');
    m_cool(j) = Qs(j)/(H10(j)-H9(j));           %Mass flow rate of the cooling water

    % Energy efficiency of the cycle
    W_t(j) = (H4(j)-H5(j))/1000;          %kJ/kg
    Qin(j) = (H4(j)-H3(j))/1000;          %kJ/kg
    W_net(j) = (W_t(j)-W_p(j));           %kJ/kg
    eff(j) = (W_t(j)-W_p(j))/Qin(j);      %Cycle efficiency


% Exergy Efficiency of the cycle
    E_t(j) = W_t(j)-T0*(S5(j)-S4(j))/1000;      % Exergy output from the turbine (kJ/kg)
```

```matlab
    E_p(j) = W_p(j)-T0*(S2(j)-S1(j))/1000;     % Exergy input in the pump (kJ/kg)
    Ex_net(j) = m*(E_t(j)-E_p(j));             % Net exergy output (kJ)
    E_h(j) = m_hot(j)*((H4(j)-H3(j))-T0*(S4(j)-S3(j)));   % Exergy input from the heat source
(kJ)
    effex(j) = (Ex_net(j))/(E_h(j));     % Exergy efficiency of the cycle

    % Exergy efficiency of evaporator
    E_fh(j) = m*((H4(j)-H3(j)-T0*(S3(j)-S2(j))));
    eta_ex_h(j) = E_fh(j)/E_h(j);

    % Exergy efficiency of the condenser
    E_c(j) = m_cool(j)*((H10(j)-H9(j))-T0*(S10(j)-S9(j)));
    E_fc(j) = m*((H6(j)-H1(j)-T0*(S6(j)-S1(j))));
    eta_ex_c(j) = E_c(j)/E_fc(j);

    % Total exergy efficiency
    eta_ex_tot(j) = effex(j)*eta_ex_h(j)*eta_ex_c(j);

    % Exergy in the recuperator
    E23(j) = (H3(j)-H2(j))-T0*(S3(j)-S2(j));
    E56(j) = (H6(j)-H5(j))-T0*(S6(j)-S5(j));
    pressure(j) = Ph;               % Pressure matrix

    j = j+1;

  end

  Pr(i) = pressure(eff==max(eff));   % Pressure at maximum efficiency
  eta(i) = max(eff)*100;             % Maximum energy efficiency for the given temperature
  eta_ex(i) = effex(eff==max(eff))*100;   % Exergy efficiency at maximum energy efficiency
for the given temperature

  i = i+1;
end

plot(Ts,eta)
```

## A.2 Earth-Air-Heat-Exchanger

This MATLAB code was used to model the earth-air-heat-exchanger shown in Figure 35.

```matlab
clc
clear all

% Geometry
d = 0.25;                % Diameter of pipe (m)
```

```matlab
L = 25;                % Length of pipe
l = 0.1;               % Differential length
Ap = l*2*pi*d/2;       % Circumferential area of the pipe element
R = d/2;               % Radius
Dp = 2;                % Depth


% Air Properties
m = 0.00222;                                  % Mass flow rate (kg/s)
rho = refpropm('D','T',300.15,'P',100,'air.ppf');   % Density of air
k1 = refpropm('L','T',300.15,'P',100,'air.ppf');    % Thermal conductivity
Cp = refpropm('C','T',300.15,'P',100,'air.ppf');    % Specific heat
Mu = refpropm('V','T',300.15,'P',100,'air.ppf');    % Viscosity
V = m/rho/3.1416/R^2;                         % Air velocity
Re_d = rho*V*d/Mu;                            % Reynold's number
Pr = Cp*Mu/k1;                                % Prandtl number


% Soil Properties
k = 0.159;             % Coefficient of thermal conductivity
Cp = 800;              % Specific heat (J/kg/K)
den = 1600;            % Density
alpha = k/Cp/den;      % Thermal diffusivity of soil (m2/sec)


% Temperature variations
Tb= 273.15+19.5;       % Yearly average bulk earth temperature
Tav= 273.15+19.5;      % Annual average air temperature
As = 10;               % Surface temperature amplitude
Aa = 20;               % Air temperature amplitude

t_total = 3600*24*365; % Total time (s)
t_step = 3600;         % Time step in seconds
t1_total = t_total/t_step;  % Total number of time steps
hour = t_step/3600;

% Initialization
Ts(1,1) = Tb;      % Surface temperature
T_soil(1,1,1) = Tb - As*exp(-Dp*(2*pi/365)*23.5)*sin(2*pi/365*(0-23.5*Dp)+pi/2);   % Initial
soil temperature at the given depth

q(1,1) = 0;            % Heat transfer rate before the flow starts
delta(1) = 0;          % Penetration depth before the flow starts
Te(1) = Tb - As*exp(-Dp*(2*pi/365)*23.5)*sin(2*pi/365*(0-23.5*Dp)+pi/2);   % Initial soil
temperature at the given depth
Tair(1) = Tav - Aa*sin(2*pi/365*(0)+pi/2);  % Initial air temperature

% Assigning memory
```

```matlab
T = Tav*ones(L/l,1);
Ts = Tb*ones(L/l,1);
q = 0*ones(L/l,1);
r(1) = R;
T_s = Tb;



t1 = 2;
while (t1<=t1_total)

    t = t1*t_step;
    days = floor(t/24/3600);
    time = t-24*3600*days;

    Te(t1) = Tb - As*exp(-Dp*(2*pi/365)*23.5)*sin(2*pi/365*(days-23.5*Dp)+pi/2);
    Tair(t1) = Tav - Aa*sin(2*pi/365*(days)+pi/2);

    %   ERB'S MODEL (1984)
    a=2*pi*(time/3600-1)/24;

    if(time<=16)

        T(1,t1)=Tair(t1)+15*(0.4632*cos(a-3.805)+0.0984*cos(2*a-0.360)+0.0168*cos(3*a-
0.822)+0.0138*cos(4*a-3.513));

    else
        T(1,t1) = Te(t1);
    end

    delta(t1)  = 2.3*sqrt(alpha*t);  % Penetration depth

    n = 2;
    while(n*l<=L)

        h = k1/d*0.023*(Re_d^0.8)*(Pr^0.33);
        U = Ap*h/m/Cp;

        % Assuming air remains unsaturated
        q(n,t1) = h*(T(n-1,t1-1)-Ts(n-1,t1-1));

        Ts(n,t1) = Te(t1) - q(n,t1)*R/k/(delta(t1)/R)*(1+delta(t1)/R-R/R)^2*(1/(delta(t1)/R +
2*log(1+delta(t1)/R)))*log(1/(1+delta(t1)/R));

        T(n,t1) = ((1-U/2)*T(n-1,t1) + U*Ts(n,t1))/(1+U/2);

        % Soil temperature variation around the pipe
```

```
    r1 = R/2;
    m1 = 2;

    while(m1*r1<2)

        r(m1) = r(m1-1)+r1;

        T_soil(n,t1,m1) = Te(t1)-q(n,t1)*R/k/(delta(t1)/R)*(1+delta(t1)/R-
r(m1)/R)^2*(1/(delta(t1)/R+2*log(1+delta(t1)/R)))*log(r(m1)/R/(1+delta(t1)/R));

        m1=m1+1;

    end

    n=n+1;

  end

  Temp(t1) = T(n-1,t1);

  if(Tair(t1)<Te(t1))

    Temp(t1)=Tair(t1);
    fprintf('Air is colder than soil \n');

  end

  t1=t1+1;

end

dlmwrite ('air_temp.rtf',Tair,'\n')
dlmwrite('outlet_l_10.rtf',Temp,'\n')
dlmwrite('ground_temp.rtf',Te,'\n')
dlmwrite('along_the_length',T(:,24*30),'\n')
```

## A.3 Ground Coupled Water Cooling

This MATLAB code was used to model the ground coupled water cooling system shown

in Figure 44.

```
clc
clear all

% Design inputs
```

```matlab
Di_GHX = 0.025;        % Inner diameter
Do_GHX = 0.03;         % Outer diameter
Tw1 = 35;              % Inlet water temperature
Tw2 = 30;              % Outlet water temperature

% Soil properties
Ts = 25;               % Mean soil temperature
Ks = 0.54;             % Thermal conductivity
Us = 12;               % Overall heat transfer coefficient

i = 1;

for(n = 1:10)

   % System operational inputs
   Qc = 4.1/0.85*1000;         % Cooling load  Qs(eff==max(eff))/wnet(eff==max(eff))/Heat
exchanger effectiveness
   Qb=Qc/n;

   % Water properties
   Kw = 0.623;                 % Thermal conductivity (W/m-K)
   mu = 719.13 * 10^(-6);      % Dynamic viscosity (Pa-s)
   rho = 994;                  % Density (kg/m3)
   Cpw = 4179.3;               % Specific heat
   mw = Qb/Cpw/(Tw1-Tw2);      % Mass flow rate of water
   vw = mw/rho*4/pi/Di_GHX^2;
   Re = rho*vw*Di_GHX/mu;
   Pr = Cpw*mu/Kw;
   Nu = 0.023 * Re^0.8 * Pr^0.33;
   hw = Kw/Di_GHX*Nu;

   % Resistance due to water flow
   Rw = 1/(2*hw*pi*Di_GHX);

   % Resistance due to pipe wall
   Kp = 0.3979;       %Thermal conductivity of polyethylene pipe (W/m-K)
   Rp = log(Do_GHX/Di_GHX)/(4*pi*Kp);

   % Resistance due to soil
   F = 580/1225;
   Rs = F/(2*pi*Us*Do_GHX);

   % Length of pipe needed
   L(i) = Qb / ((Tw1+Tw2)/2-Ts) * (Rw+Rp+Rs);
   Area(i) = L(i)*pi*(Di_GHX+Do_GHX)^2/4*n;
   N0(i) = n;
```

```
    Ltotal(i) = L(i)*n;

    i=i+1;

end

plot(L,'o')
```

## A.4 Night Sky Radiative Cooling

This MATLAB code was used to model the night sky radiative cooling system described

in section 5.4.

```
clc
clear all

phi = 0.3;      % Relative humidity (%) (20 in summer, 30 in winter)
v = 2.0;        % Wind speed (m/s) (4 in summer, 2 in winter)
hc = 2.8+3*v;   % Convective heat transfer coefficient

H = 0.5;        % Height of the tank (m)
rhow = 998;     % Density of water (kg/m3)
Cpw = 4186;     % Specific heat of water
ew = 0.9;
sig = 5.67*10^(-8); %J/s/m2/K4


Tair = 5;

Tw(1) = 40;
t_total = 8*3600;
t0 = 60;
i_total = t_total/t0;

i=1;

while(i<=i_total)

    t(i) = i*t0;  %Time
    a1(i) = 2*pi*(t(i)/3600-1)/24;    %Erb's model parameter for daily temperature variation
    Ta(i) = Tair+15*(0.4632*cos(a1(i)-3.805)+0.0984*cos(2*a1(i)-0.360)+0.0168*cos(3*a1(i)-
0.822)+0.0138*cos(4*a1(i)-3.513)); %(C)
    Pa(i) = 3385.5*exp(-8.0929+0.97608*(Ta(i)+42.607)^0.5);
    Pw(i) = 3385.5*exp(-8.0929+0.97608*(Tw(i)+42.607)^0.5);
```

```matlab
    % Sky temperature calculation
    y(i) = 1/17.27*log(phi) + Ta(i)/(237.3+Ta(i));
    Tdp(i) = 237.3*y(i)/(1-y(i));  % Dew point temperature (C)
    esky(i) = 0.741 + 0.0062*Tdp(i);          % Sky emissivity
    Tsky(i) = esky(i)^0.25 * (Ta(i)+273);        % Sky temperature (K)

    % Heat transfer rates
    Qc(i) = hc*(Ta(i) - Tw(i));                  % Convectiv gain
    Qe(i) = (0.2253+0.2464*v)*(Pw(i)-phi*Pa(i))^0.82;  % Evaporative loss
    Qr(i) = ew*sig*((Tw(i)+273)^4-Tsky(i)^4);        % Radiative loss
    Q(i) = Qc(i) - Qe(i) - Qr(i);

    i=i+1;

    Tw(i) = Tw(i-1) + t0*Q(i-1)/H/rhow/Cpw;       % Water temperature (C)

end
```

## A.5 SRC with Nocturnal Cooling

This MATLAB code was used to model efficiency improvement in the SRC when combined with nocturnal cooling.

```matlab
clc
clear all

% SRC parameters
fluid = 'R134a.fld';     %Working Fluid
eta_p = 0.85;
eta_t = 0.85;
T0 = 0+273.15;                  % Reference temperature for exergy analysis (K)
Ts_out = 80+273.15;             % Source output temperature (K)
m = 3;                          % Mass flow rate of the working fluid (kg/sec)
m_cool = 21;                    % Mass flow rate of cooling water (kg/sec)
eta_HX = 0.75;                  % Recuperator heat exchanger effectiveness
Tcrit = refpropm('T','C',0,'',0,fluid);         % Critical Temperature
Pcrit = refpropm('P','C',0,'',0,fluid);         % Critical Pressure
Ts_in = 175;                    % Source inlet temperature (C)
Ts = Ts_in+273.15;              % Conversion to K

% Nocturnal cooling system parameters
phi = 0.3;        % Relative humidity (%)
v = 2;            % Wind speed (m/s)
H = 0.5;          % Height of the tank (m)
L = 20;           % Length of the tank (m)
```

```matlab
W = 20;          % Width of the tank (m)
A = L*W;         % Top surface area
rhow = 998;      % Density of water (kg/m3)
Cpw = 4186;      % Specific heat of water
ew = 0.9;        % Emissivity of reservoir
sig = 5.67*10^(-8);     %J/s/m2/K4
Tair = 30;       % Average ambient temperature
hc = 2.8+3*v;  % Convective heat transfer coefficient

Tw(1) = 40;
Tsink(1) = 40;
t_total = 24*10*3600;
t0 = 600;
i_total = t_total/t0;

i=1;
while(i<=i_total)

    t(i) = i*t0;  %Time
    days (i) = floor(t(i)/24/3600);
    time(i)=t(i)-24*3600*days(i);
    a1(i) = 2*pi*(t(i)/3600-1)/24;    %Erb's model parameter for daily temperature variation
    Ta(i) = Tair+15*(0.4632*cos(a1(i)-3.805)+0.0984*cos(2*a1(i)-0.360)+0.0168*cos(3*a1(i)-
0.822)+0.0138*cos(4*a1(i)-3.513)); %(C)
    Pa(i) = 3385.5*exp(-8.0929+0.97608*(Ta(i)+42.607)^0.5);
    Pw(i) = 3385.5*exp(-8.0929+0.97608*(Tw(i)+42.607)^0.5);

    % Sky temperature calculation
    y(i) = 1/17.27*log(phi) + Ta(i)/(237.3+Ta(i));
    Tdp(i) = 237.3*y(i)/(1-y(i));  % Dew point temperature (C)
    esky(i) = 0.741 + 0.0062*Tdp(i);          % Sky emissivity
    Tsky(i) = esky(i)^0.25 * (Ta(i)+273);        % Sky temperature (K)

    % If the reservoir is covered during the day
    if(time(i)<=5*3600 || time(i)>=21*3600)
        % Heat transfer rates
        Qc(i) = A*hc*(Ta(i) - Tw(i));                    % Convective gain
        Qe(i) = A*(0.2253+0.2464*v)*(Pw(i)-phi*Pa(i))^0.82;  % Evaporative loss
        Qr(i) = A*ew*sig*((Tw(i)+273)^4-Tsky(i)^4);          % Radiative loss

    else
        Qc(i) = 0;
        Qe(i) = 0;
        Qr(i) = 0;
    end
%
```

```matlab
%     % If the reservoir stays uncovered all the time
%     Qc(i) = A*hc*(Ta(i) - Tw(i));                    % Convective gain
%     Qe(i) = A*(0.2253+0.2464*v)*(Pw(i)-phi*Pa(i))^0.82;  % Evaporative loss
%     Qr(i) = A*ew*sig*((Tw(i)+273)^4-Tsky(i)^4);          % Radiative loss
%
%
    % SRC optimization
    Pl(i) = refpropm('P','T',Tw(i)+273.15,'Q',0,fluid);% Cycle low pressure

    j=1;

    for (Ph = 3000:100:7500)                % Cycle high pressure (kPa)

        % Pump inlet
        P1(j) = Pl(i);                          % kPa
        H1(j) = refpropm('H','P',Pl(i),'Q',0,fluid);      % J/kg
        S1(j) = refpropm('S','P',Pl(i),'Q',0,fluid);      % J/kg/K
        T1(j) = refpropm('T','P',Pl(i),'Q',0,fluid);      % K

        % Pump outlet
        P2(j) = Ph;
        S2(j) = S1(j);
        H21(j) = refpropm('H','P',Ph,'S',S1(j),fluid);
        H2(j) = H1(j)+((H21(j)-H1(j))/eta_p);
        T2(j) = refpropm('T','P',Ph,'H',H2(j),fluid);
        W_p(j) = (H2(j)-H1(j))/1000;                 %kJ/kg

        % Turbine input
        P4(j) = Ph;
        T4(j) = Ts-10;
        H4(j) = refpropm('H','T',T4(j),'P',Ph,fluid);
        S4(j) = refpropm('S','T',T4(j),'P',Ph,fluid);

        % Turbine output
        S5(j) = S4(j);
        P5(j) = Pl(i);
        H51(j) = refpropm('H','P',P5(j),'S',S5(j),fluid);
        H5(j) = H4(j)-eta_t*(H4(j)-H51(j));
        T5(j) = refpropm('T','P',P5(j),'H',H5(j),fluid);
        Hf = refpropm('H','P',P5(j),'Q',0,fluid);
        Hg = refpropm('H','P',P5(j),'Q',1,fluid);
        x5(j) = (H5(j)-Hf)/(Hg-Hf);

        if (x5(j)<0.95)
            fprintf('Vapor quality at turbine outlet is low at pressure %0.2f \n',Ph);
        end
```

```
P3(j) = Ph;
P6(j) = P5(j);

% Recuperator heat exchanger
if((T5(j)-T2(j))<5)
   T3(j) = T2(j);
   S3(j) = S2(j);
   H3(j) = H2(j);
   T6(j) = T5(j);
   S6(j) = S5(j);
   H6(j) = H5(j);

else
   H31(j) = refpropm('H','T',T5(j),'P',Ph,fluid);
   H61(j) = refpropm('H','T',T2(j),'P',Pl(i),fluid);
   Q1(j) = H31(j)-H2(j);
   Q2(j) = H5(j)-H61(j);
   Q(j) = min(Q1(j),Q2(j));

   H3(j) = H2(j)+eta_HX*Q(j);
   T3(j) = refpropm('T','P',Ph,'H',H3(j),fluid);
   S3(j) = refpropm('S','P',Ph,'H',H3(j),fluid);

   H6(j) = H5(j)-eta_HX*Q(j);
   T6(j) = refpropm('T','P',Pl(i),'H',H6(j),fluid);
   S6(j) = refpropm('S','P',Pl(i),'H',H6(j),fluid);
   x6(j) = (H6(j)-Hf)/(Hg-Hf);

end

% Heat source
T7(j) = Ts;
P7(j) = refpropm('P','T',T7(j),'Q',0,'water');
H7(j) = refpropm('H','T',T7(j),'Q',0,'water');
S7(j) = refpropm('S','T',T7(j),'Q',0,'water');

T8(j) = Ts_out;
P8(j) = P7(j);
H8(j) = refpropm('H','T',T8(j),'P',P8(j),'water');
S8(j) = refpropm('S','T',T8(j),'P',P8(j),'water');
m_hot(j) = m*(H4(j)-H3(j))/(H7(j)-H8(j));

% Heat sink
T9(j) = Tw(i)+273.15;
H9(j) = refpropm('H','T',T9(j),'P',100,'water');
```

```matlab
    S9(j) = refpropm('S','T',T9(j),'P',100,'water');
    Tcond(j) = refpropm('T','P',Pl(i),'Q',1,fluid);      % Temperature at which working fluid
starts condensing
    Qw(j) = m*(H5(j)-H6(j));                              % Heat taken out from the working fluid
    eta_cond = 0.8;                                       % Condenser heat exchanger effectiveness
    Qs(j) = eta_cond*Qw(j);
    H10(j) = H9(j) + Qs(j)/m_cool;
    T10(j) = refpropm('T','H',H10(j),'P',100,'water');
    S10(j) = refpropm('S','H',H10(j),'P',100,'water');

    % Energy efficiency of the cycle
    W_t(j) = (H4(j)-H5(j))/1000;             % kJ/kg
    Qin(j) = (H4(j)-H3(j))/1000;             % kJ/kg
    W_net(j) = (W_t(j)-W_p(j));              % kJ/kg
    eff(j) = (W_t(j)-W_p(j))/Qin(j);         % Cycle efficiency

    j = j+1;

    end

    Qw(i) = m_cool*Cpw*(Tsink(i)-Tw(i));
    Q(i) = (Qc(i) - Qe(i) - Qr(i))+Qw(i);
    effmax(i) = max(eff);
    Wmax(i) = m*W_net(eff==max(eff));             % kW

    i = i+1;
    Tsink(i) = T10(eff==max(eff))-273.15;
    Tw(i) = Tw(i-1) + t0*Q(i-1)/H/A/rhow/Cpw;     % Water temperature (C)

end

dlmwrite('Tr_c_A400.rtf',Tw,'\n')
dlmwrite('Tr_in_c_A400.rtf',Tsink,'\n')
dlmwrite('E_c_A400.rtf',effmax,'\n')
dlmwrite('W_c_A400.rtf',Wmax,'\n')
```

## A.6 Condenser Design 1

This MATLAB code was used to model the condenser design 1.

```matlab
clc
clear all

% SRC parameters
fluid = 'R134a.fld';              %Working Fluid
eta_p = 0.85;
```

```matlab
eta_t = 0.85;
T0 = 0+273.15;              % Reference temperature for exergy analysis (K)
Ts_out = 80+273.15;         % Source output temperature (K)
m = 3;                      % Mass flow rate of the working fluid (kg/sec)
m_cool = 21;                % Mass flow rate of cooling water (kg/sec)
eta_HX = 0.75;              % Recuperator heat exchanger effectiveness
Tcrit = refpropm('T','C',0,'',0,fluid);       % Critical Temperature
Pcrit = refpropm('P','C',0,'',0,fluid);       % Critical Pressure
Ts_in = 175;               % Source inlet temperature (C)
Ts = Ts_in+273.15;         % Conversion to K

% Nocturnal cooling system parameters
phi = 0.2;      % Relative humidity
v = 4;          % Wind speed (m/s)
H = 0.5;        % Height of the tank (m)
L = 20;         % Length of the tank (m)
W = 10;         % Width of the tank (m)
A = L*W;        % Top surface area
rhow = 998;     % Density of water (kg/m3)
Cpw = 4186;     % Specific heat of water
ew = 0.9;       % Emissivity of reservoir
sig = 5.67*10^(-8);     %J/s/m2/K4
Tair = 40;              % Average ambient temperature
hc = 2.8+3*v;           % Convective heat transfer coefficient

% Initialization
Tw(1) = 40;
Tsink(1) = 40;
t_total = 24*5*3600;
t0 = 600;
i_total = t_total/t0;

i=1;
while(i<=i_total)

    t(i) = i*t0;  %Time
    days (i) = floor(t(i)/24/3600);
    time(i)=t(i)-24*3600*days(i);
    a1(i) = 2*pi*(t(i)/3600-1)/24;    %Erb's model parameter for daily temperature variation
    Ta(i) = Tair+15*(0.4632*cos(a1(i)-3.805)+0.0984*cos(2*a1(i)-0.360)+0.0168*cos(3*a1(i)-0.822)+0.0138*cos(4*a1(i)-3.513)); %(C)
    Pa(i) = 3385.5*exp(-8.0929+0.97608*(Ta(i)+42.607)^0.5);
    Pw(i) = 3385.5*exp(-8.0929+0.97608*(Tw(i)+42.607)^0.5);

    % Sky temperature calculation
    y(i) = 1/17.27*log(phi) + Ta(i)/(237.3+Ta(i));
```

```matlab
Tdp(i) = 237.3*y(i)/(1-y(i));  % Dew point temperature (C)
esky(i) = 0.741 + 0.0062*Tdp(i);          % Sky emissivity
Tsky(i) = esky(i)^0.25 * (Ta(i)+273);         % Sky temperature (K)

% The reservoir stays uncovered all the time
Qc(i) = A*hc*(Ta(i) - Tw(i));                  % Convective gain
Qe(i) = A*(0.2253+0.2464*v)*(Pw(i)-phi*Pa(i))^0.82;  % Evaporative loss
Qr(i) = A*ew*sig*((Tw(i)+273)^4-Tsky(i)^4);       % Radiative loss

% Ground cooling system
n = 4;     % Number of pipes

if(time(i)>= 5*3600 && time(i)<=21*3600)
   [Tg Qg] = Heat_pump(Tw(i),n);
   T_g(i) = Tg;
   Q_g(i) = Qg;
else
   Q_g(i) = 0;
end

if(Q_g(i)<0)
   Q_g(i) = 0;
end

% SRC optimization
Pl(i) = refpropm('P','T',Tw(i)+273.15,'Q',0,fluid);% Cycle low pressure

j=1;

for (Ph = 3000:100:7500)                % Cycle high pressure (kPa)

   % Pump inlet
   P1(j) = Pl(i);                          % kPa
   H1(j) = refpropm('H','P',Pl(i),'Q',0,fluid);        % J/kg
   S1(j) = refpropm('S','P',Pl(i),'Q',0,fluid);        % J/kg/K
   T1(j) = refpropm('T','P',Pl(i),'Q',0,fluid);        % K

   % Pump outlet
   P2(j) = Ph;
   S2(j) = S1(j);
   H21(j) = refpropm('H','P',Ph,'S',S1(j),fluid);
   H2(j) = H1(j)+((H21(j)-H1(j))/eta_p);
   T2(j) = refpropm('T','P',Ph,'H',H2(j),fluid);
   W_p(j) = (H2(j)-H1(j))/1000;               %kJ/kg

   % Turbine input
```

```matlab
P4(j) = Ph;
T4(j) = Ts-10;
H4(j) = refpropm('H','T',T4(j),'P',Ph,fluid);
S4(j) = refpropm('S','T',T4(j),'P',Ph,fluid);

% Turbine output
S5(j) = S4(j);
P5(j) = Pl(i);
H51(j) = refpropm('H','P',P5(j),'S',S5(j),fluid);
H5(j) = H4(j)-eta_t*(H4(j)-H51(j));
T5(j) = refpropm('T','P',P5(j),'H',H5(j),fluid);
Hf = refpropm('H','P',P5(j),'Q',0,fluid);
Hg = refpropm('H','P',P5(j),'Q',1,fluid);
x5(j) = (H5(j)-Hf)/(Hg-Hf);

if (x5(j)<0.95)
   fprintf('Vapor quality at turbine outlet is low at pressure %0.2f \n',Ph);
end

P3(j) = Ph;
P6(j) = P5(j);

% Recuperator heat exchanger

if((T5(j)-T2(j))<5)
   T3(j) = T2(j);
   S3(j) = S2(j);
   H3(j) = H2(j);
   T6(j) = T5(j);
   S6(j) = S5(j);
   H6(j) = H5(j);

else
   H31(j) = refpropm('H','T',T5(j),'P',Ph,fluid);
   H61(j) = refpropm('H','T',T2(j),'P',Pl(i),fluid);
   Q1(j) = H31(j)-H2(j);
   Q2(j) = H5(j)-H61(j);
   Q(j) = min(Q1(j),Q2(j));

   H3(j) = H2(j)+eta_HX*Q(j);
   T3(j) = refpropm('T','P',Ph,'H',H3(j),fluid);
   S3(j) = refpropm('S','P',Ph,'H',H3(j),fluid);

   H6(j) = H5(j)-eta_HX*Q(j);
   T6(j) = refpropm('T','P',Pl(i),'H',H6(j),fluid);
   S6(j) = refpropm('S','P',Pl(i),'H',H6(j),fluid);
```

133

```matlab
    x6(j) = (H6(j)-Hf)/(Hg-Hf);

end

% Heat source
T7(j) = Ts;
P7(j) = refpropm('P','T',T7(j),'Q',0,'water');
H7(j) = refpropm('H','T',T7(j),'Q',0,'water');
S7(j) = refpropm('S','T',T7(j),'Q',0,'water');

T8(j) = Ts_out;
P8(j) = P7(j);
H8(j) = refpropm('H','T',T8(j),'P',P8(j),'water');
S8(j) = refpropm('S','T',T8(j),'P',P8(j),'water');
m_hot(j) = m*(H4(j)-H3(j))/(H7(j)-H8(j));

% Heat sink
T9(j) = Tw(i)+273.15;
H9(j) = refpropm('H','T',T9(j),'P',100,'water');
S9(j) = refpropm('S','T',T9(j),'P',100,'water');
Tcond(j) = refpropm('T','P',Pl(i),'Q',1,fluid);        % Temperature at which working fluid
starts condensing

Qw(j) = m*(H5(j)-H6(j));                                % Heat taken out from the working fluid
eta_cond = 0.8;                                          % Condenser heat exchanger effectiveness
Qs(j) = eta_cond*Qw(j);
H10(j) = H9(j) + Qs(j)/m_cool;
T10(j) = refpropm('T','H',H10(j),'P',100,'water');
S10(j) = refpropm('S','H',H10(j),'P',100,'water');

% Energy efficiency of the cycle
W_t(j) = (H4(j)-H5(j))/1000;             %kJ/kg
Qin(j) = (H4(j)-H3(j))/1000;             %kJ/kg
W_net(j) = (W_t(j)-W_p(j));              %kJ/kg
eff(j) = (W_t(j)-W_p(j))/Qin(j);         %Cycle efficiency

j = j+1;

end

Qw(i) = m_cool*Cpw*(Tsink(i)-Tw(i));

Q(i) = Qc(i) - Qe(i) - Qr(i) + Qw(i) - Q_g(i);

effmax(i) = max(eff);
```

```
    Wmax(i) = m*W_net(eff==max(eff));            %kW

    i = i+1;

    Tsink(i) = T10(eff==max(eff))-273.15;

    Tw(i) = Tw(i-1) + t0*Q(i-1)/H/A/rhow/Cpw        % Water temperature (C)
end
```

This MATLAB function was used for the ground coupled heat exchanger system and then called in the condenser script.

```
function [T_out Q_out] = Heat_pump(Tw1,n)

% Design inputs
Di_GHX = 0.02;        % Inner diameter
Do_GHX = 0.025;       % Outer diameter
L1=100;

% Soil properties
Ts = 19.5;            % Mean soil temperature
Ks = 0.159;           % Thermal conductivity
Us = 12;              % Overall heat transfer coefficient

% Water properties
Kw = 0.623;           % Thermal conductivity (W/m-K)
mu = 719.13 * 10^(-6);  % Dynamic viscosity (Pa-s)
rho = 994;            % Density (kg/m3)
Cpw = 4179.3;         % Specific heat

ii=2;

for(Tw2=Tw1-10:0.1:Tw1)
   mw = 0.15;             % Mass flow rate of water
   vw = mw/rho*4/pi/Di_GHX^2;
   Re = rho*vw*Di_GHX/mu;
   Pr = Cpw*mu/Kw;
   Nu = 0.023 * Re^0.8 * Pr^0.33;
   hw = Kw/Di_GHX*Nu;

   % Resistant due to water flow
   Rw = 1/(2*hw*pi*Di_GHX);

   % Resistance due to pipe wall
```

```
Kp = 0.3979;          %Thermal conductivity of polyethylene pipe (W/m-K)
Rp = log(Do_GHX/Di_GHX)/(4*pi*Kp);

% Resistance due to soil
Rs = 1/(2*pi*Us*Do_GHX);

T12(ii)= L1 - mw*Cpw*(Tw1-Tw2) / ((Tw1+Tw2)/2-Ts) * (Rw+Rp+Rs);

if(T12(ii-1)<0 && T12(ii)>0)

   T12(ii);
   Tf=Tw2;

end

ii=ii+1;

end

T_out = Tf;

Q_out = n*mw*Cpw*(Tw1-T_out);
```

## Appendix B: Copyright Permissions

This section includes the permissions obtained to use the copyrighted material.

- Permission to use Figure 7 used in [127].

- Permission to use Figure 8 used in [134].
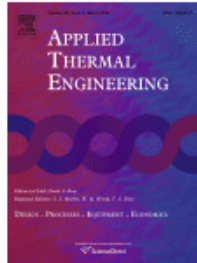
- Permission to use Figure 10 given in [82].
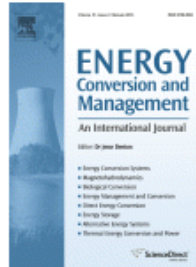
- Permission to use Figure 11 given in [150].
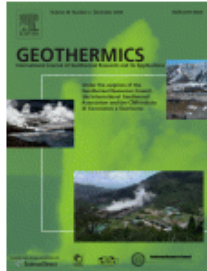
- Permission to use Figure 12 given in [157].

- Permission to use part of Figure 51 given in [186].

## Order Completed

Thank you very much for your order.

This is a License Agreement between Rachana Vidhi ("You") and Elsevier ("Elsevier"). The license consists of your order details, the terms and conditions provided by Elsevier, and the payment terms and conditions.

Get the printable license.

| | |
|---|---|
| License Number | 3422530868634 |
| License date | Jul 05, 2014 |
| Licensed content publisher | Elsevier |
| Licensed content publication | Renewable Energy |
| Licensed content title | Cooling performance of roof ponds with gunny bags floating on water surface as compared with a movable insulation |
| Licensed content author | Runsheng Tang,Y. Etzion |
| Licensed content date | July 2005 |
| Licensed content volume number | 30 |
| Licensed content issue number | 9 |
| Number of pages | 13 |
| Type of Use | reuse in a thesis/dissertation |
| Portion | figures/tables/illustrations |
| Number of figures/tables/illustrations | 1 |
| Format | electronic |
| Are you the author of this Elsevier article? | No |
| Will you be translating? | No |
| Title of your thesis/dissertation | Organic fluids and passive cooling in a Supercritical Rankine cycle for power generation from low grade heat sources |
| Expected completion date | Aug 2014 |
| Estimated size (number of pages) | 175 |
| Elsevier VAT number | GB 494 6272 12 |
| Permissions price | 0.00 USD |
| VAT/Local Sales Tax | 0.00 USD / 0.00 GBP |
| Total | 0.00 USD |

ORDER MORE...    CLOSE WINDOW

- Copyright agreement to re-use previously published article [10] in chapter 3.

The following terms of copyright assignment refer to Sections 1, 2, and 3. Sections 4 and 5 may not be subject to copyright.

The undersigned hereby assigns irrevocably to ASME all worldwide rights under copyright in the Paper.

Authors retain all proprietary rights in any idea, process, procedure, or articles of manufacture described in the Paper, including the right to seek patent protection for them. Authors may perform, lecture, teach, conduct related research, display all or part of the Paper, and create derivative works in print or electronic format. Authors may reproduce and distribute the Paper for non-commercial purposes only. Non-commercial applies only to the sale of the paper per se. For all copies of the Paper made by Authors, Authors must acknowledge ASME as original publisher and include the names of all author(s), the publication title, and an appropriate copyright notice that identifies ASME as the copyright holder.

PLEASE READ THE TERMS AND CONDITIONS WHICH ARE FULLY INCORPORATED IN THIS AGREEMENT.

1. **PAPERS OWNED BY ONE AUTHOR OR JOINT AUTHORS; DESIGNATED AUTHORS** (For jointly authored works, all authors should submit a signed Agreement, or one Designated Author may sign on behalf of the other authors, but **ONLY IF** the designated author has secured written authorization to do so from all other authors. The designated author must be able to produce such written authorization if requested.)

Designated authors, please sign below and list the names of the co-authors for whom you are signing. Please include full contact information for each author. Attach additional sheets if necessary. Author(s)/co-author(s) not covered by the Designated author, please sign in the appropriate section below and provide full contact information.

**Author, Co-Author, or Designated Author**

Name: D. Yogi Goswami        Signature: _____   1/15/13

Affiliation: University of South Florida   Job Title: Professor   _____ Energy Research Center
(Company & Institution)

Address: 4202 E. Fowler Avenue, Tampa   FL   33620   USA
(Street Address)   (City)   (State)   (Zip Code)   (Country)

Phone 813-974-0956   Fax 813-974-2050   Email goswami@usf.edu

Co-Author s (See Attached)

Name: _____   Date: _____

Affiliation: _____   Job Title: _____
(Company or Institution)

Address: _____   (City)   (State)   (Zip Code)   (Country)
(Street Address)

Phone _____   Fax _____   Email _____

2. **PAPERS OWNED BY EMPLOYER OF AUTHOR(s)** (Author may sign if so authorized; otherwise, an officer or other authorized agent of the employer should sign below.)

Name: _____   Signature: _____   Date: _____

Affiliation: _____   Job Title: _____
(Company or Institution)

Address: _____   (City)   (State)   (Zip Code)   (Country)
(Street Address)

Phone _____   Fax _____   Email _____

Author

144

- Copyright agreement to re-use previously published article *"Performance of working fluids for power generation in a Supercritical Organic Rankine cycle. Proceedings of the ASME 2012 6th International Conference on Energy Sustainability. San Diego. July, 2012"* in chapter 4.

## COPYRIGHT AGREEMENT (as of February 2010)

ASME Publishing • Three Park Avenue • New York, NY 10016
For questions about Conference paper copyright, please e-mail copyright@asme.org
For questions about Journal paper copyright, please email journalcopyright@asme.org

Before publication of your paper in a conference proceedings or journal, ASME must receive a signed Copyright Agreement. For conference papers, this form should be received by the deadline indicated by the Conference. Other forms may NOT be substituted for this form, nor may any wording on the form be changed.

PAPER NUMBER (for conference/journal papers): ESFuelCell2012-91473

TITLE: Performance of working fluids for power generation in a Supercritical Organic Rankine cycle

AUTHOR(s): Rachana Vidhi, Sarada Kuravi, Saeb M. Besarati, D. Yogi Goswami, Elias Stefanakos, Adrian S. Sabau

CONFERENCE NAME: ESFuelCell2012

JOURNAL NAME: _____

---

ASME requests that authors/copyright owners assign copyright to ASME in order for a conference or journal paper to be published by ASME. Authors exempt from this request are direct employees of the U.S. Government, whereby papers are not subject to copyright protection in the U.S., or non-U.S. government employees, whose governments hold the copyright to the paper. Otherwise, the author/ copyright owner(s) of the Paper should sign this form as instructed below. Please refer to the section below "Who Should Sign" and also to ASME's FAQ page for more information regarding copyright ownership and the copyright process.

### WHO SHOULD SIGN

Only the copyright owner(s) of the Paper, or an authorized representative, can sign this form. If one of the following applies, you may not own the copyright to the paper, or you may not be authorized to sign this agreement, and you may need to have the appropriate copyright owner(s) or organization representative sign this Agreement.
(1) You created the Paper within the scope of your employment, and your employer is the copyright owner
(2) You created the Paper under an independent contractor agreement**
(3) You received a grant that funded your Paper.

Please review your company policies regarding copyright, and if you are not authorized to sign this agreement, please forward to the appropriate organization representative. Please review applicable company, institutional, and grant policies and your employment/independent contractor agreement to determine who holds the rights to your Paper. For more information, please refer to the FAQs.

**Note to U.S. Government Contractors: If you created the Paper under contract with the U.S. Government, e.g., U.S. Government labs, the paper may be subject to copyright, and you or your employer may own the copyright. Please review your company/institutional policies and your contractor agreement. Your Paper may also require a footer acknowledging contract information and also the following statement:

"The United States Government retains, and by accepting the article for publication, the publisher acknowledges that the United States Government retains, a non-exclusive, paid-up, irrevocable, worldwide license to publish or reproduce the published form of this work, or allow others to do so, for United States Government purposes."

It is your responsibility to ensure that the final PDF version of the Paper you submit includes all necessary footers and statements required under your contract.

### COPYRIGHT ASSIGNMENT
The following terms of copyright assignment refer to Sections 1, 2, and 3. Sections 4 and 5 may not be subject to copyright.

The undersigned hereby assigns irrevocably to ASME all worldwide rights under copyright in the Paper.

Authors retain all proprietary rights in any idea, process, procedure, or articles of manufacture described in the Paper, including the right to seek patent protection for them. Authors may perform, lecture, teach, conduct related research, display all

or part of the Paper, and create derivative works in print or electronic format. Authors may reproduce and distribute the Paper for non-commercial purposes only. Non-commercial applies only to the sale of the paper per se. For all copies of the Paper made by Authors, Authors must acknowledge ASME as original publisher and include the names of all author(s), the publication title, and an appropriate copyright notice that identifies ASME as the copyright holder.

PLEASE READ THE TERMS AND CONDITIONS WHICH ARE FULLY INCORPORATED IN THIS AGREEMENT.

PAPERS OWNED BY ONE AUTHOR OR JOINT AUTHORS; DESIGNATED AUTHORS (For jointly authored works, all authors should submit a signed Agreement, or one Designated Author may sign on behalf of the other authors, but ONLY IF the designated author has secured written authorization to do so from all other authors. The designated author must be able to produce such written authorization if requested.)

Author, Co-Author, or Designated Author

Name: Rachana Vidhi   Signature: Rachana Vidhi   Date: 11 Apr 2012

Affiliation: University of South Florida   Title: Graduate Student
(Company or Institution)

Street Address: 4202, E Fowler Avenue

Tampa                    FL                    33620                United States
(City)                   (State)               (Zip Code)           (Country)

Phone: _____   Fax: _____   Email: _____

Author: (Applied only if you are signing for other)

Name: _____   Signature: _____   Date: _____

Affiliation: _____   Title: _____
(Company or Institution)

Street Address: _____

_____
(City)                   (State)               (Zip Code)           (Country)

Phone: _____   Fax: _____   Email: _____

# ASME COPYRIGHT FORM TERMS AND CONDITIONS

The following terms and conditions are fully incorporated into the Copyright Form. Please read them carefully.

## REPRESENTATIONS, OBLIGATIONS, ACKNOWLEDGEMENTS, AND INDEMNIFICATION

You represent and acknowledge that:

(A) This Paper represents: either the first publication of material or the first publication of an original compilation of information from a number of sources as specifically noted by footnotes and/or bibliography.

(B) You have the right to enter into this Copyright Form and to make the assignment of rights to ASME. If the Paper contains excerpts from other copyrighted material (including without limitation any diagrams, photographs, figures or text), you have acquired in writing all necessary rights from third parties to include those materials in the Paper, and have provided appropriate credit for that third-party material in footnotes or in a bibliography.

(C) If you are signing this Form on behalf of any co-authors or other copyright holders, you have obtained express authorizations from all those authors and/or copyright holders to make this assignment of rights to ASME.

(D) To the best of the author's knowledge, all statements contained in the Paper purporting to be facts are true or supported by reasonable scientific research, the Paper does not contain any defamatory or libelous material and does not infringe any third party's copyright, patent, trade secret, or other proprietary rights and does not violate the right of privacy or publicity of any third party or otherwise violate any other applicable law; furthermore that to the best of your ability, you are responsible for ensuring the accuracy of your research and the Paper's content.

(E) If the Paper was produced in the course of an author's employment by, or contractual relationship with, the U.S. Federal or State Government and/or contains classified material, it has been appropriately cleared for public release and such is indicated in the paper.

(F) The Paper is not subject to any prior claim, encumbrance or form and is not under consideration for publication elsewhere.

(G) You have appropriately cited and acknowledged all third parties who have contributed significantly in the Paper's technical aspects.

(H) ASME is not responsible for any misrepresentation, errors or omissions by those signing this copyright form.

(I) All print and electronic copies of the Paper submitted to ASME become ASME's physical property regardless of whether or not ASME publishes the Paper, and that ASME is not obligated to publish your paper (see the Termination Section below if your paper is not published).

(J) ASME is not responsible for any of your expenses incurred in connection with preparing the Paper or attending meetings to present it, nor will ASME pay you any financial compensation if it publishes your Paper.

(K) Subject to and to the maximum extent permitted by law, you agree to indemnify and hold harmless ASME from any damage or expense related to a breach of any of the representations and warranties above.

## TERMINATION

If ASME decides not to publish your Paper, this Form, including all of ASME's rights in your Paper, terminates and you are thereafter free to offer the Paper for publication elsewhere.

## GENERAL PROVISIONS

This Copyright Form, the Terms & Conditions, and ASME Copyright Guidelines, constitutes the entire agreement between you and ASME, and supersedes all prior or current negotiations, understandings and representations, whether oral or written, between you and ASME concerning the Paper.

This Agreement is governed by, and should be construed in accordance with, the laws of the State of New York, United States of America, applicable to agreements made and performed there, except to the extent that your institution is prohibited by law from entering contracts governed by New York law, in which limited case this Agreement is governed by, and should be construed in accordance with, the laws of the jurisdiction in which your institution is located. Any claim, dispute, action or proceeding relating to this Agreement may be brought only in the applicable state and federal courts in the State and County of New York, and you expressly consent to personal jurisdiction and venue in any of those courts.

## Appendix C: Nomenclature

| | | | |
|---|---|---|---|
| *T* | *Temperature* | | |
| *U* | *Overall heat transfer coefficient* | | |
| *h* | *Convective heat transfer coefficient* | *Subscripts* | |
| *Cp* | *Specific heat* | | |
| *m* | *Mass flow rate* | *n* | *Element from inlet* |
| *A* | *Differential area* | *s* | *Surface of the tube* |
| *δ* | *Penetration depth* | *e* | *Earth* |
| *r* | *Radial distance* | *f* | *Fluid* |
| *W* | *Humidity* | *g* | *Gas* |
| *H* | *Enthalpy* | *o* | *Outer wall* |
| *D* | *Diameter* | *i* | *Inner wall* |
| *L* | *Length* | | |
| *k* | *Thermal conductivity* | | |
| *q'* | *Heat transfer per unit area* | | |

## ABOUT THE AUTHOR

Rachana Vidhi was born in Chhapra, Bihar, India to a doctor father and a professor mother. She entered the Indian Institute of Technology, more commonly known as IIT around the world, in the year 2006 to study Energy Engineering. At the end of the junior year of college, she travelled to the Universiti Teknologi Malaysia, Johor Bahru for a 10 week internship.

After obtaining Bachelor of Technology degree in 2010, she came to the United States to pursue higher education and perform research in the field of clean energy. She joined the Clean Energy Research Center at the University of South Florida to work under the guidance of Dr. Yogi Goswami on power generation from low temperature heat sources. During the doctoral study, she was also involved in raising awareness about clean energy in the community. For her research and services in the field of solar energy, she was awarded the John and Barbara Yellott award by the American Solar Energy Society in 2014. She expects to graduate with a Doctor of Philosophy in Chemical Engineering from the University of South Florida in 2014.